EUROPEAN ORGANIZATION FOR NUCLEAR RESEARCH

NP/Int./64- 5
27 May, 1964

EXPERIMENTAL STUDY OF PARTICLE PRODUCTION AT SMALL ANGLES IN NUCLEON-NUCLEON COLLISIONS*)

D. Dekkers, J.A. Geibel, R. Mermod, G. Weber†, T.R. Willitts and K. Winter

CERN, Geneva

B. Jordan and M. Vivargent
Institut du Radium, Orsay

N.M. King and E.J.N. Wilson
Rutherford High Energy Laboratory, Chilton

ABSTRACT

Differential cross sections are presented for the production of pions, kaons, protons and antiprotons at the angles 0° and 5.7°, produced in proton collisions with H_2, Be and Pb targets at primary momenta of 18.8 and 23.1 Gev/c, and in some cases at 8.65 and 11.8 Gev/c. The data are discussed with special reference to the rôle of isobar excitation in the production of secondary particles. All qualitative features of the experimental data are shown to be consistent with a dominant rôle of isobar decay in the production of pions, positive kaons and protons at small angles. Excitation of isobars is shown to proceed without exchange of isospin between the colliding nucleons. Direct excitation of strange isobars can be ruled out. Evidence is presented for reduced probability of isobar production at 0°.

Submitted for publication to The Physical Review

*) A first account of this work was presented at the International Conference on Elementary Particles, Siena 1963.

†) Now at DESY, Hamburg, Germany.

I. INTRODUCTION

The experimental data presented in this paper were obtained during a detailed investigation of particle production at small angles. For the first time absolute cross sections for the production of pions, kaons, protons and antiprotons in proton - proton collisions were obtained at 0°. For an investigation of the dynamics of particle production, data on proton - proton collisions are most relevant. Information on the angular distribution was obtained by repeating the experiment at an angle of 5.7° (100 mrad). The primary momenta were 18.8 and 23.1 Gev/c, in some cases also 8.65 and 11.8 Gev/c. Data were also taken for collisions of protons with complex nuclei, beryllium and lead; they have mainly practical use for the design of secondary beams. The data on particle production from proton collisions with complex nuclei gave also information on proton - neutron collisions and reabsorption phenomena. In particular, they were of importance for an improved calculation of the neutrino spectrum in the CERN neutrino experiment[1]. It was for this purpose that this investigation was originally started. In total, more than 300 differential cross sections have been measured.

Previous experimental studies of particle production in nucleon - nucleon collisions, with cosmic rays and accelerators, have established some general characteristics of this process. They will be recalled in the following[2] without giving special reference to individual contributions.

1. The mean inelasticity in high-energy collisions, defined as the mean fraction of energy available for particle production, remains small throughout the primary energy range 10 to 10^5 Gev.

2. The mass spectrum of secondary particles remains approximately the same up to the highest energies studied with cosmic rays. The total energy carried away by pions is a small fraction, about 30% of the primary nucleon energy.

3. In the centre-of-mass system, the longitudinal momentum spectrum of protons is peaked towards the maximum possible momentum, in contrast with the pion spectrum which is peaked at low momenta. The mean energy carried away by the nucleon component is approximately 60% of the initial energy.

4. The momentum spectrum of pions is characterized by an exponential tail at the high-energy end. As the primary energy, E_o, is raised, the mean kinetic centre-of-mass energy of pions remains constant, the mean pion multiplicity increasing roughly as $E_o^{1/4}$.

5. Pions and kaons are produced with transverse momenta distributed approximately as a Boltzmann law. The average transverse momentum is about 400 Mev/c and remains constant up to cosmic ray energies. There is some evidence that the baryonic component has a similar distribution of transverse momentum, but the average transverse momentum seems to increase slightly with the mass of the baryon.

Several models were proposed (statistical model, fire ball model, one pion exchange model, multiperipheral model, etc), to account for these general characteristics. They either reproduce some average features, such as the centre-of-mass energy spectra, averaged over all angles (statistical model), or some dynamical features, such as the angular distribution (peripheral model). The best description is obtained by a set of empirical rules[3] as suggested by the data.

Some finer details of the experimental data about the dynamics of particle production have however been left out in this list of general characteristics.

At low primary momenta, of a few Gev/c, the process of particle production has been successfully described[4] by the formation of isobars and their subsequent decay. Detailed calculations, using an explicit mechanism for exciting the incident nucleon as well as the target nucleon through one pion exchange, gave quantitative agreement with the experimental data[5].

At the highest accelerator energies there is also experimental evidence from near elastic proton scattering for the excitation of the nucleons[6]. However, the exchange phenomena leading to this isobar excitation were found to be drastically different. The angular distribution

of isobar excitation was observed to follow the diffraction pattern of elastic proton - proton scattering, up to momentum transfers which are far outside the range of validity of the one pion exchange model. Moreover, the excitation of the first isobar with isospin $I = 3/2$, was observed to disappear very rapidly as the primary energy was increased; at the highest accelerator energies, only excitation of isobars with isospin $I = 1/2$ was observed experimentally. This difference in the exchange phenomena at low and high primary energies was attributed to the vanishing of inelastic contributions with exchange of one unit of isospin (such as the one pion exchange), and the increasing importance of processes without exchange of isospin[7].

In the following we shall try to investigate the rôle of isobar excitation in the production of secondary particles[8]. Kinematically, particles emitted in the decay of isobars may be distinguished by the high velocity of the parent isobar in the laboratory system. In the decay to the ground state by single pion emission, the mean total energy retained by the pion is :

$$\frac{M_B^2 - M_p^2 + m_\pi^2}{2M_B} ,$$

where M_B is the isobar mass. For an average mass of $M_B = 1.6$ Gev, each isobar will, on the average, transfer 30% of its energy to one or sometimes two pions. As a consequence of the high velocity of their parent isobar, decay pions can carry a large fraction of the primary momentum. The average fraction is determined by the isobar mass and is approximately independent of the primary momentum. As a consequence of this, the average secondary momentum of decay pions will scale linearly with the primary momentum.

The kinetic energy remaining in the collision rest system as the colliding nucleons go on in an excited state will also contribute to secondary particle production. This process will produce the bulk of secondaries observed at large angles. The average momentum in the collision rest system, $\langle \bar{p} \rangle$, is known to be small and constant, independent of the primary momentum.

In the laboratory system this contribution is characterized by small secondary momenta, of the order of $\langle \bar{p} \rangle \bar{\gamma}_c$, where $\bar{\gamma}_c$ is the Lorentz factor of the c.m.s., scaling roughly as the square root of the primary momentum. These kinematical differences will be useful in the discussion of the experimental results.

In the following section II, the experimental set-up is described. The main qualitative features of the experimental data will be discussed in section III, with special reference to the rôle of isobar excitation. Finally, in section IV, the observations on the experimental data from section III will be summarized and their consistency will be discussed.

In the appendix, all differential cross sections obtained during this experiment are presented in tables 1 - 7 .

II. EXPERIMENTAL METHOD

Targets were placed in the focus of a scattered out proton beam of the CERN proton synchrotron, containing some 10^7 protons per burst in an image 2 cm wide by 3 cm high, with a momentum band of ±1% and a divergence of ±3 mrad. The number of protons hitting the target was monitored by a counter telescope M_2 M_3 (Fig.1), looking at secondaries which leave the target at a mean angle of 100 mrad; it was calibrated using in coincidence a small scintillator M_1, placed in front of the target. This calibration was found to be reproducible to within ±3%.*) A differential ion chamber[9], placed in front of the target, monitored the position of the proton beam.

Secondary particles produced in the target were analyzed in momentum and brought to a focus on counter S_5 by a spectrometer consisting of a quadrupole triplet Q_8 Q_9 Q_{10} and a bending magnet B_4 ; in the 0 mrad position, the bending magnet separated secondaries from the incident proton beam, giving a spatial separation at counter S_1 of 25 to 70 cm for positive particles and more for negative particles. In the 100 mrad measurements, the whole set-up was rotated around the target; the incident proton beam then cleared the spectrometer completely.

*) The neutron contamination was found to be smaller than 1%.

Secondaries were then defined in direction by the counter telescope S_1 to S_5 and identified by the Čerenkov counters C_1 C_2 C_3 [10] (threshold) and C_d (differential) [11]. Using appropriate combinations of the signals of these counters, all particles of the same charge (π^+, K^+, p or π^-, K^-, $\bar{p}$) were identified simultaneously. A large scintillator, S_6, placed behind 1 m of iron was used to reject muons by anticoincidence.

Severe experimental problems arise in the 0 mrad measurements from the fact that the proton beam traverses the spectrometer together with secondaries produced in the target. The following figures depict the situation in two typical cases in which the spectrometer is set for 10 Gev/c secondaries of positive and negative charge.

Table I

Number of particles traversing the spectrometer (per burst)			
Protons of the incident beam : 2×10^7	70 π^+	1.2 K^+	400 p
	35 π^-	0.35 K^-	0.04 $\bar{p}$

Secondaries may be also produced by protons of the incident beam hitting the pole pieces of the quadrupoles. The protons producing these intersections come from the halo surrounding the incident beam. There is also a finite probability for any proton of the incident beam to be scattered into the counter telescope, giving rise to false proton or false kaon counts; one should notice here that the β of 10 Gev/c kaons is roughly equal to that of 18 Gev/c protons. Both these effects result in a counting rate without target which is a significant fraction of that with target; moreover the effect is target dependent because the number of protons through the spectrometer is reduced when the target is in position.

The following precautions helped to improve this situation :

1. Thin targets were used to avoid excessive blowing up of the proton beam by multiple scattering.

2. Multiple and nuclear scattering from the air throughout the spectrometer was minimized by inserting He bags.

3. All secondaries produced in the pole pieces of the spectrometer and liable to reach the counter telescope were vetoed by guard counters placed inside the spectrometer. They also served to define a simple diaphragm for particles produced in the target which greatly simplified a reliable calculation of the solid angle.

4. The high counting rate of the guard counters gave rise to losses due to accidental anticoincidences. These were therefore continuously monitored and used for correcting the data. This effect was always smaller than 10%.

The measured cross sections for production of $\pi^{\pm}$, $K^{\pm}$, p and $\bar{p}$ at 0 and 100 mrad from p - p, p - Be and p - Pb interactions at 18.8 and 23.1 Gev/c are given in the appendix, tables 1 - 7, each table corresponding to one particle of given charge. The cross sections are expressed in mb sr^{-1} $(Gev/c)^{-1}$ per nucleus and not in number of secondaries per interaction; this would have implied the use of the total cross section which is not well known for nuclei.

Corrections have been applied for particle decay, for accidental coincidences, for absorption, multiple scattering and diffraction scattering in the target and the telescope and for differential Cerenkov counter efficiency. The errors quoted include both statistical and systematical uncertainties; the latter arise from approximations in the computation of the corrections as well as from the uncertainty in the intensity of the incident beam. Error bars are shown for $K^{\pm}$ and $\bar{p}$; errors on $\pi^{\pm}$ and p are of the same order as the size of the points.

Absorption corrections are important as the simultaneous identification of three kinds of particles requires several counters and consequently introduces a certain amount of material in the path of the secondaries.

K and $\bar{p}$ - nucleus absorption cross sections are often not available and have been computed from cross sections on hydrogen with the help of a semi-theoretical formula derived by R.W. Williams[12], which is more accurate than the "geometrical" formula $\sigma = \sigma_0 A^{2/3}$. Typical corrections are of the order of 20% for 6 Gev/c positive pions.

No simple evaluation of losses by multiple scattering can be done when the scatterer is extended, as in the case of our counter telescope; consequently a Monte-Carlo calculation was done. This considers both the particles which are scattered out of the telescope and those which would leave the telescope but are scattered back into it, taking into account the spatial distribution of the beam, which was not uniform in our case because of the focusing action of the lenses. Typically, corrections are smaller than 10% for 6 Gev/c secondaries.

The problem of losses by diffraction scattering is similar; minor modifications to the computer programme allowed the calculation of the fraction of diffraction scattered secondaries which are lost for the telescope, yielding a typical correction of 5% for 6 Gev/c positive pions.

The effect of the finite average angular acceptance of ± 8 mrad on the 0 mrad data has been investigated. Extrapolation to zero solid angle requires assumptions on the detailed shape of the angular distribution. This is strongly momentum dependent. An upper limit for this correction was estimated with the help of the empirical formula given by Cocconi, Koester, Perkins[3], which over-estimates this effect. These limiting corrections varied from less than 1% to less than 10% for 1 Gev/c and 12 Gev/c secondaries respectively, and were neglected.

III. EXPERIMENTAL RESULTS

1. Pion Spectra

The differential momentum spectra of positive and negative pions observed at 0 and 100 mrad in the laboratory system, for different primary momenta and targets are presented in Figs. 2 and 3.

Inspection of these spectra and a comparison with other data, on negative pion production in proton - beryllium collisions in the angular range 25 - 125 mrad[13] and on neutral pion production in proton - proton collisions in the angular range 30 - 500 mrad[14] leads us to the following general observations:

i) The differential momentum spectra of positive and negative pions at 0° differ strongly in shape. This is best observed on a linear plot in Fig.4 . The spectrum of positive pions exhibits a pronounced maximum at 5.8 Gev/c for 18.8 Gev/c primary momentum, which is shifted to 6.8 Gev/c for 23.1 Gev/c primary momentum. In contrast to this, a smooth spectrum is observed for negative pions; only the high momentum tail is observed to shift linearly with the primary momentum.

ii) At small angles, the cross section for production of pions with secondary momenta below 5 Gev/c is approaching a constant value in the laboratory system, independent of the primary momentum.

iii) At fixed secondary momentum, the production of pions increase strongly as the angle is decreased. However, in the very small angle range between 0 - 25 mrad, and for higher secondary momenta, the production hardly changes.

iv) There is experimental evidence that the production of pions with low secondary momenta is more abundant at small angles than at 0°.

These general observations will now be discussed in more detail in connection with the model for particle production which was given in section 1.

Spectra of Positive and Negative Pions

The pronounced difference in shape of the spectra observed for positive and negative pions can also be demonstrated by considering the ratio of positive to negative pions, $N(\pi^+) / N(\pi^-)$. This quantity is shown in Figs. 5 and 6 as a function of secondary momentum for different angles and primary momenta. At low secondary momenta, it is close to one, as the momentum increases a steep rise is observed and finally a constant value is reached, varying only with the angle. The step in the momentum dependence of the ratio $N(\pi^+) / N(\pi^-)$, as well as the position of the peak in the π^+ spectrum are observed to shift approximately linearly with the primary momentum. If the incident nucleon were excited in a near elastic collision, pions emerging from its decay to the nucleon ground state would exhibit this dependence on the primary momentum. The average fraction of energy which an excited nucleon can transfer to a single decay pion is about 30% for an average isobar mass of 1.6 Gev, as calculated in section 1. The peak in the positive pion spectrum (Fig. 4), is indeed observed to occur at about 30% of the primary momentum. The maximum fraction of energy which an isobar can transfer to a single decay pion is about 70% for an isobar mass of 1.68 Gev. This is unfortunately outside the momentum range of this experiment. Observation of a fast, sudden drop in the pion spectrum at high momenta could in fact be used to put a lower limit on the masses of isobars frequently excited in nucleon-nucleon collisions.

Here we have assumed that isobars decay preferentially by the emission of a single pion. Decay into other channels are known to contribute about 20% to the total rate[20]. The contribution from more complicated decays, for instance into two pions[21], is evidenced by the shift, with primary momentum, of the high-momentum tail in the π^- spectrum. In decays into two pions, the average fraction of energy transferred to each pion is about 15%. The maximum observed in the π^- spectrum at 18.8 Gev/c primary momentum does indeed occur at about $0.15 \cdot p_o$.

But apparently, few negative pions are produced by single pion decay of isobars. This surprising result implies that the incident nucleon does not change its charge when it is excited, a statement equivalent to the observation that at high primary energies the exchange phenomena responsible for isobar excitation are processes without exchange of isospin[6,7].

This result is further supported by the experimental evidence from our data, that the ratio $N(\pi^+)/N(\pi^-)$ is independent of the target nucleus, a result which is to be expected when isobar excitation is proceeding through processes without exchange of isospin.

Further direct evidence against the excitation of isobars with isospin $I = 3/2$ is obtained from the ratio of positive to neutral pions at fixed secondary momentum. On the basis of isospin conservation the decay probabilities of a positively charged isobar into π^+ or π^0 are in the ratio of $N(\pi^+)/N(\pi^0) = 2$ for isospin 1/2, and of 1/2 for isospin 3/2. A comparison of our data on π^+ production with other data[14] on π^0 production at 100 mrad gives a ratio of 1.6 ± 0.3 in the relevant range of secondary momenta (see Fig.6), compatible with $I = 1/2$ but excluding $I = 3/2$.

This experimental fact of unequal population of the different isospin states could certainly not be understood on the basis of a statistical model. This model, on the contrary, predicts that all isospin and spin states are populated according to their respective statistical weights. The statistical model, however, may be adequate to describe particle production from the kinetic energy remaining in the collision rest system as the colliding nucleons go on in an excited state. It, in fact, predicts the observed constant mean kinetic c.m.s. energy[16] and gives also excellent agreement with experimental data on the c.m. spectrum, averaged over all angles[14]. This agreement shows that, though pions created by the decay of isobars carry high energy, their number, averaged over all angles, is small as compared to the pion multiplicity in pionization processes.

With this justification in mind, it will be instructive to compare the experimental data at 0°, transformed to the c.m.s., with the momentum spectrum predicted by the statistical model[16]. This comparison is shown for positive and negative pions in Fig.7; the spectrum given by the statistical model is supposed to give a good approximation to particle production in the collision rest system. Fair agreement is found for small momenta where mainly multipion production is contributing. The comparison at high momentum gives an indication of the strong contribution from isobar decays[4]. The

respective average momenta, $\langle \bar{p} \rangle$, are given in Table II, together with data from bubble chamber work[15] on events with charged pion multiplicities ≥ 4, averaged over all angles.

Table II

Average momenta in c.m.s. compared to the prediction of the statistical model[16] and to experimental results from bubble chamber work[15], averaged over all angles.

	This experiment 0°	Statistical[16] model	Bubble chamber[15] (averaged over all angl.)
$\langle \bar{p}_{\pi^+} \rangle$	1.00 Gev/c	0.540 Gev/c	0.550 Gev/c
$\langle \bar{p}_{\pi^-} \rangle$	0.70 Gev/c		

This comparison shows unambiguously the strong contributions from isobar decays to both positive and negative pions at 0°; note, however, the good agreement with the statistical model for high multiplicity events, averaged over all angles.

Excitation Curves

Varying the primary momentum, it was observed (see Figs. 8a and 8b) that the cross section in the laboratory system for production of pions at 0° with secondary momenta below 5 Gev/c tends to approach a constant value. This was in fact predicted by a multi-peripheral model[17]. The decoupling from the primary momentum is introduced in this model, by assuming that pion production in the collision rest system takes place by multi-pion interaction in the exchange process between the colliding nucleons. For secondaries of small momentum a unique laboratory spectrum is predicted which depends on the mass and on the transverse momentum of the secondaries, but not on the primary energy. It would be interesting to search for such a behaviour over a wider range of primary and secondary momenta.

Angular Distribution at High Secondary Momentum

The variation of pion production with laboratory angle and secondary momentum has already been investigated by several authors[18]. In the range of angles larger than 5^0, it was found that the probability for emission of a pion with secondary momentum p and transverse momentum $p_t = p.\sin\Theta$ can be expressed as a product of two probability distributions, $g(p)$ and $f(p_t)$. Using the general characteristics of particle production, as mentioned in section 1, Cocconi et al[3] obtained an excellent fit to all data on pion production[22] in the angular range $\Theta > 5^0$ with the empirical formula :

$$\frac{d^2\sigma}{d\Omega dp} = \frac{n_\pi}{2\pi} \frac{p^2}{p_0^2 < p >} \exp\left(-\frac{p}{< p >}\right) \exp\left(\frac{-2p_t}{< p_t >}\right).$$

Here n_π is the effective pion multiplicity, p_0, $< p >$ and $< p_t >$ are the primary momentum, the mean secondary momentum and the mean transverse momentum respectively. Typical values obtained for these parameters are $< p_t > = 350$ Mev/c, $< p > = 2$ Gev/c. The validity of this empirical rule in the small angle range can be tested by plotting the ratio of cross sections for pion production at 0 and 100 mrad against secondary momentum. The empirical rule predicts this ratio to be given by the expression

$$\exp\left(2p\Theta / < p_t >\right).$$

The experimental data are shown in Fig.9; the solid lines give the prediction of the empirical rule for different average transverse momenta. The plotted ratio is seen to follow an exponential with a slope of $< p_t > = 0.40$ Gev/c for positive pions and $< p_t > = 0.46$ for negative pions respectively in good agreement with data at larger angles[3]. However, a ratio equal to one, predicted by the empirical rule for zero secondary momentum, is observed to occur at a momentum of about 2 Gev/c; extrapolating to zero momentum gives

a ratio of 0.4 for positive pions and of 0.5 for negative pions. Since a good fit of the data for angles $\Theta > 5^{\circ}$ was obtained with this rule, as mentioned before, we conclude that for angles close to 0° the production of pions of both polarities is increasing less rapidly with decreasing transverse momentum. To investigate this apparent suppression of pion production at 0° further, a comparison with other data, at angles between 25 and 30 mrad has been done. The high-momentum tail of the π^{+} spectrum at 0° has been compared to data on π^{0} production in proton - proton collisions[14]. In doing this comparison, one should keep in mind that both positive and neutral pions of high secondary momentum, $p_{\pi} \geq 6$ Gev/c, are supposed to emerge from the decay of positively charged isobars of isospin 1/2. Consequently, the expected ratio $N(\pi^{+}) / N(\pi^{0}) = 2$ has been taken into account in Fig. 10. One notices that the production in the secondary momentum range considered is hardly changing between 0 and 30 mrad. Remembering the finite angular acceptance of $\pm$ 8 mrad in this experiment, an actual dip in the angular distribution at 0° cannot be excluded. A similar conclusion is reached for the high-momentum tail of negative pion production at 0°, as compared to unpublished data at 25 mrad[13].

Considering now the angular distribution of parent isobars, one could in principle, using some information on the different partial waves contributing to the decay of different isobars, deduce it by unfolding the observed angular distribution of decay pions. In practice this analysis would only be significant if the probabilities of exciting different isobars, decaying into different partial waves were known. We can, however, arrive at the more qualitative conclusion that the probability for exciting the incident nucleon is reduced when the angle is not changed during the collision. Some more quantitative statements will be given later, from an analysis of the proton momentum spectrum at 0°. This suppression of isobar excitation at small angles has in fact already been observed in experiments on near eleastic scattering of protons[6].

Isobars are known to have high spin values which are increasing with increasing mass. Classically, the change in orbital angular momentum without change in direction is related to the change in momentum in the c.m.s.

before and after the excitation. Quantum mechanically this means that the probability for changing the orbital angular momentum by one or more units is reduced if the direction is not changed in the collision.

This speculation gives actuality to several experimental studies:

1. Investigation on the pion momentum spectrum up to the maximum possible momentum would give confidence in the limitation of isobar masses contributing to pion production.

2. Experimental studies of the pion production in the small angle range, up to the maximum possible momentum, would be valuable to determine the reduction of the probability for exciting isobars of different masses.

3. The main contribution to pion production at 0° may be due to the hypothetical $P_{1/2}\ 1/2$ πN resonance[19] of mass 1480 Mev which can be excited without change in orbital angular momentum. Experimental observation of a sudden break in the high-momentum part of the π^+ spectrum would give the mass and an answer to the question of the existence of a $P_{1/2}\ 1/2$ πN resonance.

Angular Distribution at Low Momenta

The observation of more abundant production of pions of small secondary momentum at finite angles as compared to 0° (see Fig. 10) may direct this discussion to consider the dependence on the impact parameter of the amount of kinetic energy remaining available for particle production in the collision rest system when the colliding nucleons fly away in an excited state. The angular distribution of excited nucleons was found[6] to be characterized by an exponential decrease of the differential cross section with increasing (four-momentum transfer)^2 = t, exp $(-b|t|)$. At small angles, close to 0°, the collision is dominated by isobar excitation in two-body reactions. The kinetic energy remaining in the collision rest system is, in the statistical average, necessarily small and its contribution to pion production at 0° vanishes as compared to isobar decay. As the angle is

increased, the probability for the incident nucleons to separate from the collision rest system in an excited state decreases rapidly. Consequently, the kinetic energy remaining available for particle production in the c.m.s. will, in the statistical average, increase with decreasing impact parameter and its contribution to pion production will grow. This effect is apparently observed in the low momentum region of pion spectra at small angles as compared to 0°, most strikingly in Fig. 10, where production of π^+ at 0° and π^0 at small angles is compared.

Using the arguments given in the preceding paragraph, the relative numbers of pions at 0° produced in the collision rest system and by isobar decay, are estimated from Fig. 7, to 1/3 , their relative total energy content to 1/8, respectively.

2. Kaon Spectra

Production of positive kaons at small angles (Fig. 11) is characterized by a striking similarity with the spectra of positive pions. This is observed most directly in Fig. 12, showing the ratio K^+/π^+ as a function of secondary momentum for 0 and 100 mrad. One notices that this ratio is constant, close to 10% , independent of angle and primary momentum. Consequently, we consider that the conclusions reached for production of positive pions apply to the production of positive kaons as well; in particular, that there is a high probability of exciting the incident nucleon in a near elastic collision with decay by the emission of a single positive kaon.

Before entering into a discussion of the probability of isobar decay into kaon and hyperon, a few remarks about the data on negative kaon production will be given. This is characterized by a strong dependence on secondary momentum, both at 0 and 100 mrad (Fig. 14) and by the strong dependence on primary momentum. These characteristics of K^- production are seen to be in contrast with the observations for negative pions, as is evidenced by the ratio K^-/π^- , shown in Fig. 13, as a function of secondary momentum. The production of K^- seems to be dominated by phase space, whereas most negative pions of high momentum are produced in decays of isobars by emission of two pions.

This conclusion is supported further by a comparison of the momentum spectrum at 0°, transformed to the c.m.s., with the prediction of the statistical model; the shape of both spectra is observed to be very similar.

With this conclusion in mind, the possibility of exciting a strange isobar in a near elastic nucleon - nucleon collision may be investigated[8]. Strange isobars, such as the Y_0^* (1520 Mev) and Y_0^* (1815 Mev), for instance, are known to decay to the nucleon ground state by the emission of a single K^-, with a probability of 30% and 60% respectively[23]. The average fraction of energy transferred to a decay kaon would be 36% and 40% respectively. No peak in the K^- spectrum at secondary momenta around $0.4 \cdot p_0$ has been found at 0°. We therefore conclude that the excitation of strange isobars, requiring an exchange of strangeness between the colliding nucleons, is very improbable as compared to non - strange isobars.

This can also be demonstrated by the production ratio K^+/K^-. If a strange isobar were excited directly in a near elastic collision, with exchange of strangeness between the colliding nucleons, a K^+ would have to be produced simultaneously at the other nucleon. Strong excitation of strange isobars would thus tend to give a ratio $(K^+/K^-) \cong 1$, averaged over all momenta. Experimentally, however, this ratio is observed to be larger than one and to increase strongly with increasing secondary momentum, roughly as an exponential (see Fig. 12).

We are now prepared to discuss the probability of non-strange isobar decay into kaon and hyperon. The isobar $N^*_{1/2\ 5/2}$ of mass 1688 Mev is known[20,24] to decay to $K^+\Lambda_0$ (d wave) with a probability of about 3%. Assuming that all positive pions of high momentum are emitted in the decay of the two isobars $N^*_{1/2\ 3/2}$ (1512 Mev) and $N^*1/2, 5/2$ (1688 Mev), which are known to be excited with about equal probability[6], we would expect a ratio $K^+/\pi^+ \simeq 1.5\%$. It is, however, necessary to take into account the respective momenta of the pion and kaon in the isobar rest system and to correct the decay probability by the Jacobian, which for small angles is equal to

$$\left(\frac{p^*_{\pi}}{p^*_K}\right)^2 = 6 ,$$

to arrive at the ratio K^+/π^+ as observed in the laboratory system per fixed element of solid angle and per unit momentum interval. Using this correction, we in fact arrive with the given decay probability, at the observed ratio of 10%.

As a consequence of the smaller momentum of K^+ in the isobar rest system, the angular distribution in the laboratory will be more peaked forward. Thus, the suppression of production at 0°, due to the reduced probability of isobar excitation in the forward direction, should be more marked for kaons as compared to pions. This can be observed in Fig. 15, showing the ratio of K^+ production at 0 and 100 mrad, as a function of secondary momentum. The data are well fitted by an exponential

$$a \cdot \exp\left(2p^{\circ}/\langle p_t \rangle\right),$$

using a value of $\langle p_t \rangle = 0.37$ Gev/c for the average transverse momentum. Extrapolation to zero secondary momentum gives $a = 0.2$ demonstrating the suppression of K^+ production at 0°, as compared to 100 mrad, by a factor of 5. The production of π^+ at 0° was found to be suppressed by a factor 2.5. This consistent observation then helps to increase the confidence in our conclusion about abundant production of positive kaons and pions from the decay of isobars with isospin 1/2.

3. Proton Spectra

Unlike pions and kaons, protons observed at small angles are not "produced" in the proper sense of the word; they are identical to the incident protons and have lost a certain fraction of their primary energy which went into proper production phenomena.

This is strongly exhibited in the momentum spectrum at 0° (Fig.16), which is observed to increase as an exponential with increasing secondary momentum and to be peaked towards the maximum possible momentum, as already found previously in bubble chamber investigations[25]. It was the observation

of this behaviour which first stimulated the discussion of particular processes of particle production in which the nucleon retains a large fraction of its primary momentum. To come to more quantitative statements, let us consider a diagram in the c.m.s. where the longitudinal momentum, $\bar{p}_L$, of an event is plotted against the transverse momentum, p_t . Each event is represented by the end point of its total momentum vector. A projection of the density distribution in this diagram on the axis p_t and $\bar{p}_L$ gives the probability distribution of these variables. These distributions have been assumed to be independent of each other in a previous analysis[3] of experimental data[22] obtained at laboratory angles $\Theta \geq 5^0$. Using this assumption, good agreement for pion production and for proton fluxes was obtained.

In the forward direction the transverse momentum is zero and a transformation of the observed momentum spectrum to the c.m.s. gives directly the probability distribution in longitudinal momentum, $\bar{p}_L$. This distribution, expressed as the probability per steradian, Gev/c, and interaction is shown in Fig. 17. The high momentum part is well approximated by an exponential, peaked towards $\bar{p}_o$, the primary c.m. momentum. As the primary momentum is increased, the probability for fixed $\bar{p}_L$ decreases. This effect is obviously related to the fact that the total area under the distribution, the number of protons per steradian and interaction at 0^0 remains constant, i.e. the probability of near elastic charge exchange is independent of the primary momentum. This number of protons at 0^0 per steradian and interaction is also found to be independent of the target nucleus, to within 20%. These observations may be taken as the most convincing confirmation of our preceding conclusion, reached in the discussion of pion and kaon spectra, that only isobars with isospin 1/2 are excited with high probability in high-energy nucleon-nucleon collisions.

Protons emitted in the decay of isobars, produced at small angles at a primary momentum of 18.8 Gev/c, have a minimum momentum of 6.5 Gev/c, for an average isobar mass of 1.6 Gev. Their maximum momentum is close to the primary momentum. Unlike decay pions, these protons are collimated in a narrow angular cone of ± 40 mrad opening angle around the direction of the isobar;

consequently, isobars produced at an angle Θ will contribute by their decay protons to the momentum spectrum at 0°, with a momentum depending on the angle Θ. The resulting spectrum could then in fact be calculated, if more information on the angular distribution of isobars were available. In the light of our conclusion about the importance of isobar excitation and decay in the production of particles, the unique distribution of transverse momentum, according to a Boltzmann law observed for pions and kaons at all angles, including the very small angle range, appears to be the result of a strange accident, produced by the combined action of dynamics, in the production of isobars, and of kinematics, in their decay. In fact, in the case of protons this accident does not occur.

Figure 18 shows the plot of the ratio of protons observed at 0 and 100 mrad against secondary momentum. The slope of the momentum dependence is observed to increase with increasing momentum. For secondary momenta $p \geq 6.5$ Gev/c, the data may be fitted by a single exponential

$$a \cdot \exp\left(2p\Theta / \langle p_t \rangle\right),$$

using a value of $\langle p_t \rangle = 0.290$ Gev/c. Extrapolating to zero momentum, a ratio $a = 0.05$ is obtained. The apparent break in the slope of the data is observed to occur at the minimum momentum of protons emitted in isobar decay. The dashed curve in Fig. 18 indicates the prediction on the basis of a unique distribution in transverse momentum, $\exp\left(2p\Theta / \langle p_t \rangle\right)$, using $\langle p_t \rangle = 0.44$ Gev/c, a value which gave a satisfactory fit to the data at angles $\Theta \geq 5^\circ$ [3]. The striking disagreement with the experimental data invalidates the assumption of unique and independent distributions of transverse and longitudinal momentum. This is illustrated more quantitatively by comparing the mean energy loss per steradian and interaction at 0° in the c.m.s., $\langle \bar{E}_0 - \bar{E}_L \rangle$, as calculated from our data,

$$\langle \bar{E}_0 - \bar{E}_L \rangle_{exp} = 2.0 \text{ Gev sr}^{-1} \text{ (interaction)}^{-1} ,$$

to the corresponding value, calculated from a spectrum at 0° as predicted, on the basis of unique and independent distributions of p_t and $\bar{p}_L$, from data at larger angles, including our data at 100 mrad,

$$< \bar{E}_o - \bar{E}_L >_{pred.} = 4.3 \text{ Gev sr}^{-1} \text{ (interaction)}^{-1}.$$

The striking difference may be taken as an indication that the contribution at 0° to the total mean inelasticity is reduced by a factor 2. If this result is not to affect the established value of the mean inelasticity, we have to conclude that the probability for isobar excitation at small angles around 0° is indeed reduced by the limitation in change of orbital angular momentum. This conclusion is strongly supported by the observed shape of the proton momentum spectrum at 0°. The momentum of protons emerging from isobar decay is determined by the angle of emission. Only protons with a momentum around 6.5 Gev/c are contributed from isobars produced at zero degree, protons of higher momentum are emitted at an angle Θ by isobars produced at the same angle. Taking into account the Jacobian of the transformation from the isobar rest system to the laboratory system and the finite angular resolution in this experiment, one can deduce the angular distribution of isobar production from the observed momentum spectrum. If the angular distribution of isobar production were peaked at 0°, following an exponential in t = (four-momentum transfer)^2 with the slope observed at larger angles[6], the resulting momentum spectrum at 0° would drop by a factor of 8 from 7 to 12 Gev/c. We have therefore to conclude that the observed increase in the proton spectrum at 0° with increasing momentum reflects a rise in isobar production with increasing angle around 0°.

4. Antiproton Spectra

So far the production of antiparticles in high-energy collisions has been described by statistical theories. In comparing these calculations with experiments one meets in general the difficulty that the calculations refer to an elementary process whereas the targets in experiments are complex nuclei. For some time it was thought[26] that the discrepancies between theory[16] and experiment, in particular regarding the production of antiprotons, may partly be due to reabsorption in the same nucleus where the particle was produced. Since then, reabsorption effects in complex nuclei have been calculated on the basis of a model[27] and were found to be an order of magnitude too small to account for the observed discrepancies. This result is confirmed here by a comparison of antiproton production from hydrogen and from nuclei, as shown in Fig. 19; for the comparison the experimental data are given as probabilities per interaction[28]. One notices that the probabilities per interaction obtained with different targets are indeed very close to each other.

The shape of the spectra reflects the importance of phase space effects : strong dependence on secondary momentum and pronounced excitation with increasing primary momentum. As an example, the yield of 10 Gev/c antiprotons was found to increase by a factor of 10 as the primary momentum was raised from 18.8 to 23.1 Gev/c. One should notice the similarity to K^- production; the ratio $\bar{p}/K^-$ is constant, equal to about 0.12, independent of the emission angle, primary and secondary momentum in the range covered in this experiment.

The ratio of antiprotons to negative pions, as shown in Fig. 20, decreases from 10^{-2}, at 4 Gev/c, to 10^{-3} at 12 Gev/c, and increases as either the primary momentum or the angle is increased. At 4 Gev/c the statistical model[16] predicts a ratio of 0.2 . This prediction is valid for central collisions, in which all the c.m. energy is available for production of particles. From the preceding discussion of pion production we inferred that the colliding nucleons rather separate off before an equilibrium state, containing all available energy, is reached and fly away in an excited state,

the remaining kinetic energy available for particle production being in the statistical average a function of the impact parameter. The fraction of central collisions may in fact be very small, of the order of[29]

$$\frac{\sigma_{\text{central}}(pp)}{\sigma_{\text{inel.}}(pp)} = \frac{\pi(\hbar / M_p \cdot c)^2}{32 \text{ mb}} \simeq 1/30 .$$

Antiprotons are only produced when the remaining kinetic energy, left by the colliding nucleons is high. Pions are produced in the decay of excited nucleons as well. Using the estimated fraction of central collisions, the prediction of the statistical model may be reconciled with the experimental data.

One is surprised to observe that particles such as antiprotons which are produced only in central collisions, show the same characteristic Boltzmann distribution of transverse momentum as particles emitted in the decay of excited nucleons. The ratio of antiproton fluxes measured at 0 and 100 mrad, as plotted against secondary momentum in Fig. 21, is indeed well fitted by an exponential corresponding to an average transverse momentum $< p_t > = 0.55$ Gev/c.

Central collisions seem to be distinguished from peripheral collisions only by the occurrence of higher transverse momenta[30].

IV. CONCLUSIONS

Several experimental studies[6] provided information about the dynamics of isobars excitation in high-energy near elastic proton scattering. Here we investigated the rôle of isobars in the production of secondary particles. It was found that at small angles around 0° the production of positive pions is predominantly due to the decay of isobars. Negative pions were not found to be emitted in the decay by emission of a single pion. This result was shown to imply that the incident nucleon conserves the same charge in the excited state. It is equivalent to say that the exchange process responsible for isobar excitation at high energy does not change the isospin.

This result seems to be of general validity in high-energy interactions[7]. Independently, the same result was derived from the observation that the number of protons per steradian at 0° does not depend on the charge of the target nucleon. We can also rule out the occurrence of simultaneous excitation of the incident and of the target nucleon to states of isospin 3/2; this possibility could not be excluded in previous experiments[6].

The high probability for isobar excitation leads us then to conclude that the colliding nucleons rather separate off before an equilibrium state containing all available energy is reached and go on in an excited state. The kinetic energy remaining in the collision rest system is in the statistical average a function of the impact parameter. Experimentally we found that the production of pions in the collision rest system increased with increasing angle.

Also positive kaons at small angles were observed to emerge predominantly from isobars decaying into $K^{+}\Lambda_{0}$. The known branching ratio[20,24] for isobar decay into positive pion and kaon gives quantitative agreement with the observed ratio K^{+}/π^{+} at small angles; this ratio is predicted to be constant at all primary energies where the parent isobar is strongly excited. Direct excitation of strange isobars[8] can be ruled out on the basis of the observed spectrum of negative kaons.

Previous experiments[18] on the angular distribution of secondaries produced in nucleon - nucleon collisions have demonstrated as a common feature a unique distribution of transverse momentum around an average value, according to a Boltzmann law. The average transverse momentum was found to be independent of the longitudinal momentum at larger angles[3]. Here we could show that in particle production at small angles which is dominated by isobar decay this appears to be the result of a strange accident, produced by the combined action of dynamics, in the production of isobars, and of kinematics, in their decay. In fact an exception from the rule was found for protons. However, this exception was demonstrated to be produced by the particular dynamics of isobar excitation at 0°; the probability to excite the incident nucleon at 0° was found to be reduced. We have tentatively interpreted this phenomenon by a limitation in the orbital angular momentum change imposed at 0°.

Isobars are known to have high spin values. Their excitation therefore requires a change in orbital angular momentum. At 0° the probability to change the orbital angular momentum by one or more units is reduced.

An indication that the excitation of colliding nucleons remains important and of roughly constant probability up to cosmic ray energies may be found in the experimental fact that high-energy collisions are characterized by small mean inelasticities. To account for this observation one has to invoke a process in which the nucleon retains a large fraction of its primary energy. Guided by the experimental evidence at accelerator energies presented here and on the basis of cosmic ray data[8] at 3000 Gev, we tentatively identify this process at all energies with the excitation of colliding nucleons. The observed small inelasticity then limits the mass of strongly contributing isobars to less than $2\ M_p$[8]. This is certainly a very strange observation. It would be much more natural to assume that there is a continuous transition from isobars of increasing mass to central collisions. If the spin of isobars would continue to increase with the mass, the reduced probability for changing the orbital angular momentum by the amount required to excite a high mass isobar at small angles could be effective to limit the mass of strongly contributing isobars. The limitation of isobar mass inferred from the small inelasticity is of course the basis of the model for particle production which was discussed here.

ACKNOWLEDGEMENTS

This investigation was originally started to provide information on pion and kaon production for an improved calculation of the neutrino spectrum in the CERN neutrino experiment. We wish to thank Professors Van Hove, Preiswerk and Puppi for their interest in extending the aim of this study to a more general investigation of particle production at small angles.

The CERN proton synchrotron division has contributed a great effort to this experiment; we wish to acknowledge gratefully their whole-hearted collaboration. We also thank Messrs. L. Velati and B. Friend for their assistance in setting up and running the experiment, and Mr. R. Tannenbaum for his help during the data taking.

Table I

POSITIVE PION PRODUCTION $d^2\sigma/d\Omega dp$ mb $sr^{-1}(GeV/c)^{-1}$ per nucleus

Production Parameters			Momentum of Secondaries GeV/c							
Target	Angle mrad	Primary momentum GeV/c	1	2	3	4	6	8	10	12
H_2	0	18.8	28.2±3.5	35.5±3.5	52.0±5.0	60.0±5.0	83.0±6.0	56.0±7.0	24.5±1.7	11.9±.8
H_2	0	23.1				60.0±4.5	86.2±6.5	80.4±5.5	46.4±3.0	30.6±2.0
H_2	100	18.8		38.8±4.0	26.2±2.4	19.6±1.4	7.71±.49	2.02±.13	.54±.03	.083±.005
Be	0	18.8	240±29	300±30	370±37	376±30	448±35	305±40	138±10	61±4
Be	0	23.1				341±28	428±32	380±28	233±16	154±11
Be	100	18.8		297±35	207±18	135±10	49±3	13.0±.8	3.1±.2	.42±.03
Be	100	23.1				168±12	70±5	24.5±1.6	7.1±.45	1.39±.09
Pb	0	18.8	4070±500	3900±400	4200±420	3380±260	3460±230	2100±135	990±65	390±26
Pb	0	23.1				3660±280	3860±270	2940±195	1790±120	1170±80
Pb	100	23.1				1810±130	712±46	247±16	79±5	15.9±1

Errors quoted are due to systematic uncertainties.

PS/4303

Table 2 NEGATIVE PION PRODUCTION $d^2\sigma/d\Omega dp$ mb sr^{-1} $(GeV/c)^{-1}$ per nucleus

Production parameters			Momentum of secondaries GeV/c							
Target	Angle mrad	Primary momentum GeV/c	1	2	3	4	6	8	10	12
H_2	0	18.8	26.2±3.2	30.0 ± 3.0	34.0 ± 3.4	28.0 ± 4.0	21.6 ±1.7	13.3±.9	7.8 ± .5	2.45 ± .15
H_2	0	23.1				39.0 ± 4.0	34.1 ± 2.5	23.6±1.5	16.2 ±1.2	9.9 ± .7
H_2	100	18.8		22.5 ± 2.5	17.9 ± 1.6	10.6 ± 1.0	3.75 ± .27	1.06± .07	.21 ± .014	.023 ± .0014
Be	0	18.8	229 ±26	273 ± 27	265 ± 27	215 ± 30	152 ±13	92 ±7	50.0 ±3.5	15.4 ±1.2
Be	0	23.1				267 ± 27	211 ±16	157 ±12	94.4 ±6.5	54.9 ±4.5
Be	100	18.8		296 ± 32	144 ± 13	82.8 ±7.7	29.1± 2.1	7.76 ± .53	1.56 ± .1	.187 ± .012
Be	100	23.1				125 ± 11	46.1± 3.3	14.2 ± 1.0	3.73 ± .25	.72 ± .05
Pb	0	18.8	4000±500	3420 ±340	2970 ±300	2080±290	1290 ±100	680 ±50	340 ± 24	107 ± 7
Pb	0	23.1				2790±260	1940±150	1200±85	714 ± 52	400 ± 30
Pb	100	23.1				1360±125	470 ± 34	146 ±10	38.0 ± 2.5	7.7 ± .5

Errors quoted are due to systematic uncertainties.

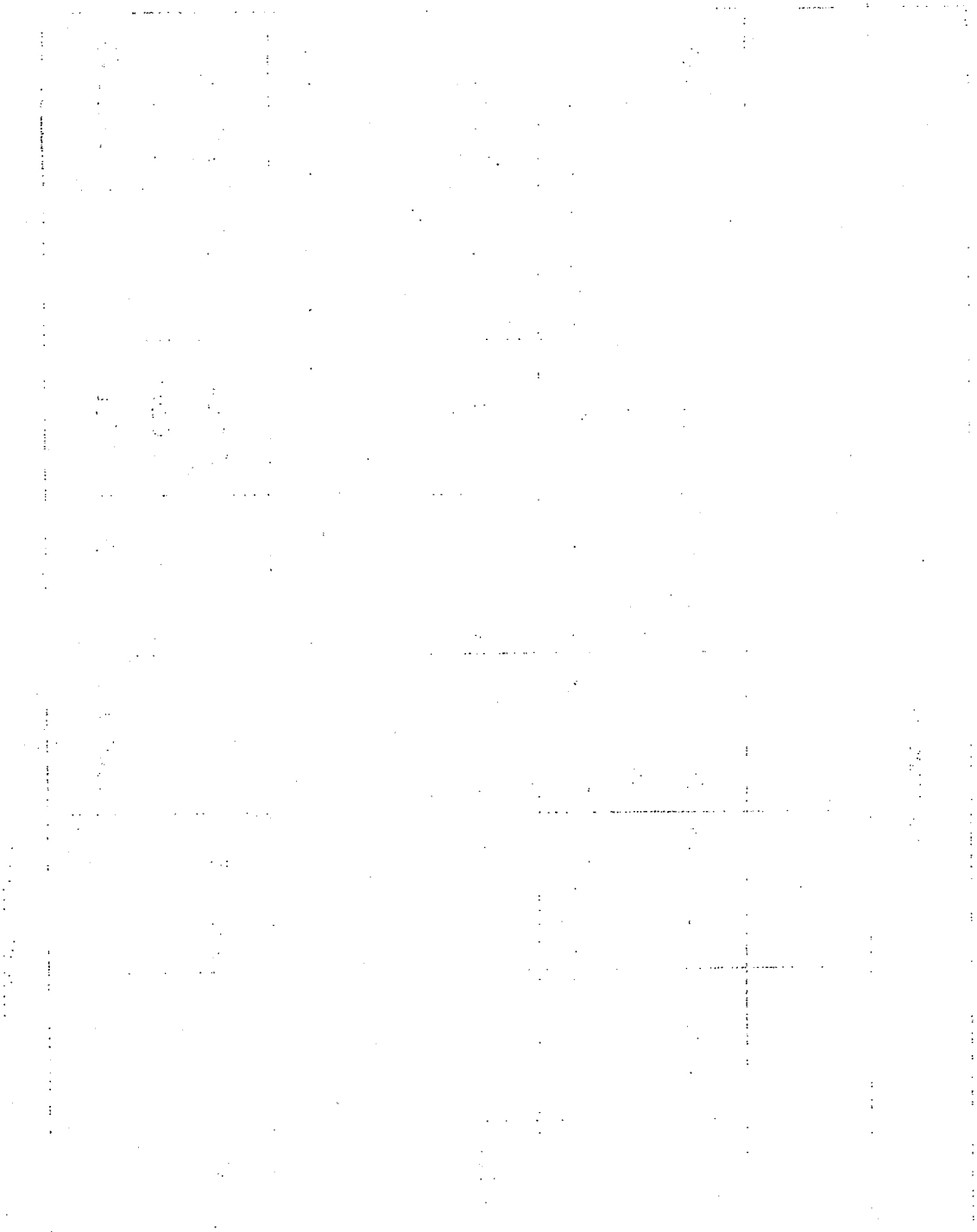

Table 3 POSITIVE KAON PRODUCTION $d^2\sigma/d\Omega dp$ mb sr^{-1} $(GeV/c)^{-1}$ per nucleus

Production Parameters			Momentum of secondaries GeV/c				
Target	Angle mrad	Primary momentum GeV/c	4	6	8	10	12
H_2	0	18.8	3.18 ± .60	4.26 ± .70	3.09 ± .40	2.62 ± .70	.98 ± .11
H_2	0	23.1	5.00 ± .85	5.55 ± .72	4.27 ± .48	4.00 ± .56	2.21 ± .63
H_2	100	18.8	1.7 ± .2	.80 ± .11	.21 ± .02	.056 ± .007	.008 ± .004
Be	0	18.8	30.2 ± 3.4	29.5 ± 4.8	18.5 ± 3.0	14.8 ± 6.0	7.6 ± 1.2
Be	0	23.1	32.9 ± 3.0	38.9 ± 5.3	25.8 ± 2.8	24.1 ± 3.2	11.3 ± 3.8
Be	100	18.8	16.3 ± 1.4	6.8 ± .5	1.9 ± .14	.55 ± .05	.046 ± .01
Be	100	23.1	21.0 ± 1.8	10.6 ± .7	3.9 ± .3	1.04 ± .09	.21 ± .03
Pb	0	18.8	421 ± 67	281 ± 76	235 ± 63		62 ± 13
Pb	0	23.1	469 ± 75	520 ± 88	260 ± 52	234 ± 54	
Pb	100	23.1	295 ± 24	148 ± 13	57.0 ± 5.0	18.0 ± 1.6	3.50 ± .37

Errors quoted include both statistical and systematic uncertainties.

Table 4 NEGATIVE KAON PRODUCTION $d^2\sigma/d\Omega dp$ mb sr^{-1} $(GeV/c)^{-1}$ per nucleus

Production Parameters			Momentum of secondaries GeV/c				
Target	Angle mrad	Primary momentum GeV/c	4	6	8	10	12
H_2	0	18.8	1.18 ± .46	.83 ± .16	.34 ± .03	.09 ± .02	.055 ± .010
H_2	0	23.1	3.03 ± .61	1.92 ± .29	.93 ± .09	.56 ± .05	.20 ± .02
H_2	100	18.8	1.16 ± .14	.31 ± .03	.037 ± .005		
Be	0	18.8	13.1 ± 1.4	6.75 ± .71	3.13 ± .25	.902 ± .062	.168 ± .027
Be	0	23.1	20.5 ± 2.7	11.8 ±1.1	5.98 ± .47	3.37 ± .24	1.16 ± .09
Be	100	18.8	7.3 ± .8	2.30 ± .20	.25 ± .02	.031 ± .005	
Be	100	23.1	13.3 ± 1.2	3.90 ± .30	.63 ± .06	.14 ± .015	.017 ± .004
Pb	0	18.8	169 ± 35	73 ± 12	30.0 ± 4.4	6.46 ± 1.30	2.50 ± .65
Pb	0	23.1	304 ± 52	177 ± 20	68.0 ± 5.0	27.7 ± 2.8	7.62 ±1.10
Pb	100	23.1	153 ± 16	44.0 ± 4.4	7.80 ± .90	1.36 ± .21	.31 ± .10

Errors quoted include both statistical and systematic uncertainties.

Table 5 PROTON SPECTRA $d^2\sigma/d\Omega dp$ mb sr^{-1} $(GeV/c)^{-1}$ per nucleus

Production Parameters			Momentum of secondaries GeV/c							
Target	Angle mrad	Primary momentum GeV/c	1	2	3	4	6	8	10	12
H_2	0	18.8	5.0 ±.6		14.0±1.3	24.2±2.0	48.4±3.4	95.1±6.6	170 ± 12	267 ±18
H_2	0	23.1				25.8±2.2	39.4±2.9	70.0±4.9	102 ± 7	151 ±10
H_2	100	18.8			9.1 ±.8	10.6 ±.9	11.4 ±.8	7.73±.53	4.19 ±.28	1.44 ±.1
Be	0	18.8	57.0±6.5		136 ± 11	208 ±19	362 ± 26	614 ± 43	903 ± 61	1340 ±91
Be	0	23.1				164 ±14	251 ± 18	444 ± 31	652 ± 44	959 ±80
Be	100	18.8			94.5 ±8.5	103 ± 9	99.4 ± 7.3	59.7±4.2	30.3±2.1	10.1±.69
Be	100	23.1				94.4±7.9	90.6 ± 6.6	61.0±4.3	31.8±2.2	12.9±.9
Pb	0	18.8	1910 ±230		2117±200	2870±240	3550±250	5100±350	6440±430	8700±580
Pb	0	23.1				2510±210	2870±210	4090±280	5210±350	7150 ±480
Pb	100	23.1				1460±120	1100 ±80	720 ±50	400 ±27	160 ± 11

Errors quoted are due to systematic uncertainties.

Table 6 ANTIPROTON PRODUCTION $d^2\sigma/d\Omega dp$ mb sr^{-1} $(GeV/c)^{-1}$ per nucleus

Production Parameters			Momentum of secondaries GeV/c				
Target	Angle mrad	Primary momentum GeV/c	4	6	8	10	12
H_2	0	18.8	.154 ± .046	.077 ± .022			
H_2	0	23.1	.281 ± .055	.291 ± .042	.137 ± .018	.063 ± .012	.025 ± .006
H_2	100	18.8	.063 ± .020	.032 ± .008	.0054 ± .0015		
Be	0	18.8	1.04 ± .17	.62 ± .10	.19 ± .04	.048 ± .019	
Be	0	23.1	2.08 ± .33	1.41 ± .19	.76 ± .08	.306 ± .035	.073 ± .015
Be	100	18.8	.531 ± .100	.191 ± .027	.029 ± .004	.0032 ± .001	
Be	100	23.1	1.22 ± .20	.460 ± .064	.122 ± .017	.017 ± .005	
Pb	0	18.8	12.2 ± 3.3	4.80 ± 1.40	2.00 ± .60		
Pb	0	23.1	28.7 ± 4.9	14.1 ± 2.7	7.20 ± 1.00	2.40 ± .75	1.00 ± .50
Pb	100	23.1	14.0 ± 2.3	3.80 ± .70	.61 ± .24		

Errors quoted include both statistical and systematic uncertainties.

DATA FROM P- Be AT 8.65 AND 11.8 GeV/c PRIMARY MOMENTUM

Table 1' POSITIVE PION PRODUCTION $d^2\sigma/d\Omega dp$ mb sr^{-1} $(GeV/c)^{-1}$ per nucleus

Production Parameters			Momentum of Secondaries GeV/c			
Target	Angle mrad	Primary momentum GeV/c	4	5	6	7
Be	0	8.65	58 ± 12			
Be	0	11.8	318 ± 64	142 ± 28	90 ± 18	42 ± 8

Table 2' NEGATIVE PION PRODUCTION $d^2\sigma/d\Omega dp$ mb sr^{-1} $(GeV/c)^{-1}$ per nucleus

Production Parameters			Momentum of Secondaries GeV/c			
Target	Angle mrad	Primary momentum GeV/c	4	5	6	7
Be	0	8.65	35 ± 7			
Be	0	11.8	124 ± 25	91 ± 18	43 ± 9	20 ± 4

Table 5' PROTON SPECTRA $d^2\sigma/d\Omega dp$ mb sr^{-1} $(GeV/c)^{-1}$ per nucleus

Production Parameters			Momentum of Secondaries GeV/c			
Target	Angle mrad	Primary momentum GeV/c	4	5	6	7
Be	0	8.65	244 ± 65			
Be	0	11.8	263 ± 50	390 ± 70	575 ± 110	885 ± 180

REFERENCES

1 G. Bernardini et al, Proc. of Int. Conf. on Elementary Particles, Siena 1963 (to be published).

2 See e.g. for a review up to 1958: D.H. Perkins, in Progress in Cosmic Ray and Elementary Particle Physics, Vol. 5 (North-Holland Publishing Co., Amsterdam 1960).

3 G. Cocconi, L.J. Koester and D.H. Perkins, High Energy Physics Seminar, No. 28 (2), UCLD 1444 (1961), UCRL SS-28-2 (unpublished).

4 A.C. Melissinos, G.G. Fazio, T. Yamanouchi, S.J. Lindenbaum and L.C.L. Yuan, Phys.Rev.Letters 7, 454 (1961).

5 G.B. Chadwick, G.B. Collins, P.J. Duke, T. Fujii, N.C. Hien, M.A.R. Kemp, F. Turkot, Phys.Rev. 128, 1823 (1962).

6 A.N. Diddens, E. Lillethun, G. Manning, A.E. Taylor, T.G. Walker, A.M. Wetherell, Proc. of 1962 Int. Conf. On High-Energy Physics at CERN, p. 576;
G. Cocconi, A.N. Diddens, E. Lillethun, G. Manning, A.E. Taylor, T.G. Walker, A.M. Wetherell, Phys.Rev.Letters 87, 450 (1961);
G. Cocconi, E. Lillethun, J.P. Scanlon, C.A. Ståhlbrandt, C.C. Ting, J. Walters, A.M. Wetherell, Physics Letters 8, 134 (1964).

7 D. Amati, L.L. Foldy, A. Stanghellini and L. van Hove, Nuovo Cim. (to be published).

8 B. Peters, Proc. of 1962 Int. Conf. on High-Energy Physics at CERN, p. 623.

9 A.J. Metheringham and T.R. Willitts, Nucl.Instr.Methods 15, 297 (1962).

10 M. Vivargent, G. von Dardel, R. Mermod, G. Weber and K. Winter, Nucl.Instr. Methods 22, 165 (1963).

11 R. Mermod, K. Winter, G. Weber and G. von Dardel, Proc. Int.Conf. on Instrumentation for High-Energy Physics, Berkeley 1960, p. 172.

12 R.W. Williams, preprint (University of Washington), Seattle.

13 A.N. Diddens et al, private communication.

14 M. Fidecaro, G. Finocchiaro, G. Gatti, G. Giacomelli, W.C. Middelkoop and T. Yamagata, Nuovo Cim. 24, 73 (1962).

PS/4303/kl

15 S.J. Goldsack et al, Nuovo Cim, 23, 941 (1962).

16 R. Hagedorn, Nuovo Cim. 15, 434 (1960).

17 D. Amati, S. Fubini, A. Stanghellini and M. Tonin, Nuovo Cim. 22, 569 (1961).

18 See for complete list of references: D.R.O. Morrison, Review Lecture for Ultra High-Energy Nuclear Physics Conf, of the Institute of Physics and the Physical Society, Bristol 1963.

19 G. Cocconi, E. Lillethun, J.P. Scanlon, C.A. Ståhlbrandt, C.C. Ring, J. Walkers, A.M. Wetherell, Physics Letters 8, 134 (1964); P. Bareye, C. Bricman, G. Valladas, G. Villet, J. Bizard, J. Seguinot, L.D. Roper, Phys.Rev.Letters 12, 340 (1964).

20 P. Falk-Vairant and G. Valladas, Rev.Mod.Phys. 33, 362 (1961).

21 The ratio π^+ / π^- expected from the decay of the 1688 MeV isobar is estimated to 3.2 from data given in Ref. 20.

22 W.F. Baker et al., Phys.Rev.Letters 7, 101 (1961).

23 A.H. Rosenfeld, UCRL 8030 Rev. April 1963 (unpublished).

24 J.A. Anderson et al., Proc. of the 1962 Int. Conf. on High-Energy Physics at CERN, p. 271.

25 D.R.O. Morrison, Aix-en-Provence Conf. on High-Energy Physics 1961, Vol.1, p407.

26 G. Cocconi, Proc. of 1960 Int.Conf.on High-Energy Physics at Rochester, p.801.

27 J. Von Behr and R. Hagedorn, Nuovo Cim. 23, 339 (1962).

28 The following values for the inelastic cross sections were used: $\sigma_{in}(p\,p) = 31$ mb, $\sigma_{in}(p\,Be) = 180$ mb, $\sigma_{in}(p\,Pb) = 1692$ mb.

29 G. Cocconi, Nuovo Cim. (to be published).

30 This point will be discussed in connection with experimental data on deuteron production in proton-proton collisions in a later publication.

/4303/kl

FIGURE CAPTIONS

Fig.1 : Experimental layout of the spectrometer and the counter telescope. M_{1-3} monitor, $Q_8 - Q_{10}$ quadrupole lenses, B_4 bending magnet, G guard counters, $S_1 - S_6$ scintillators, $C_1 - C_3$ threshold Čerenkov counters, C_d differential Čerenkov counter, Fe 1 m iron absorber.

Fig.2 : Momentum spectra of positive pions at 0 and 100 mrad, for primary momenta of 18.8 and 23.1 Gev/c, as observed in a) p - p collisions, b) p - Be collisions and c) p - Pb collisions.

Fig.3 : Momentum spectra of negative pions at 0 and 100 mrad, for primary momenta of 18.8 and 23.1 Gev/c, as observed in a) p - p collisions, b) p - Be collisions and c) p - Pb collisions.

Fig.4 : Comparison of momentum spectra of positive and negative pions observed at 0° in p - p collisions with primary momenta of 18.8 and 23.1 Gev/c.

Fig.5 : Ratio π^+/π^- as a function of secondary momentum at 0 and 100 mrad observed in p - Be collisions at 23.1 Gev/c.

Fig.6 : Ratios π^+/π^- and π^+/π^0 versus secondary momentum as observed at different primary momenta in p - p collisions. Data for $p_0 = 3.8$ Gev/c are taken from Melissinos et al[4].

Fig.7 : Momentum spectra of positive and negative pions at 0° for p - p collisions at 18.8 and 23.1 Gev/c transformed to the centre-of-mass system versus longitudinal c.m. momentum $\bar{p}_L$. The dashed curve gives the prediction of the statistical model[16].

Fig.8 : a) Production of positive pions at 0° in p - Be collisions at fixed secondary momentum for primary momenta of 8.65, 11.8, 18.8 and 23.1 Gev/c.

b) Production of negative pions at 0° in p - Be collisions for different primary momenta.

Fig.9 : Angular distribution of positive and negative pions in p - Be collisions at 18.8 Gev/c. Plotted is the ratio of cross sections at 0 and 100 mrad versus secondary momentum.

Fig.10 : Comparison of momentum spectra of positive and neutral pions in p - p collisions at small angles. Data on π^0 production are from M. Fidecaro et al[14]. The cross sections for π^+ production are shown also taking into account a ratio $\pi^+/\pi^0 = 2$, expected from the decay of a positive isobar of isospin 1/2.

Fig.11 : Momentum spectra of positive kaons at 0 and 100 mrad, for primary momenta of 18.8 and 23.1 Gev/c, as observed in a) p - p collisions, b) p - Be collisions and c) in p - Pb collisions.

Fig.12 : Observed ratio K^+/π^+ at 0 and 100 mrad and K^+/K^- at 0 mrad in p - p collisions at 23.1 Gev/c.

Fig.13 : Ratio K^-/π^- observed at 0 and 100 mrad in p - Be collisions at 23.1 Gev/c.

Fig.14 : Momentum spectra of negative kaons at 0 and 100 mrad, for primary momenta of 18.8 and 23.1 Gev/c, as observed in a) p - p collisions, b) p - Be collisions and c) p - Pb collisions.

Fig.15 : Angular distribution of positive kaons produced in p - p collisions at 18.8 Gev/c. Plotted is the ratio of cross sections at 0 and 100 mrad versus secondary momentum. The solid curve is a fit with $a \cdot \exp(2p\Theta/\langle p_t \rangle)$ using $a = 0.2$, $\langle p_t \rangle = 0.37$ Gev/c.

Fig.16 : Momentum spectra of protons at 0 and 100 mrad, for primary momenta of 18.8 and 23.1 Gev/c, as observed in a) p - p collisions, b) p - Be collisions and c) p - Pb collisions.

Fig.17 : Probability distribution in longitudinal c.m. momentum, $\bar{p}_L$, per steradian, of protons observed at 0° in p - p collisions at 18.8 and 23.1 Gev/c. Also shown is the distribution predicted by the statistical model[16] for central collisions.

Fig.18 : Angular distribution of protons observed in p - p collisions at 18.8 Gev/c. Plotted is the ratio of differential cross sections at 0 and 100 mrad versus secondary momentum. The dashed curve gives the prediction for a unique distribution in transverse momentum, using $\langle p_t \rangle = 0.44$ Gev/c, the solid curve is a fit to the high momentum data with $a \cdot \exp(2p\Theta/\langle p_t \rangle)$, using $a = 0.05$ and $\langle p_t \rangle = 0.290$ Gev/c.

3/kl

Fig.19 : Probability of antiproton production per interaction versus secondary momentum as observed in p - p, p - Be and p - Pb collisions at 18.8 and 23.1 Gev/c. For clarity, errors are not shown, they are given in table 6.

Fig.20 : Ratio of $\bar{p}/\pi^-$ versus secondary momentum as observed at 0° in p - p collisions at 23.1 Gev/c and at 0 and 100 mrad in p - Be collisions at 23.1 Gev/c.

Fig. 21 Angular distribution of antiprotons produced in p - Be collisions at 18.8 Gev/c. Plotted is the ratio of differential cross sections at 0 and 100 mrad versus secondary momentum. The solid line is a fit to the data with $a \cdot \exp(2p\Theta/\langle p_t \rangle)$, using $\langle p_t \rangle = 0.55$ Gev/c.

PS/4303/kl

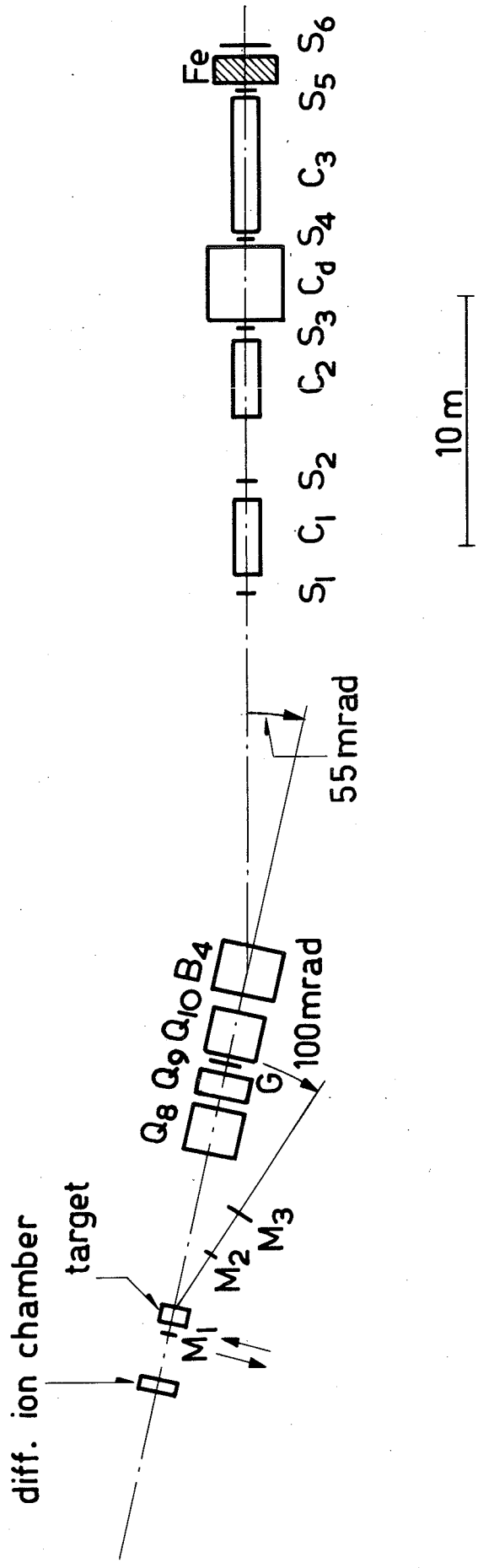

FIG. 1 SPECTROMETER AND COUNTER TELESCOPE

DIA - 18970

SIS/R/7365

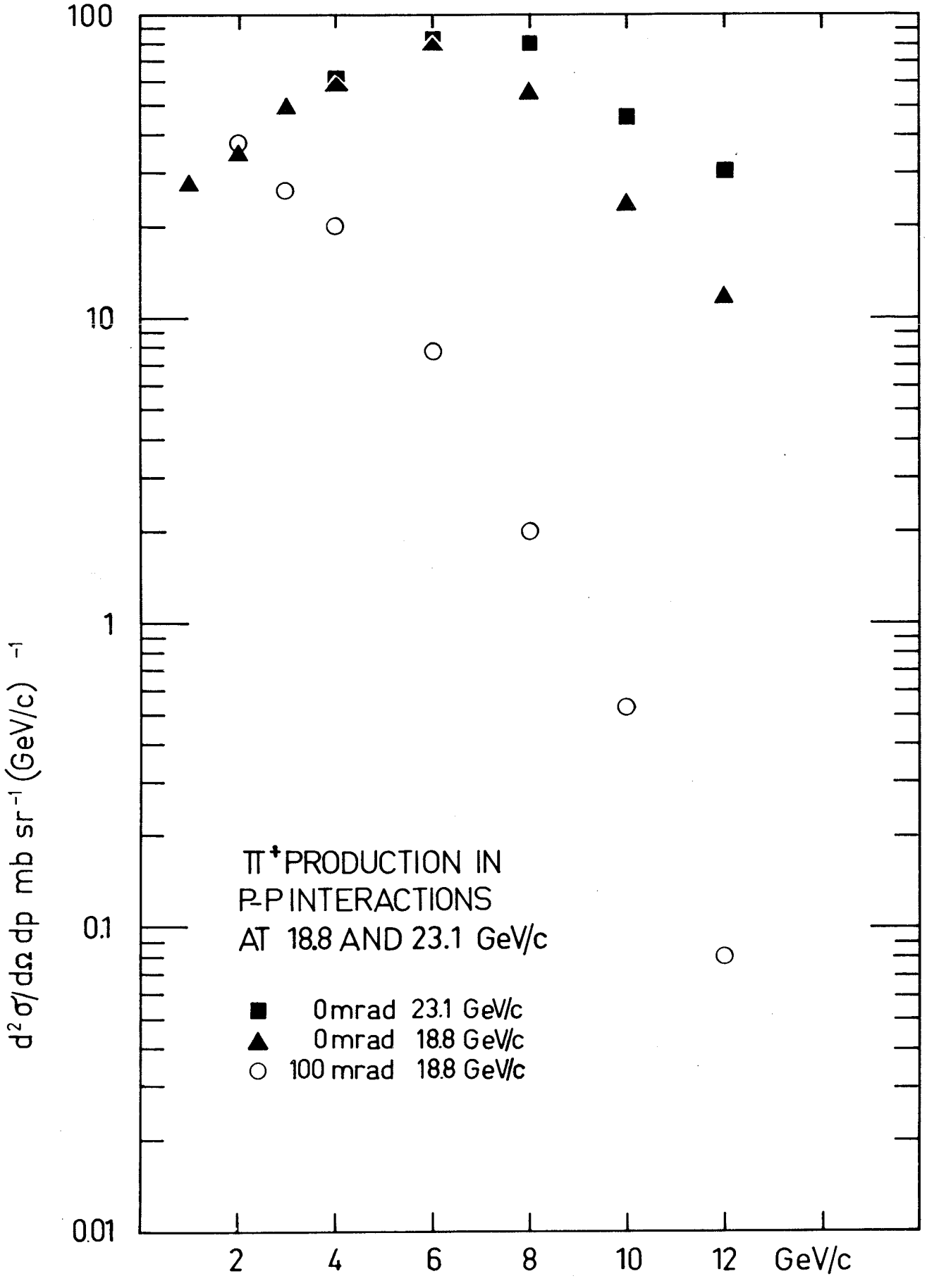
100
10
1
0.1
0.01
2
4
6
8
10
12
GeV/c
$d^2\sigma/d\Omega\,dp$ mb sr^{-1} (GeV/c) $^{-1}$
π^+ PRODUCTION IN
P-P INTERACTIONS
AT 18.8 AND 23.1 GeV/c
0 mrad 23.1 GeV/c
0 mrad 18.8 GeV/c
100 mrad 18.8 GeV/c

FIG. 2a

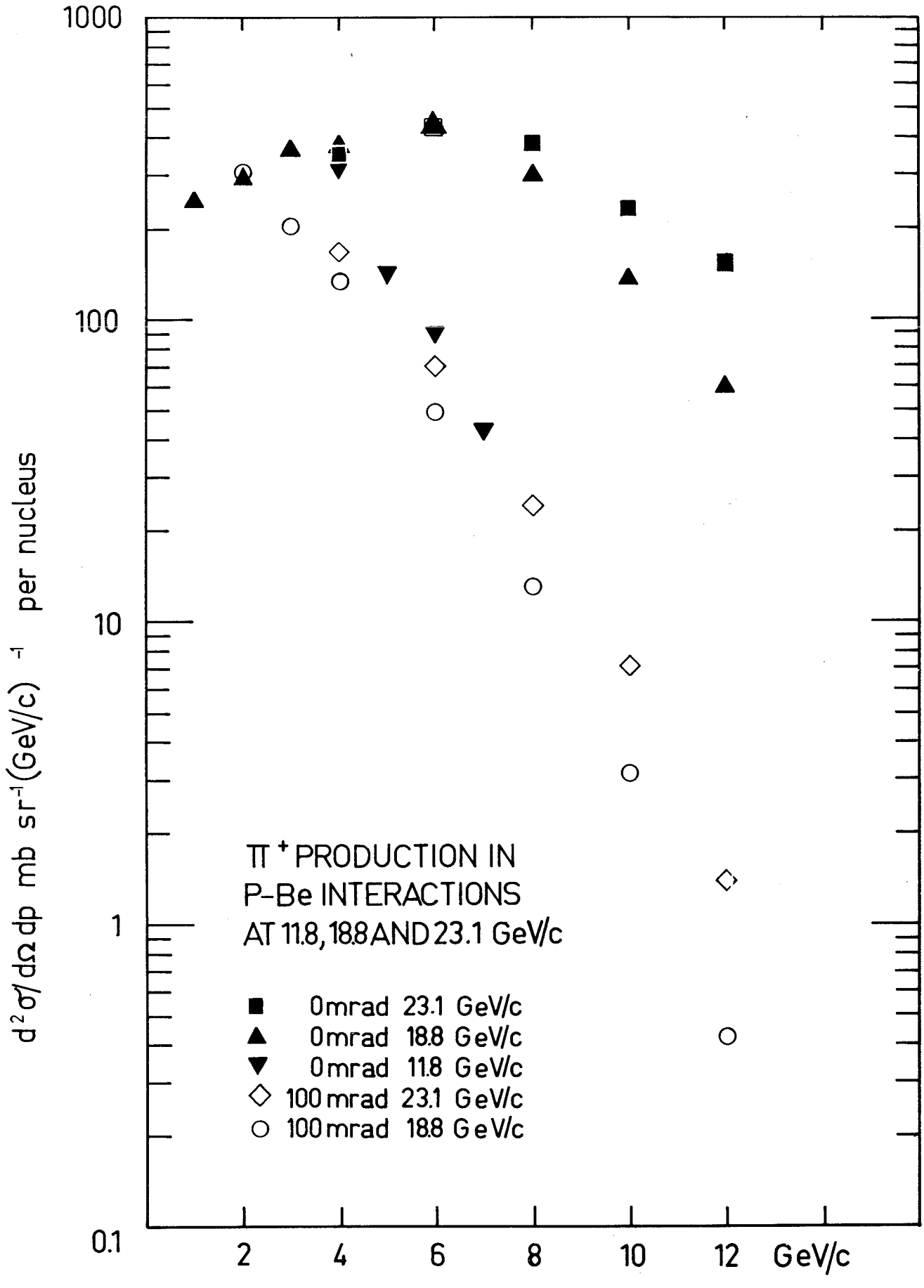

FIG. 2b

DIA - 19856

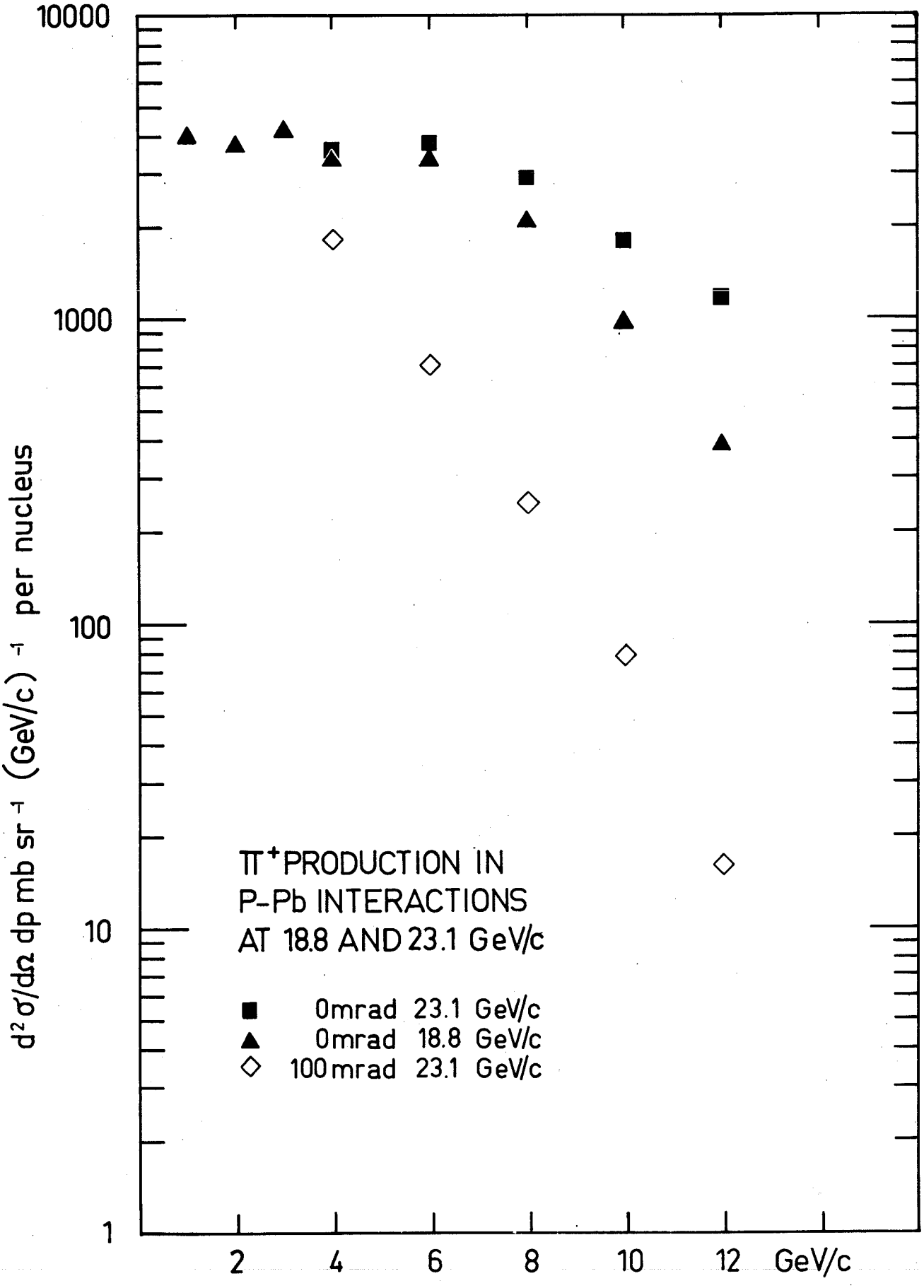

FIG. 2c

DIA - 19868

SIS/R/8566

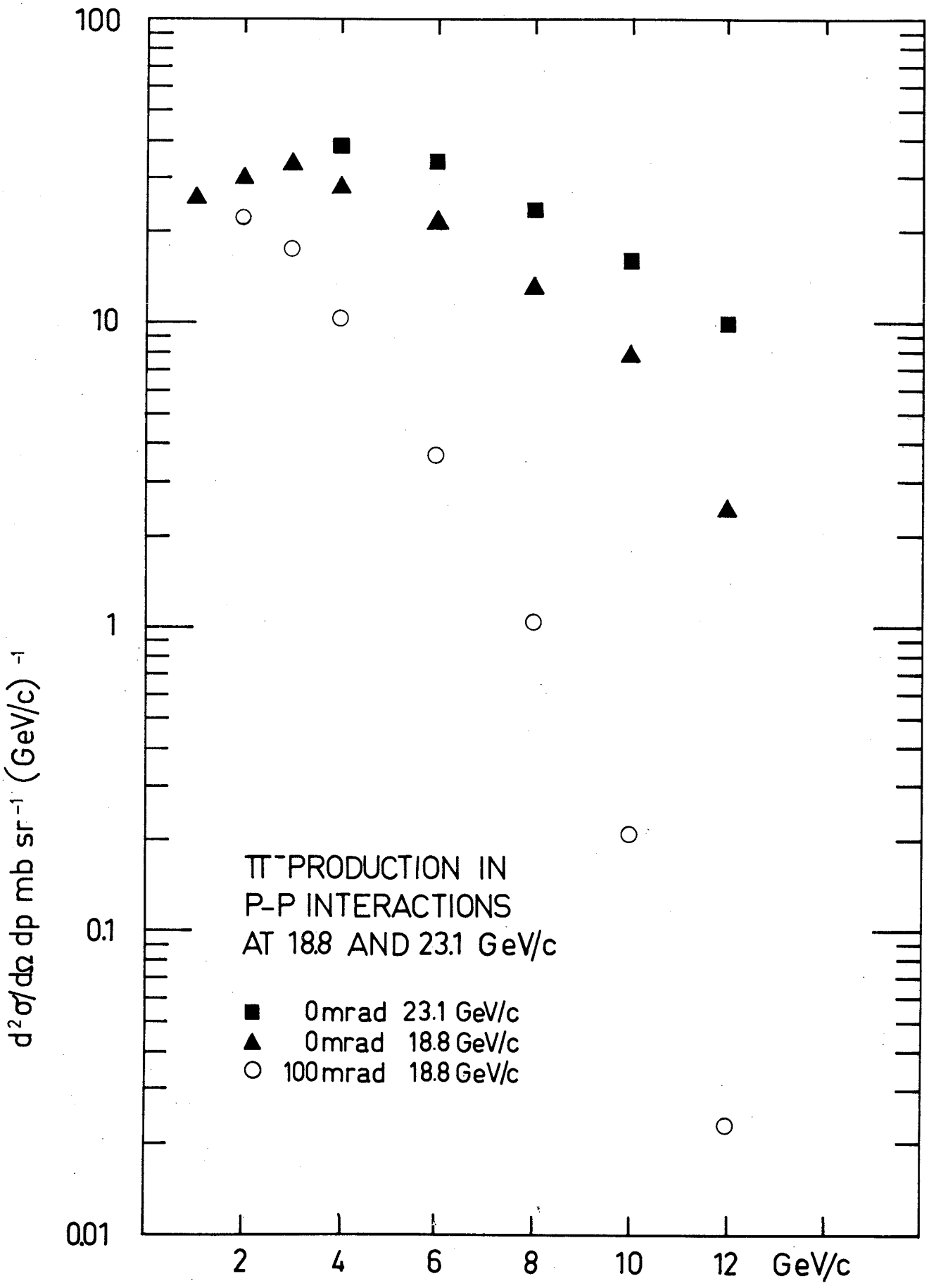

FIG. 3a

DIA - 19865

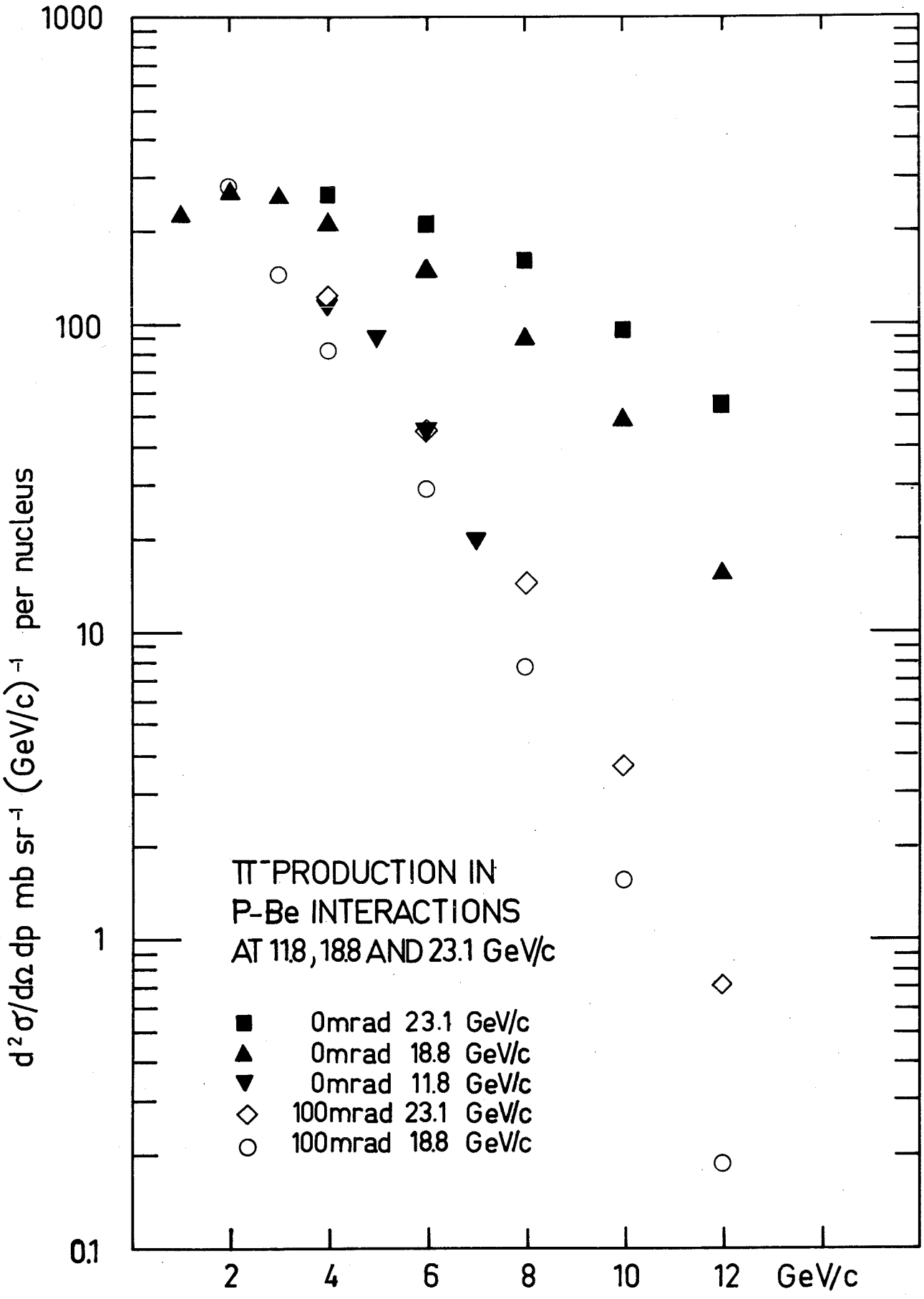

FIG. 3b

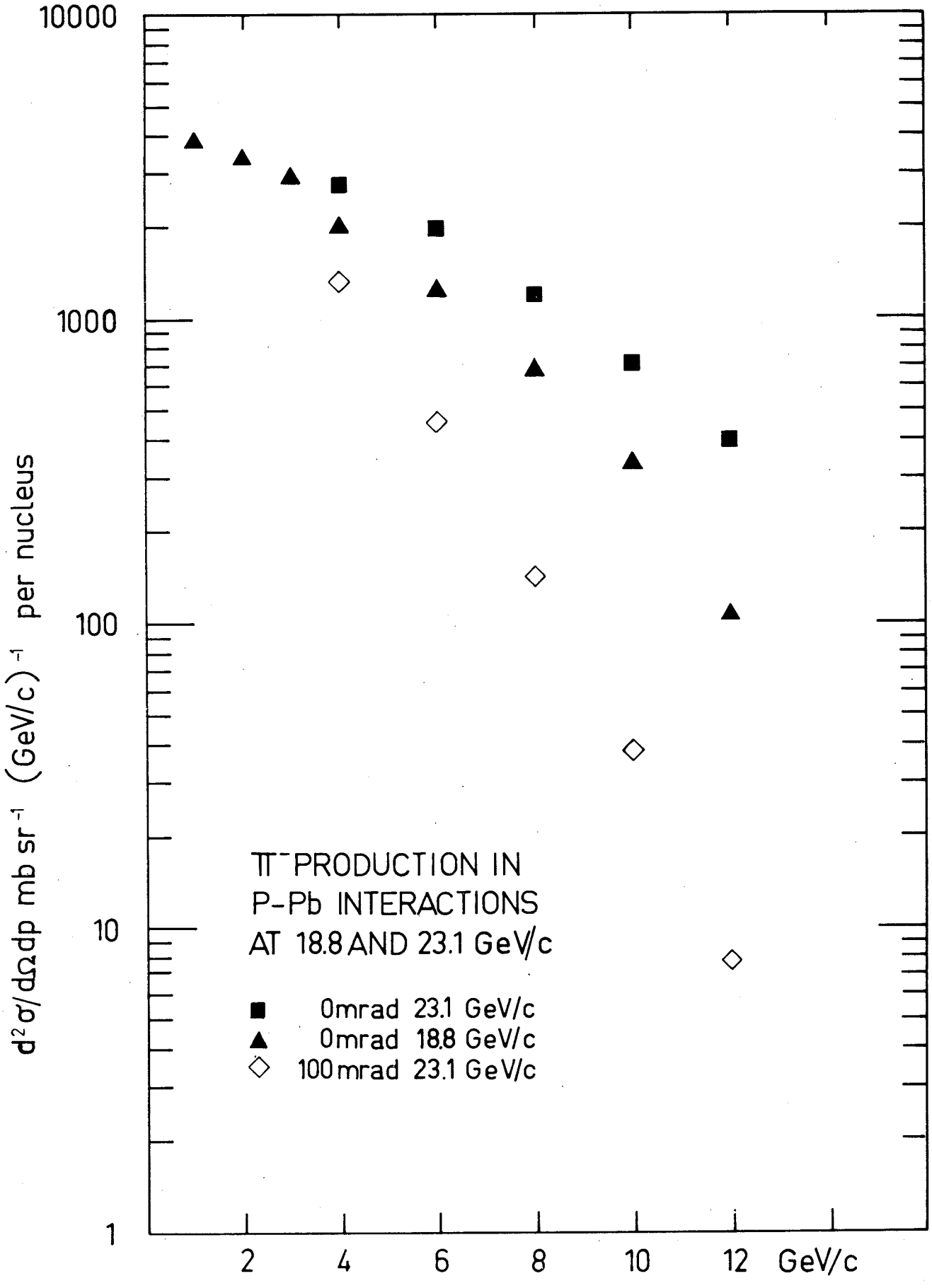

FIG. 3c

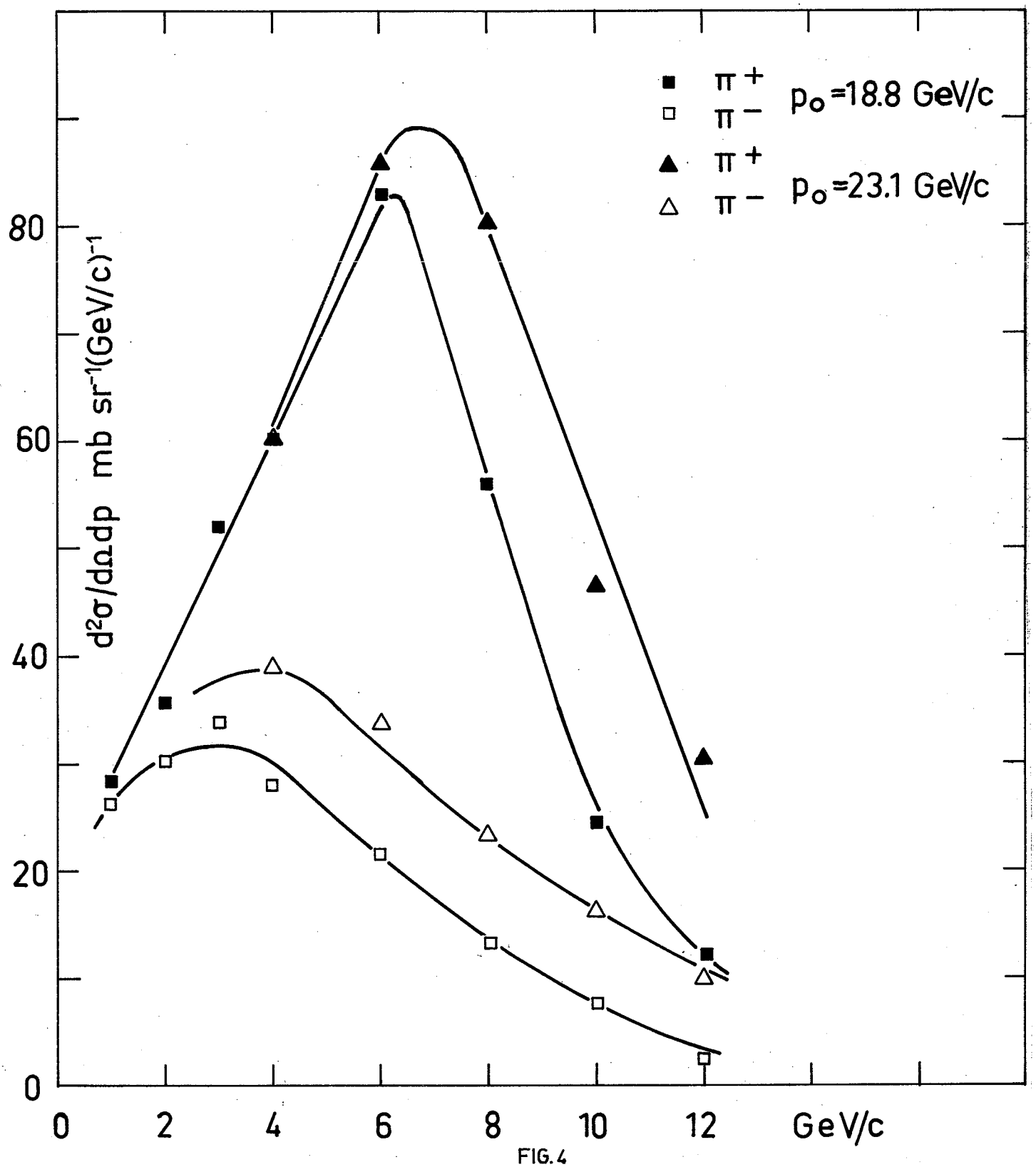
π+
π−
p₀=18.8 GeV/c
π+
π−
p₀=23.1 GeV/c
d²σ/dΩdp mb sr⁻¹(GeV/c)⁻¹
0
20
40
60
80
0
2
4
6
8
10
12
GeV/c

FIG. 4

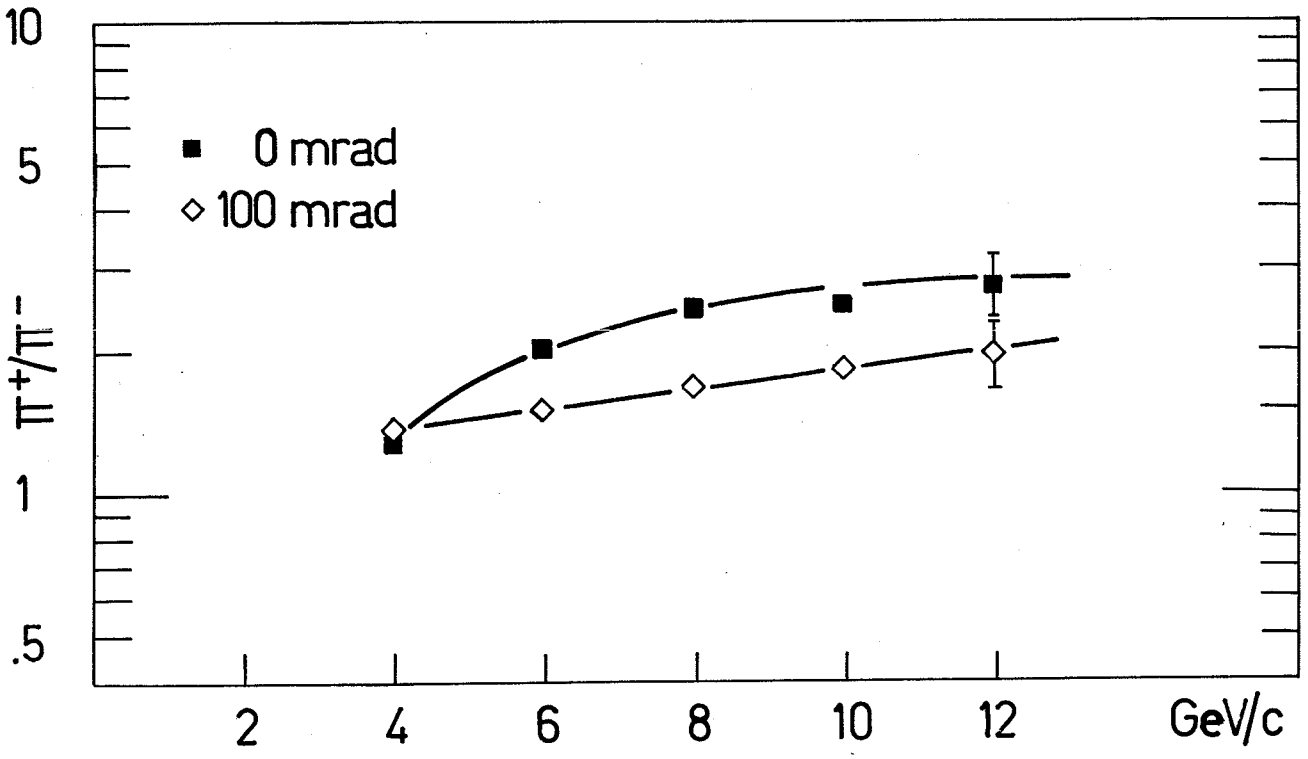
10
5
1
.5
π^+/π^-
■ 0 mrad
◇ 100 mrad
2
4
6
8
10
12
GeV/c

FIG.5

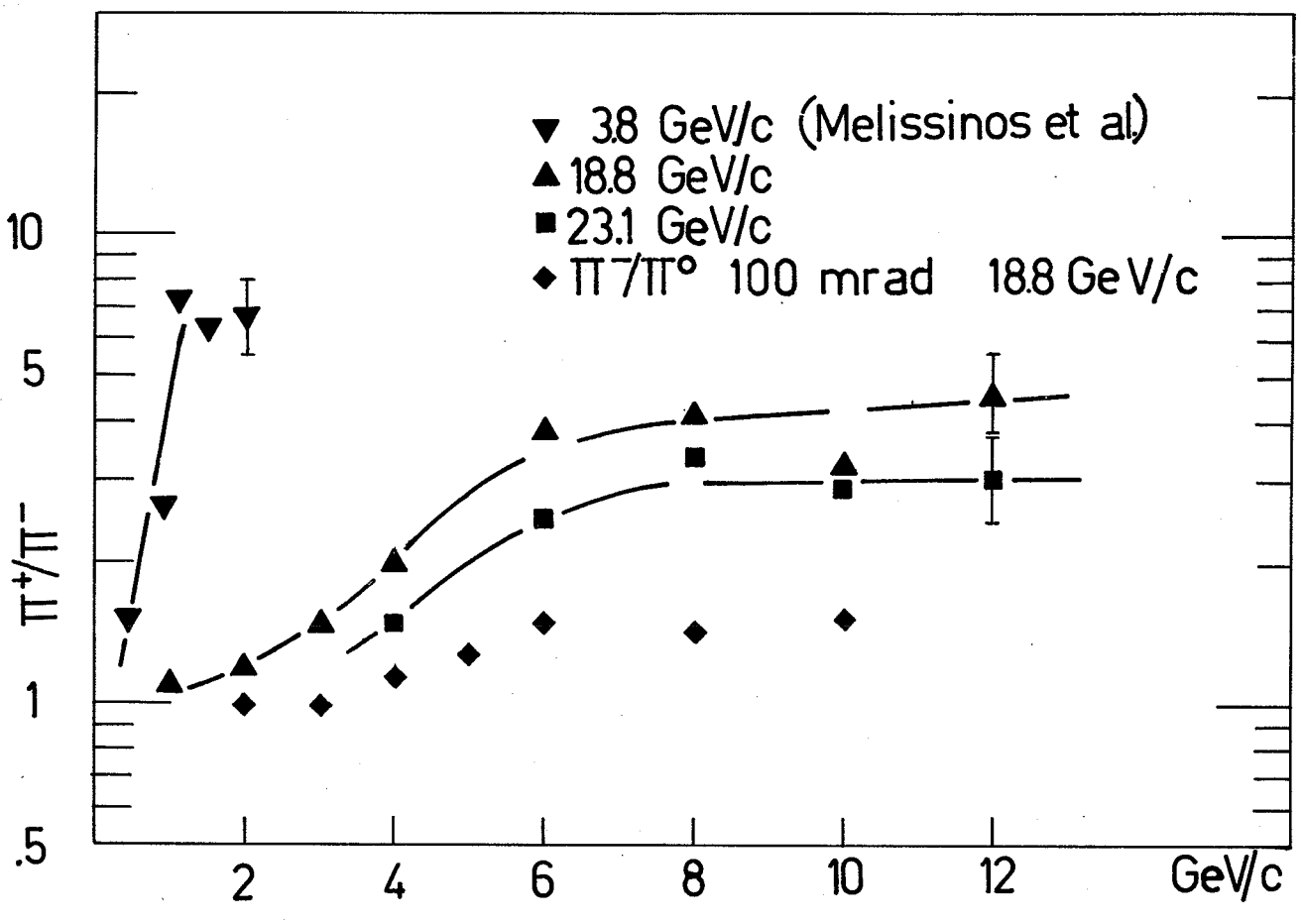
▼ 3.8 GeV/c (Melissinos et al.)
▲ 18.8 GeV/c
■ 23.1 GeV/c
◆ π^-/π^0 100 mrad 18.8 GeV/c
10
5
1
.5
π^+/π^-
2
4
6
8
10
12
GeV/c

FIG.6

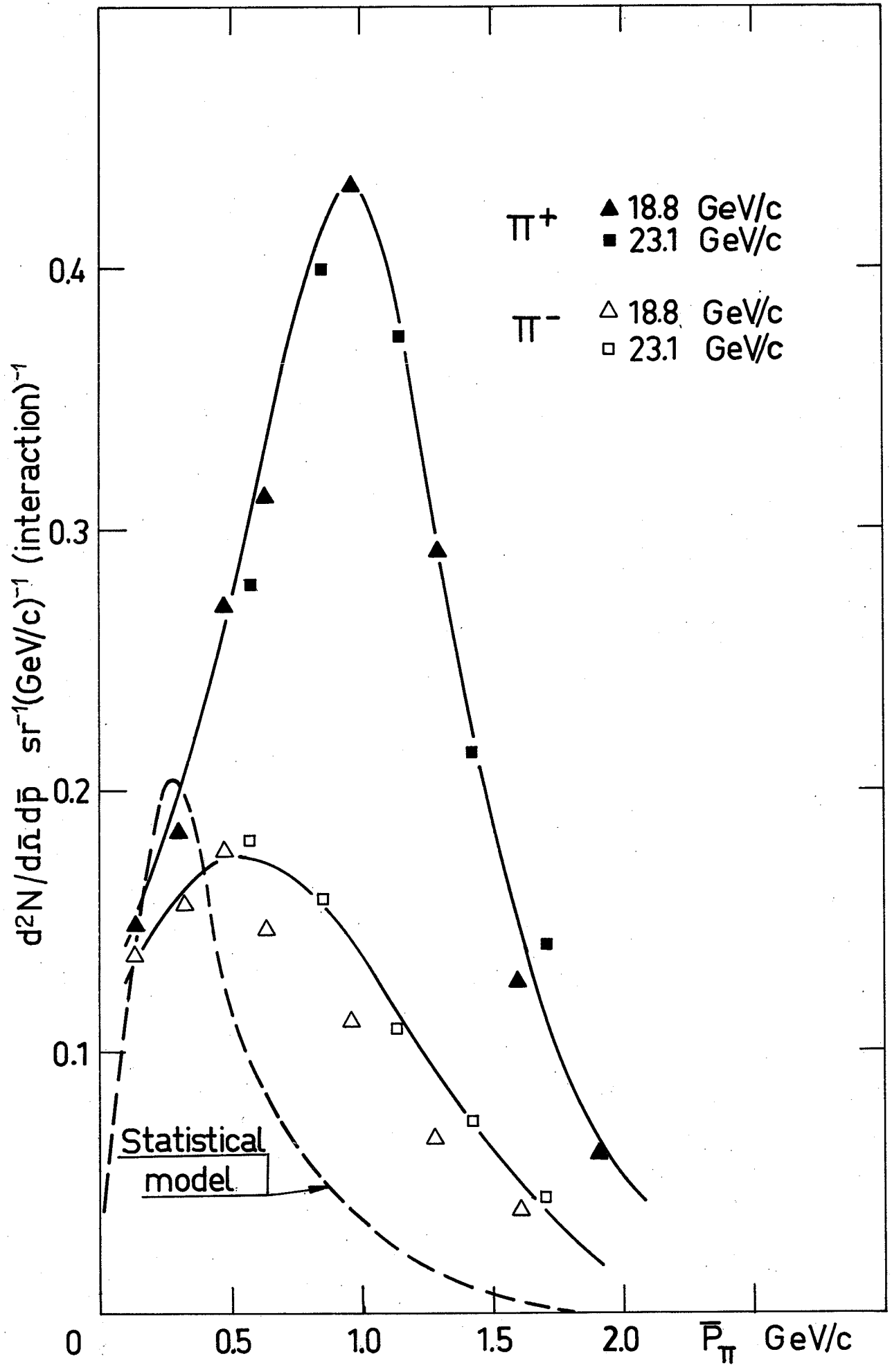

FIG. 7

SIS/R/8573

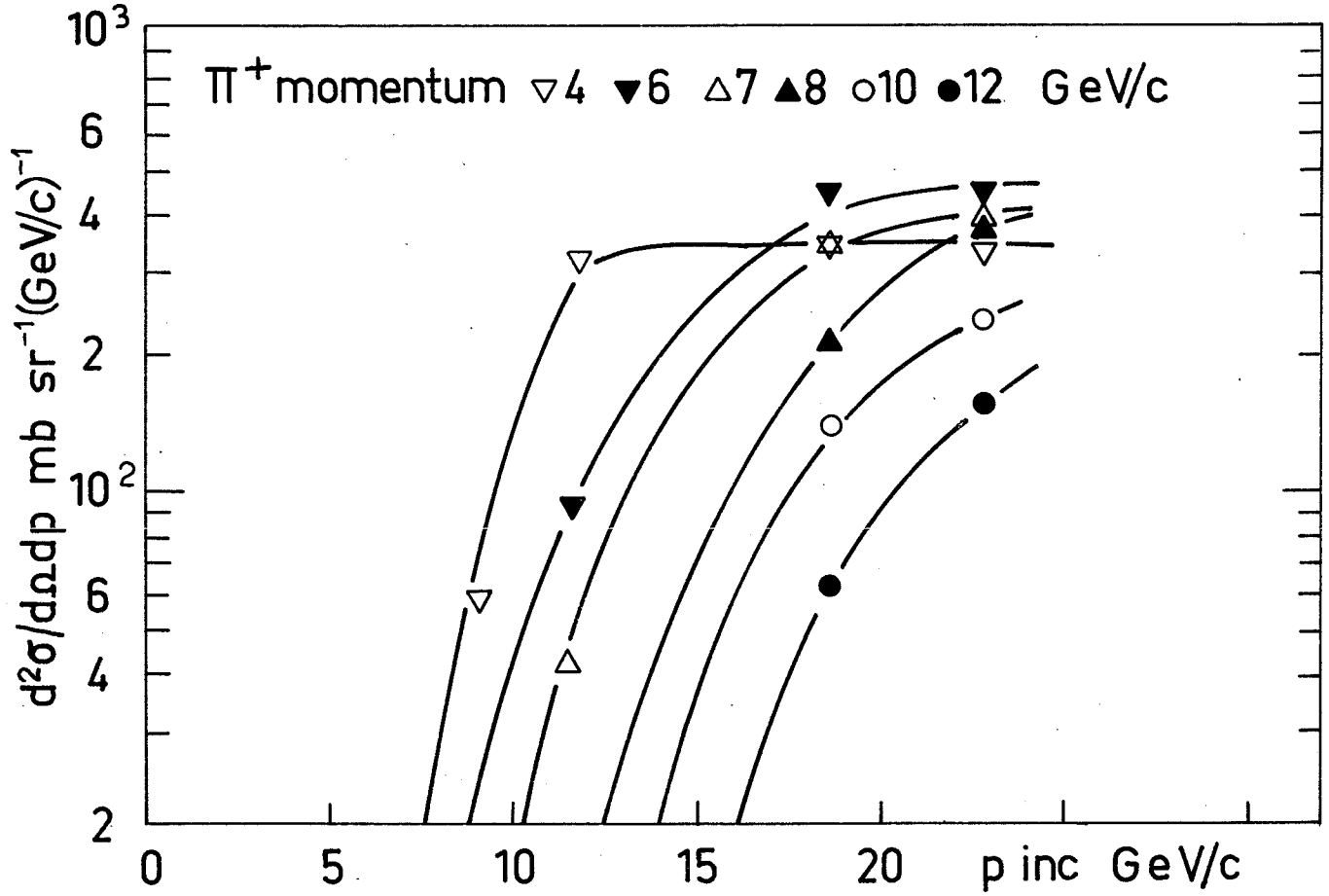
π^+ momentum ▽4 ▼6 △7 ▲8 ○10 ●12 GeV/c
$d^2\sigma/d\Omega dp$ mb $sr^{-1}(GeV/c)^{-1}$
10^3
6
4
2
10^2
6
4
2
0
5
10
15
20
p inc GeV/c

FIG. 8a

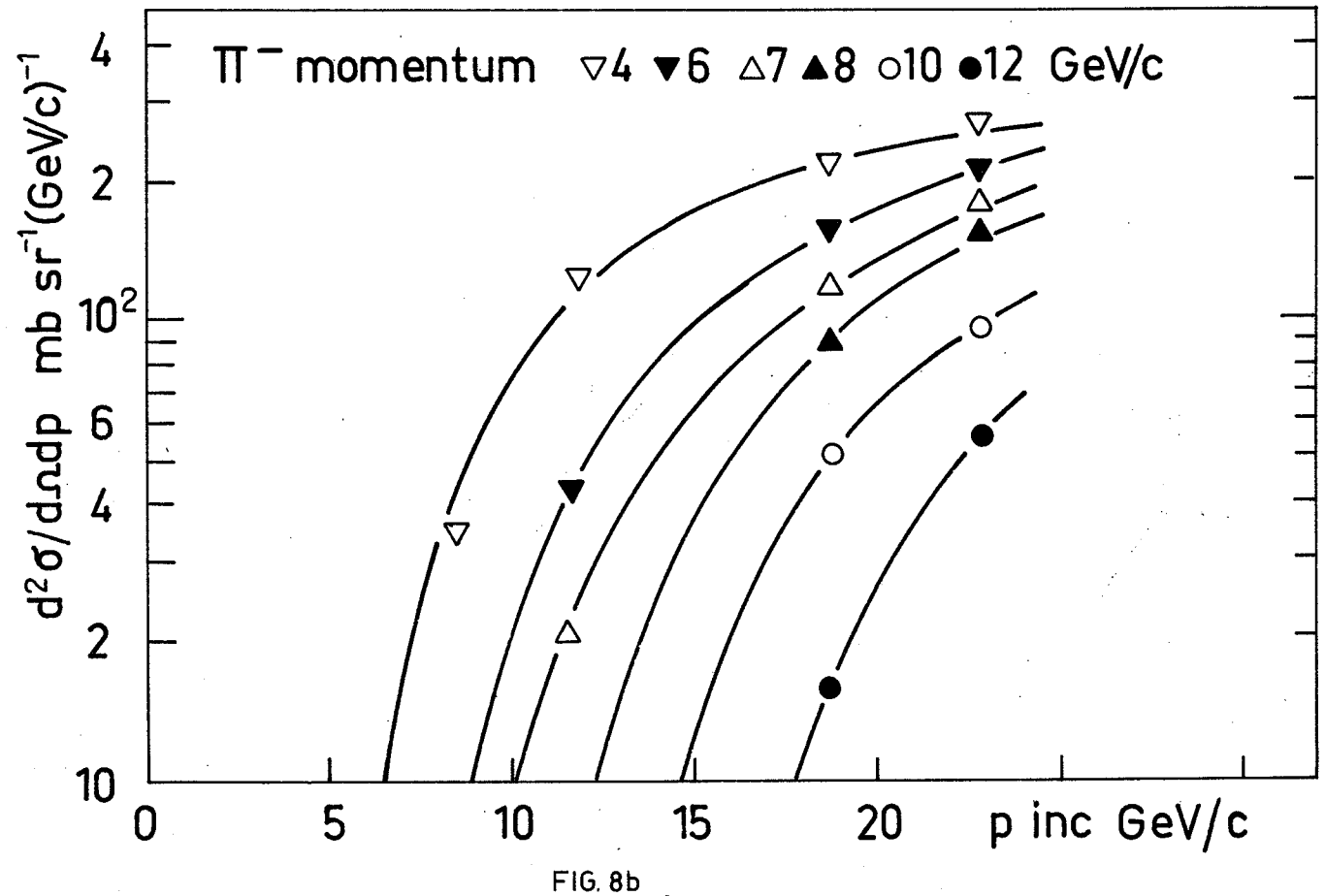
π^- momentum ▽4 ▼6 △7 ▲8 ○10 ●12 GeV/c
$d^2\sigma/d\Omega dp$ mb $sr^{-1}(GeV/c)^{-1}$
4
2
10^2
6
4
2
10
0
5
10
15
20
p inc GeV/c

FIG. 8b

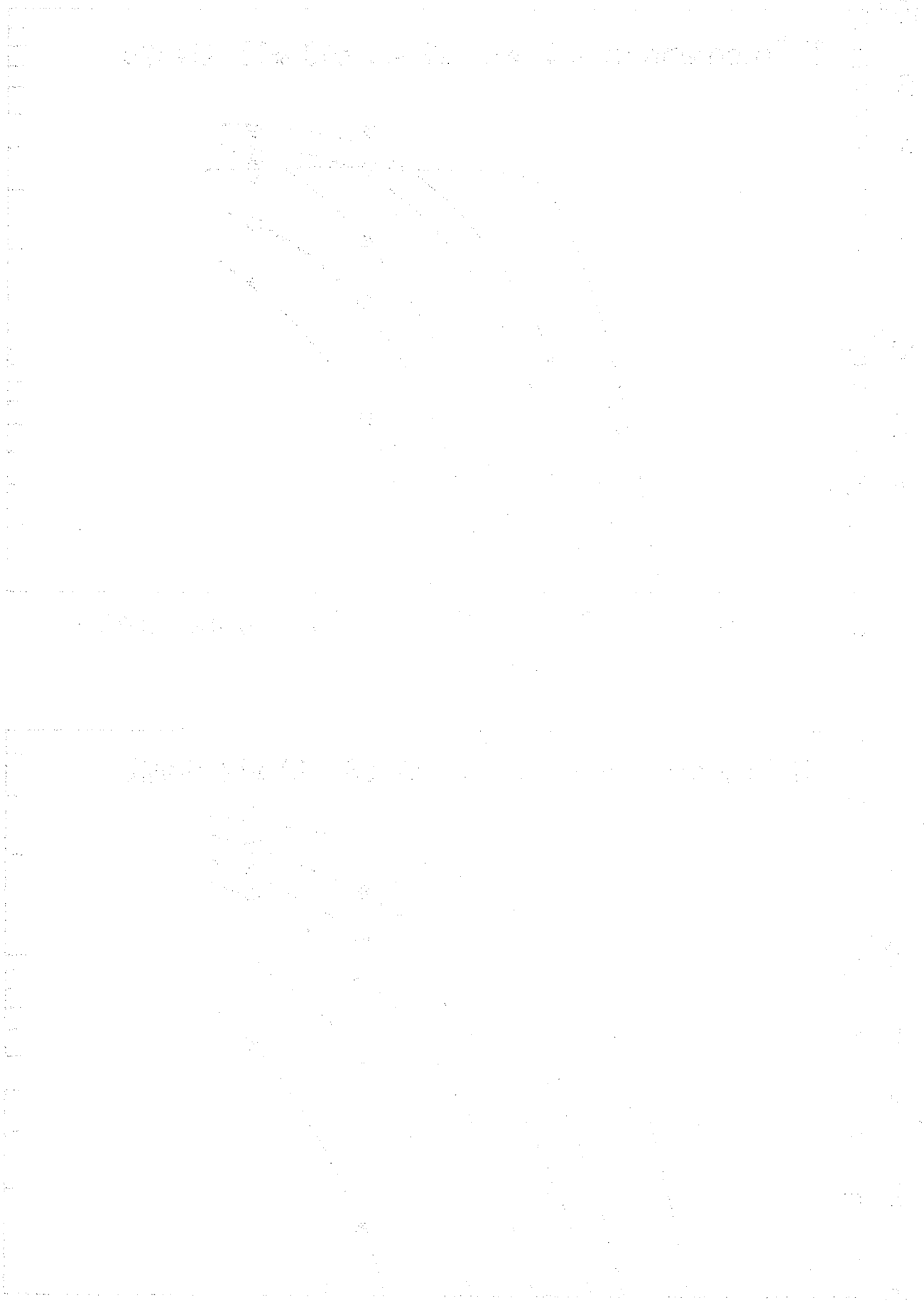

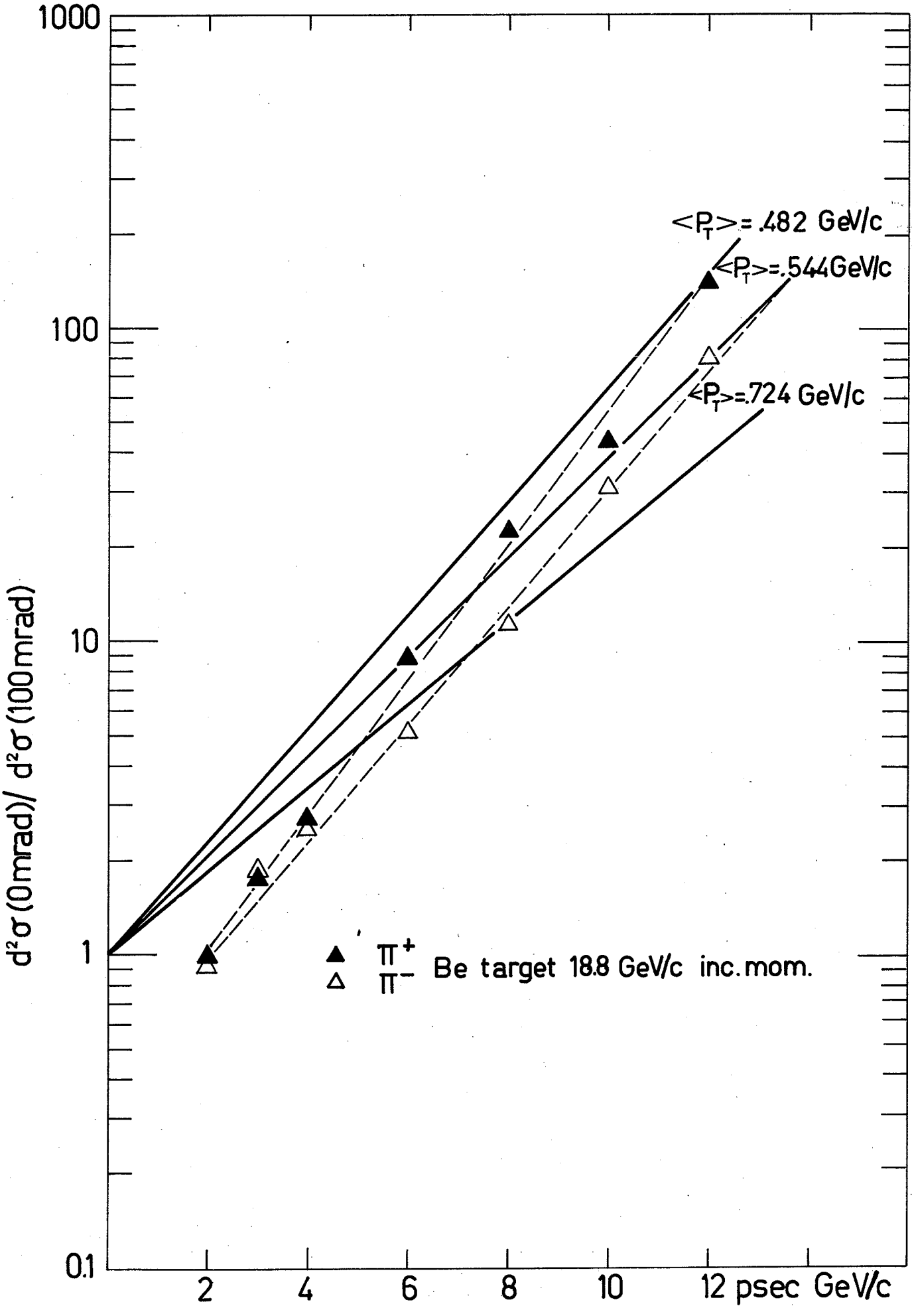

FIG. 9

SIS/R/8571

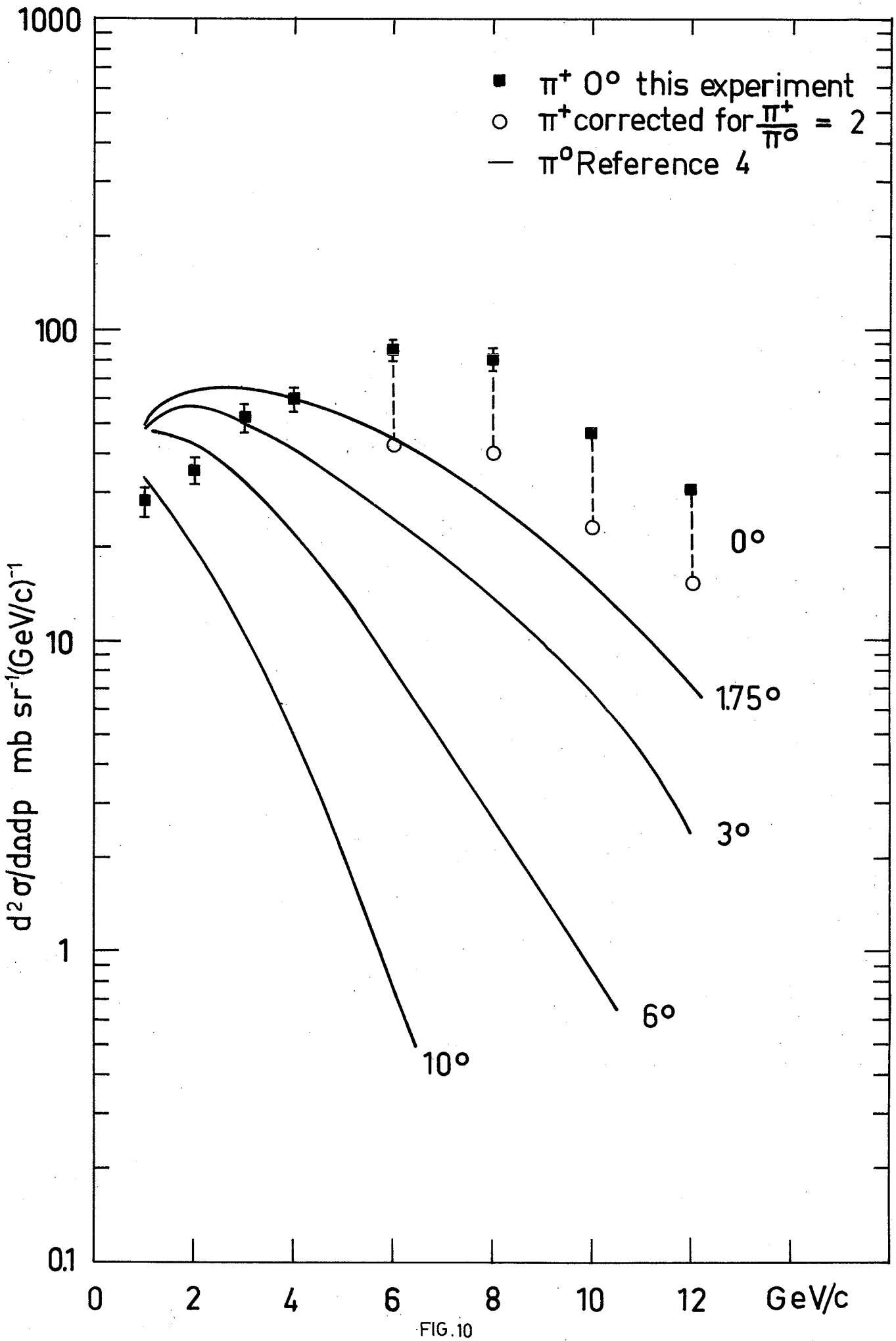

FIG. 10

SIS/R/8572

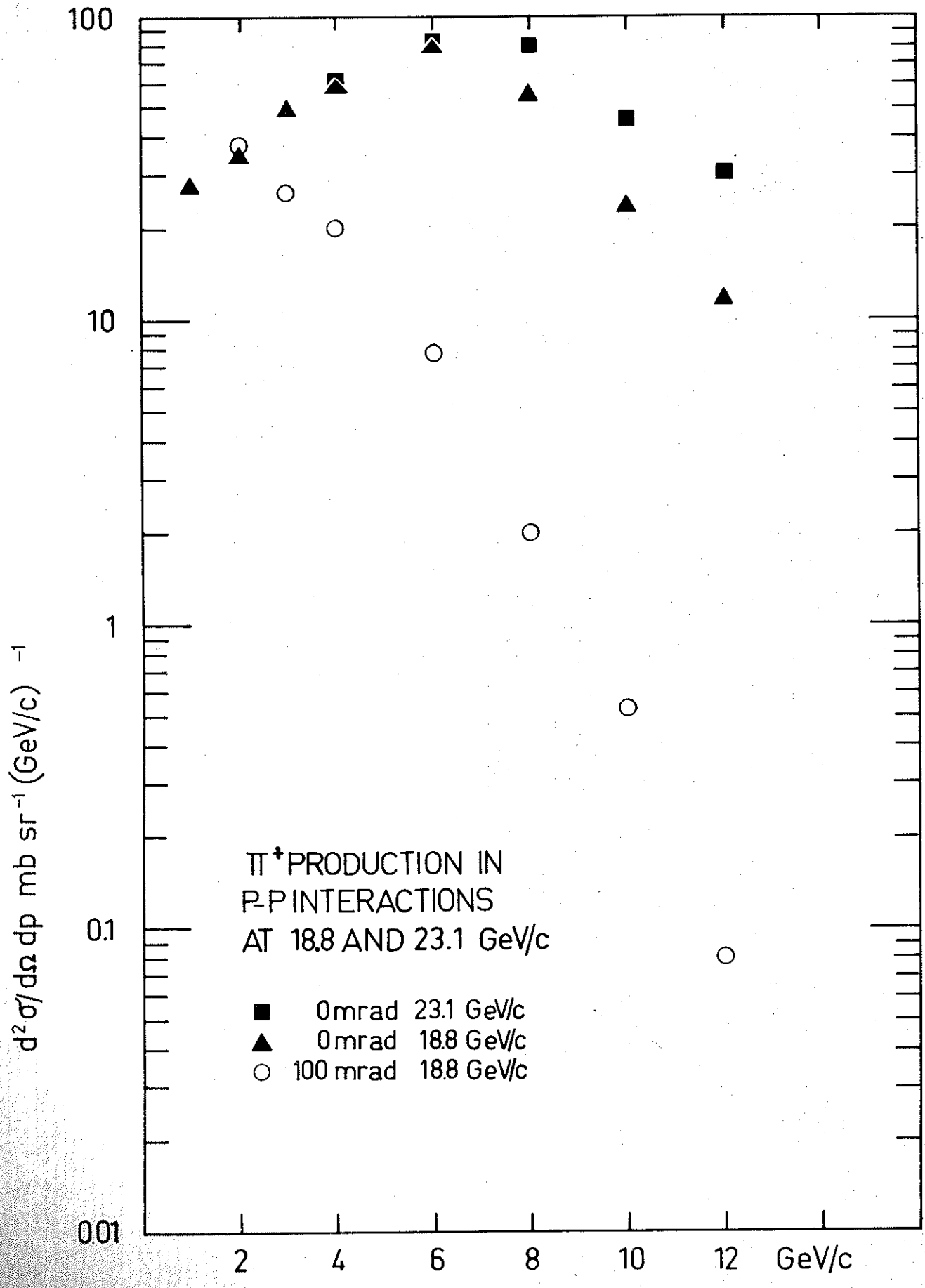
100
10
1
0.1
0.01
$d^2\sigma/d\Omega\,dp$ mb sr^{-1} $(GeV/c)^{-1}$
π^+ PRODUCTION IN
P-P INTERACTIONS
AT 18.8 AND 23.1 GeV/c
0 mrad 23.1 GeV/c
0 mrad 18.8 GeV/c
100 mrad 18.8 GeV/c
2
4
6
8
10
12
GeV/c

FIG. 2a

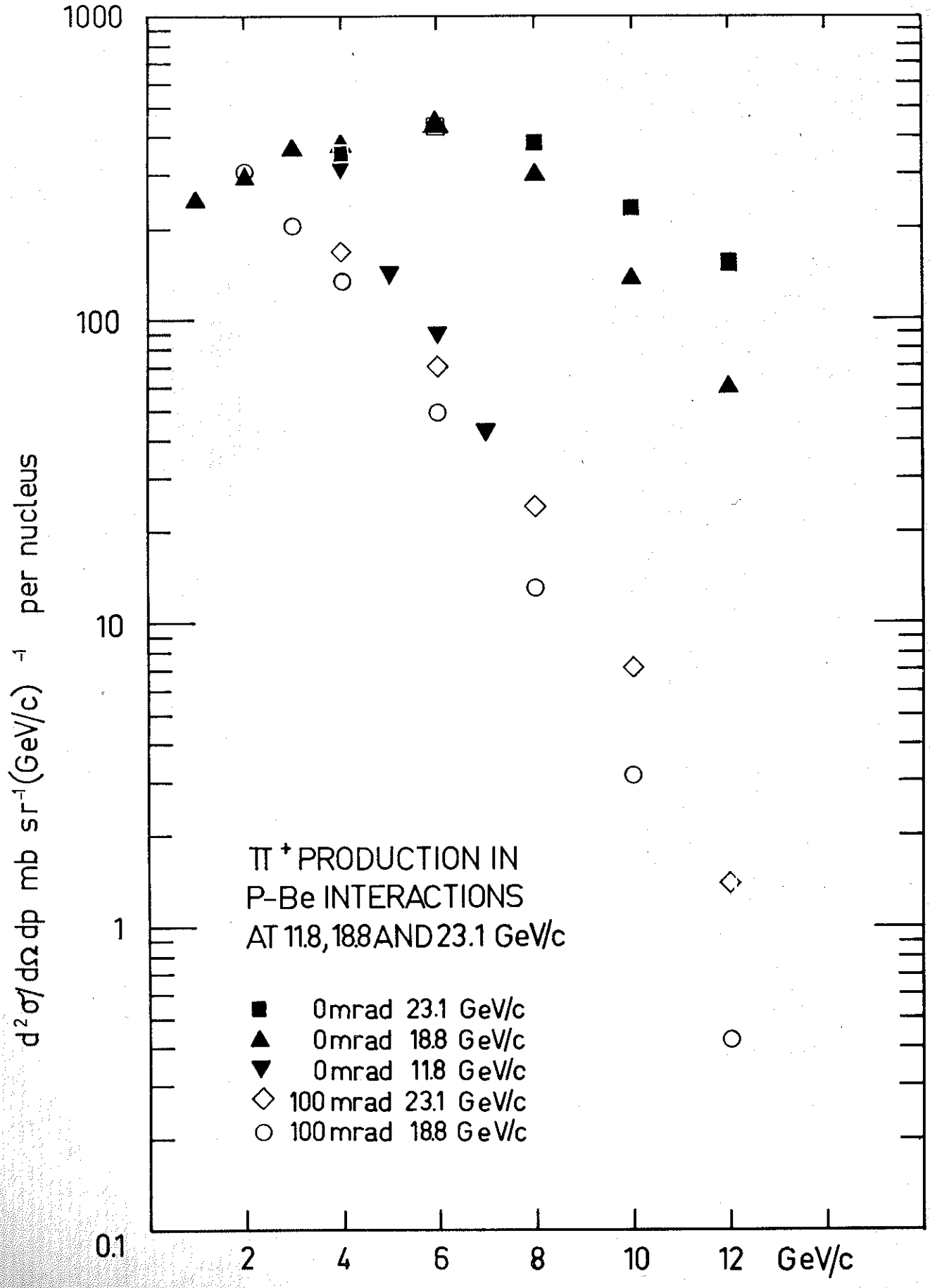
1000
100
10
1
0.1
2
4
6
8
10
12
GeV/c
d²σ/dΩ dp mb sr⁻¹(GeV/c)⁻¹ per nucleus
π⁺ PRODUCTION IN
P-Be INTERACTIONS
AT 11.8, 18.8 AND 23.1 GeV/c
0 mrad 23.1 GeV/c
0 mrad 18.8 GeV/c
0 mrad 11.8 GeV/c
100 mrad 23.1 GeV/c
100 mrad 18.8 GeV/c

FIG. 2b

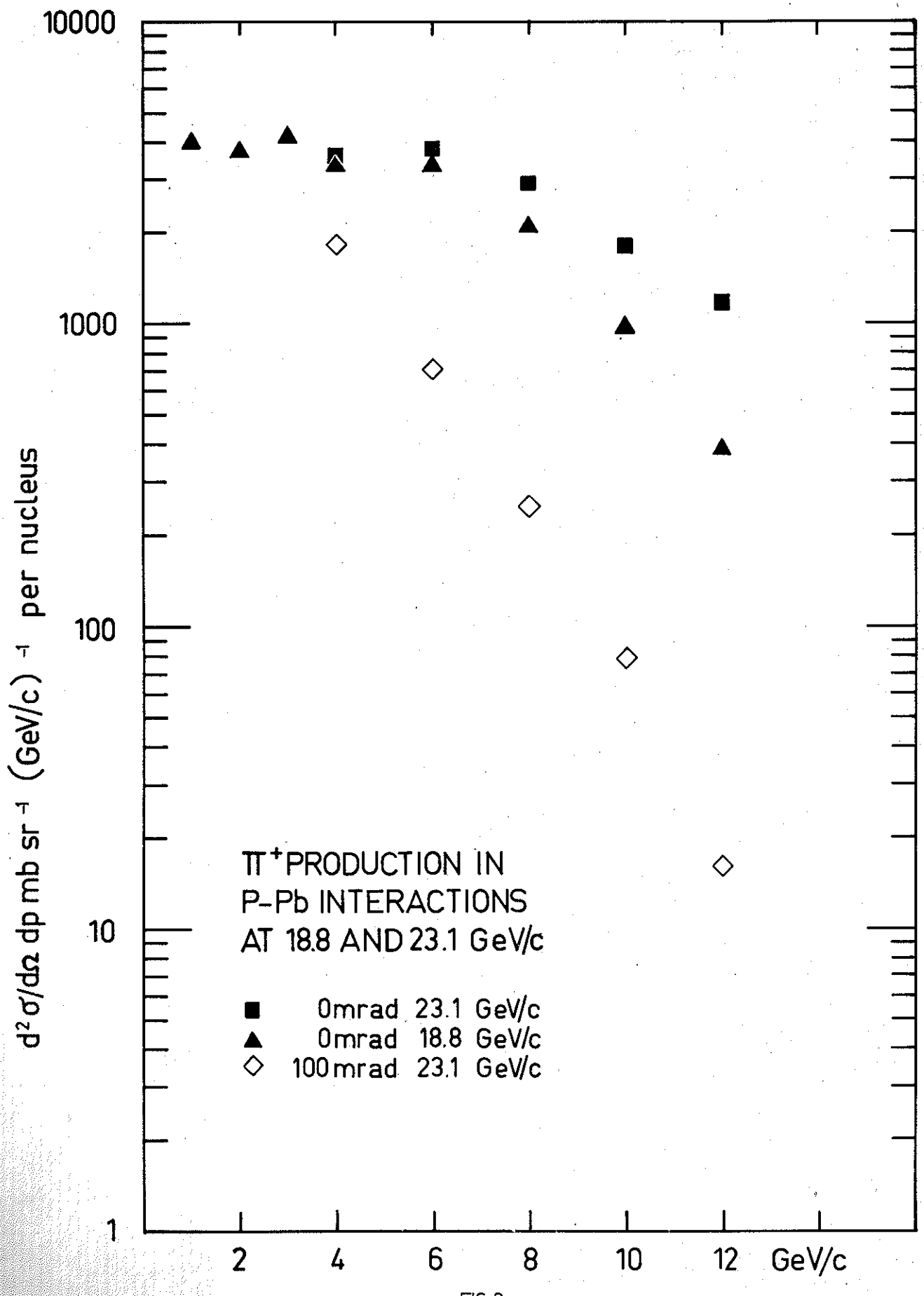

FIG. 2c

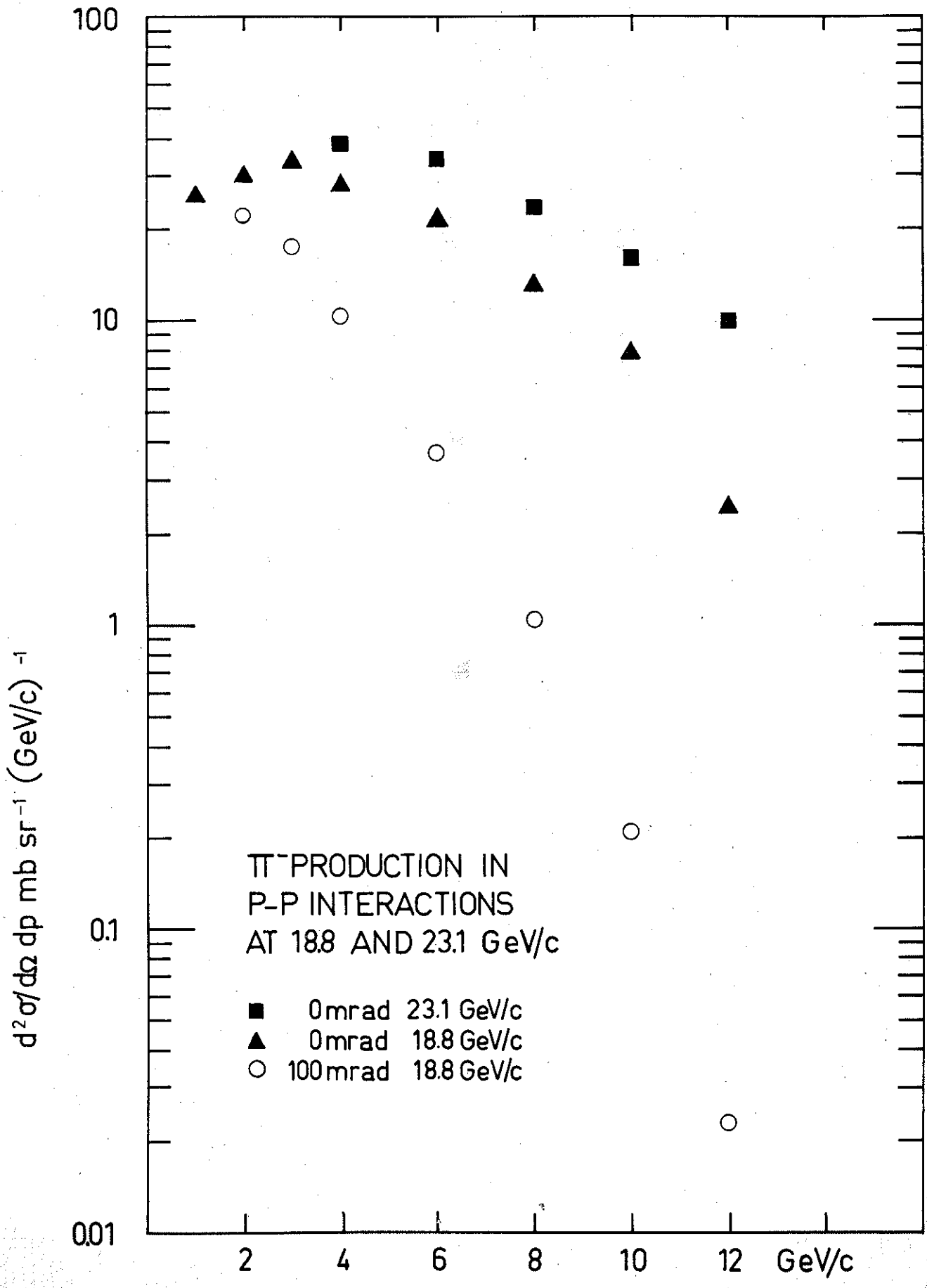

FIG. 3a

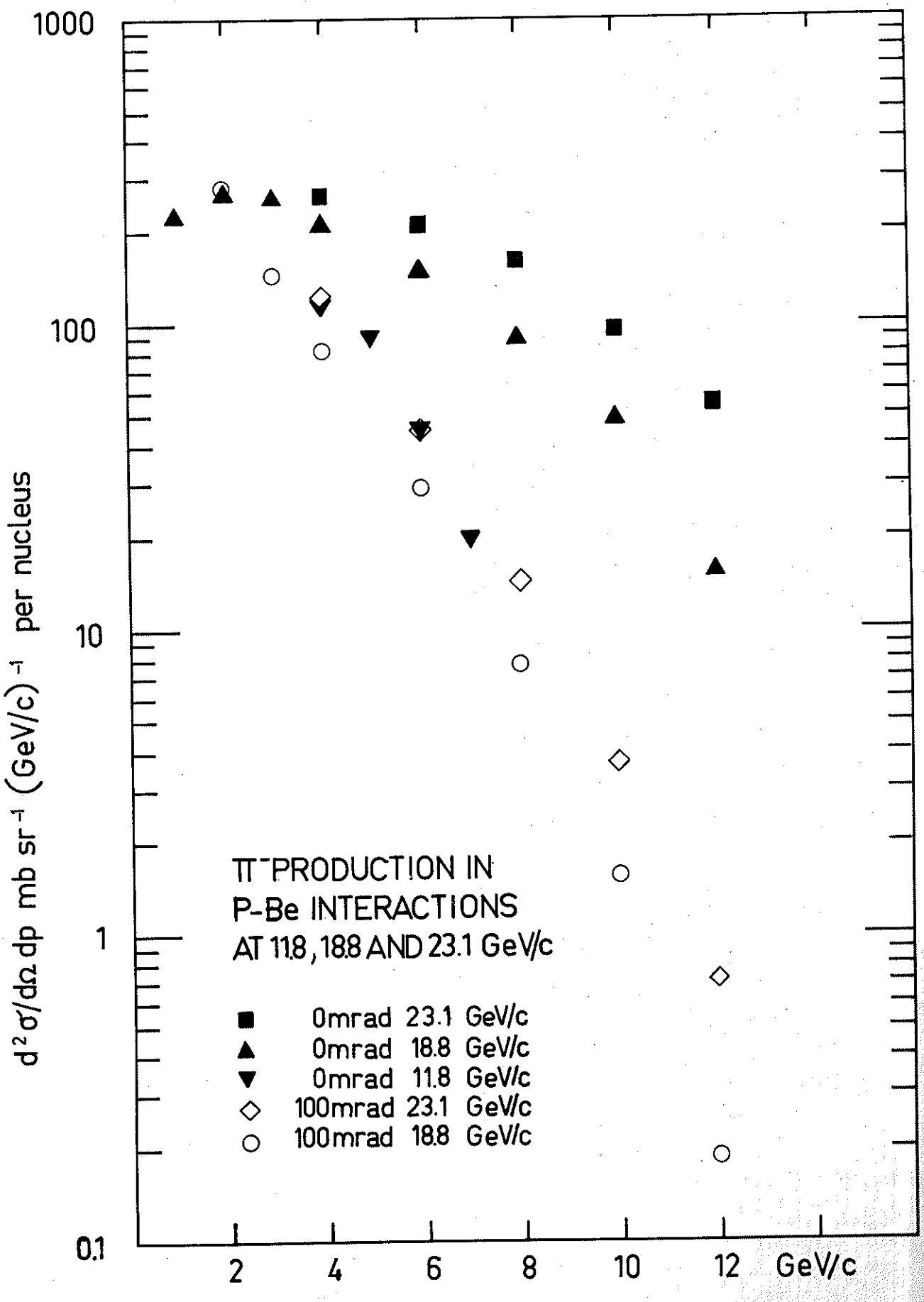

FIG. 3b

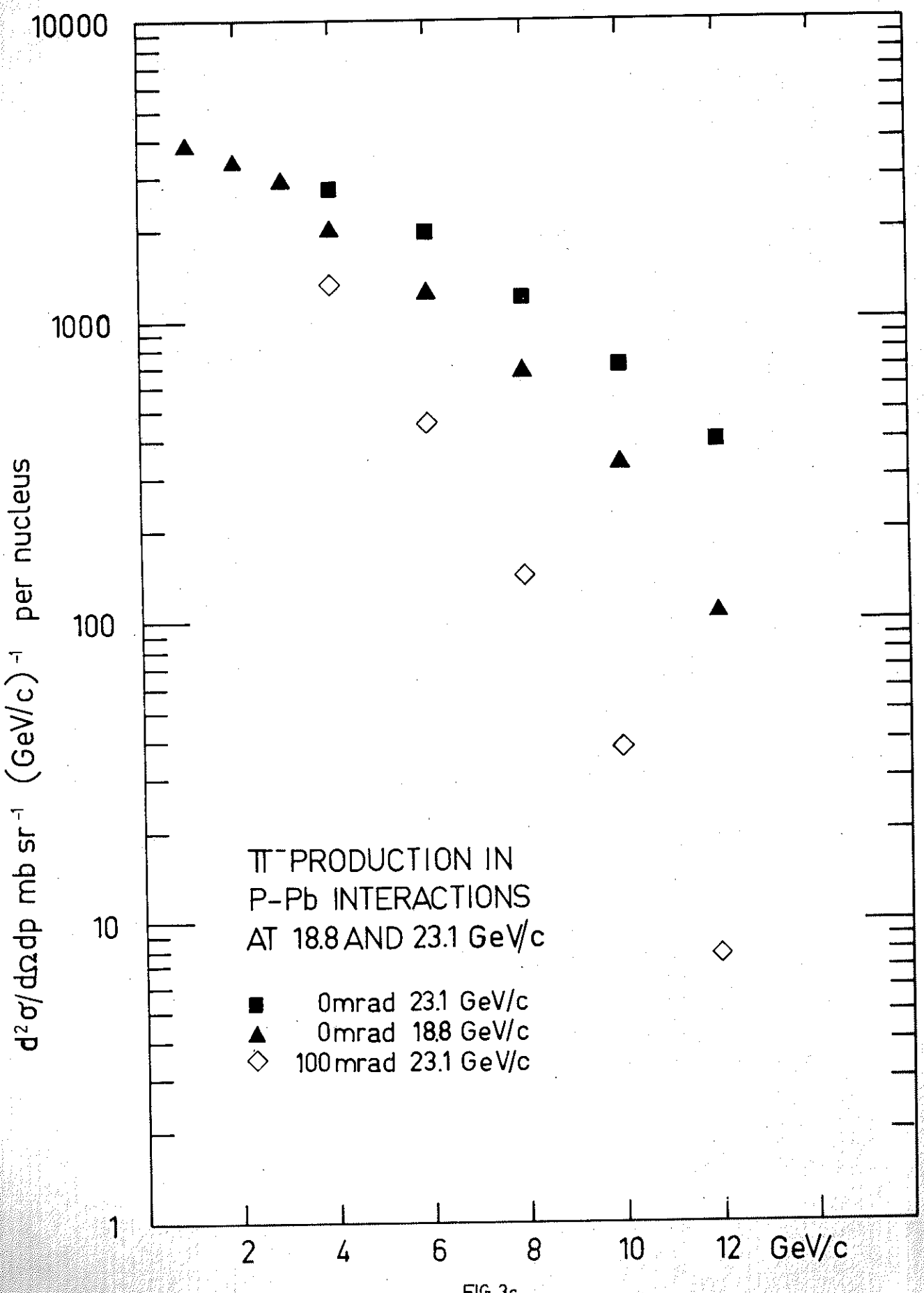
10000
1000
100
10
1
$d^2\sigma/d\Omega dp$ mb sr^{-1} $(GeV/c)^{-1}$ per nucleus
π^- PRODUCTION IN
P-Pb INTERACTIONS
AT 18.8 AND 23.1 GeV/c
0mrad 23.1 GeV/c
0mrad 18.8 GeV/c
100mrad 23.1 GeV/c
2
4
6
8
10
12
GeV/c

FIG. 3c

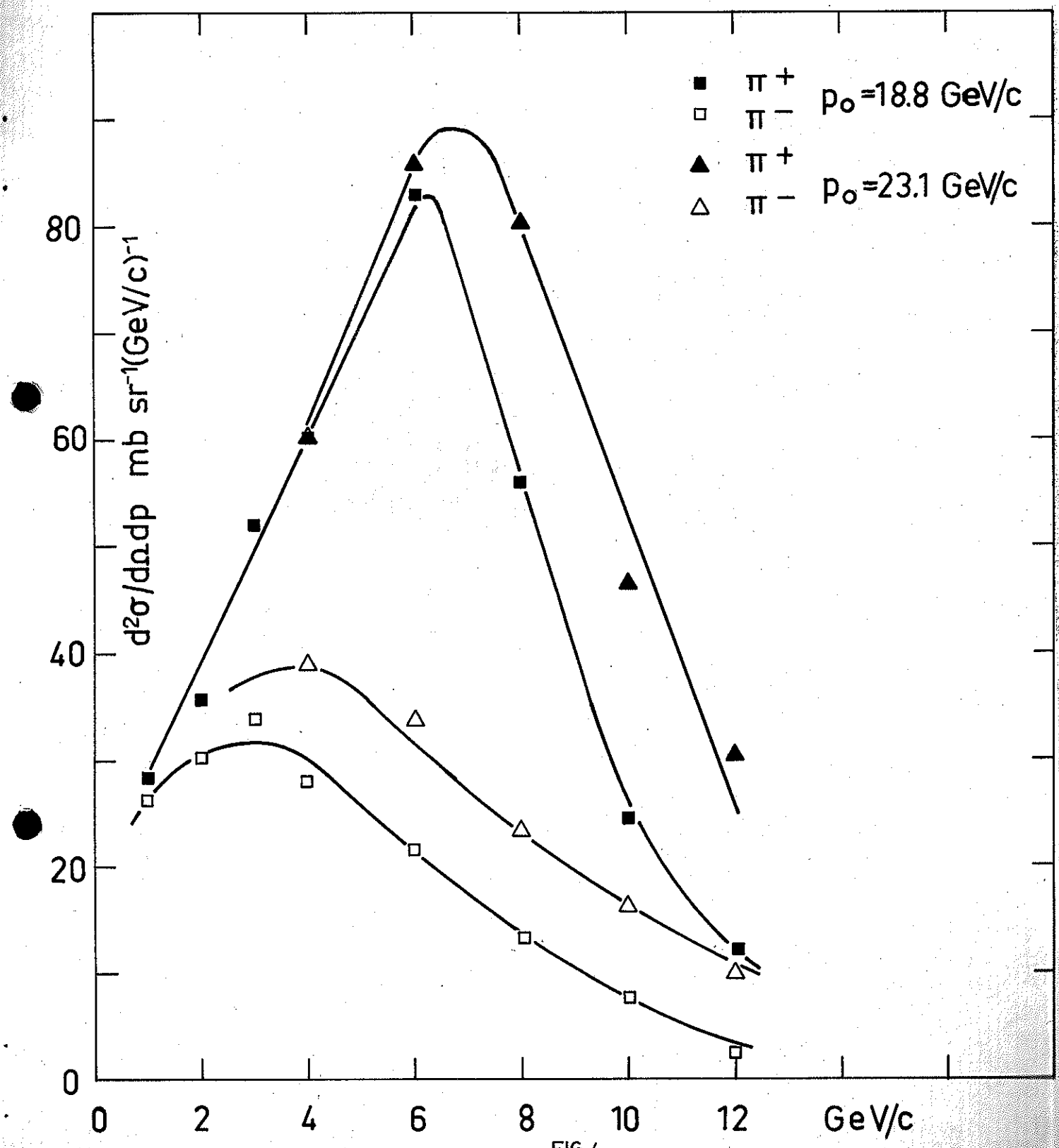
π +
π −
p₀ =18.8 GeV/c
π +
π −
p₀ =23.1 GeV/c
d²σ/dΩdp mb sr⁻¹(GeV/c)⁻¹
0
20
40
60
80
0
2
4
6
8
10
12
GeV/c

FIG. 4

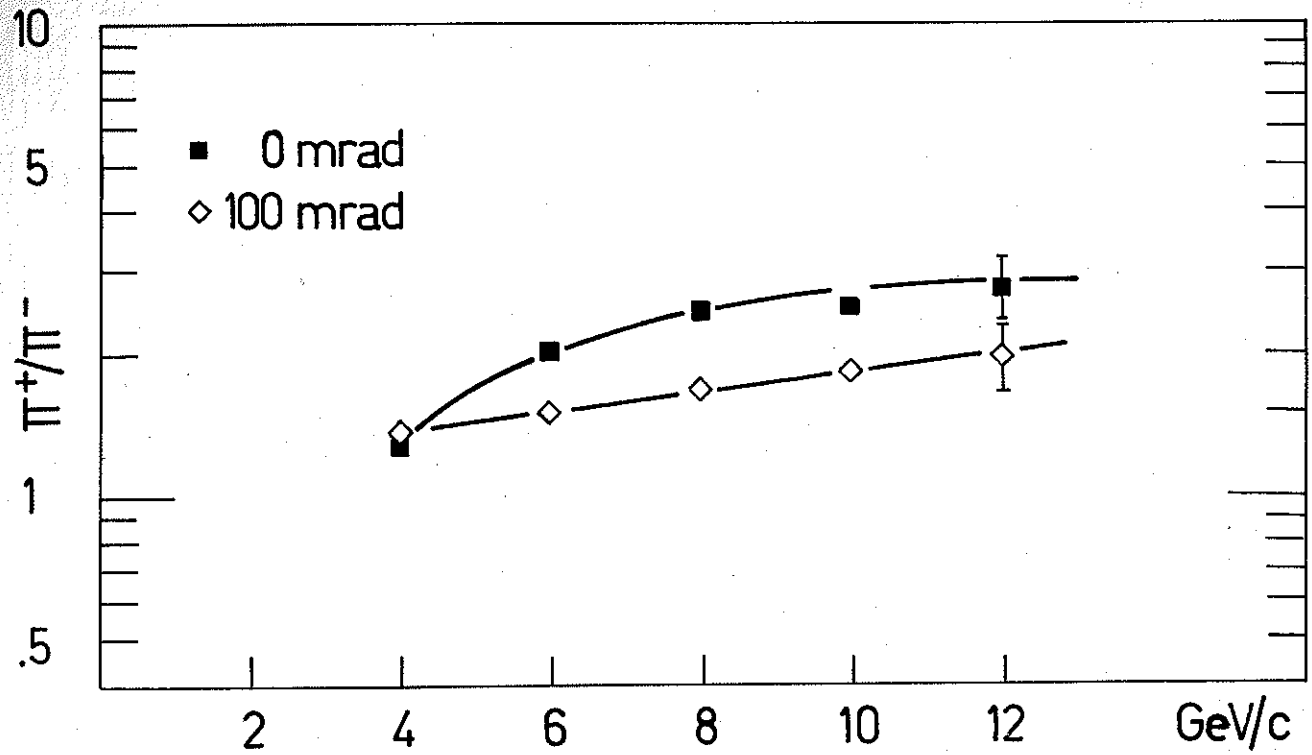
10
5
1
.5
π^+/π^-
0 mrad
100 mrad
2
4
6
8
10
12
GeV/c

FIG. 5

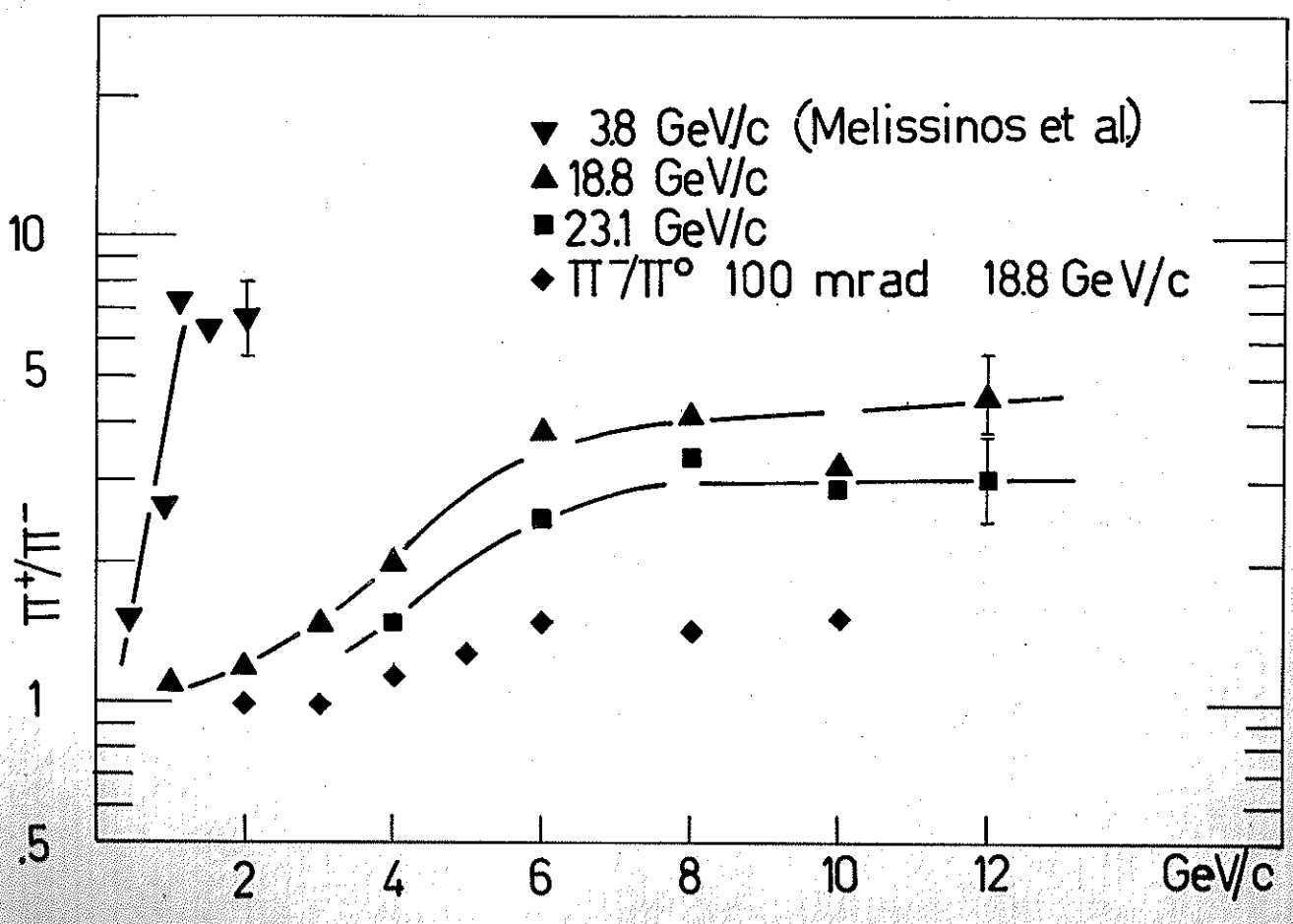
3.8 GeV/c (Melissinos et al.)
18.8 GeV/c
23.1 GeV/c
π^-/π° 100 mrad 18.8 GeV/c
10
5
1
.5
π^+/π^-
2
4
6
8
10
12
GeV/c

FIG. 6

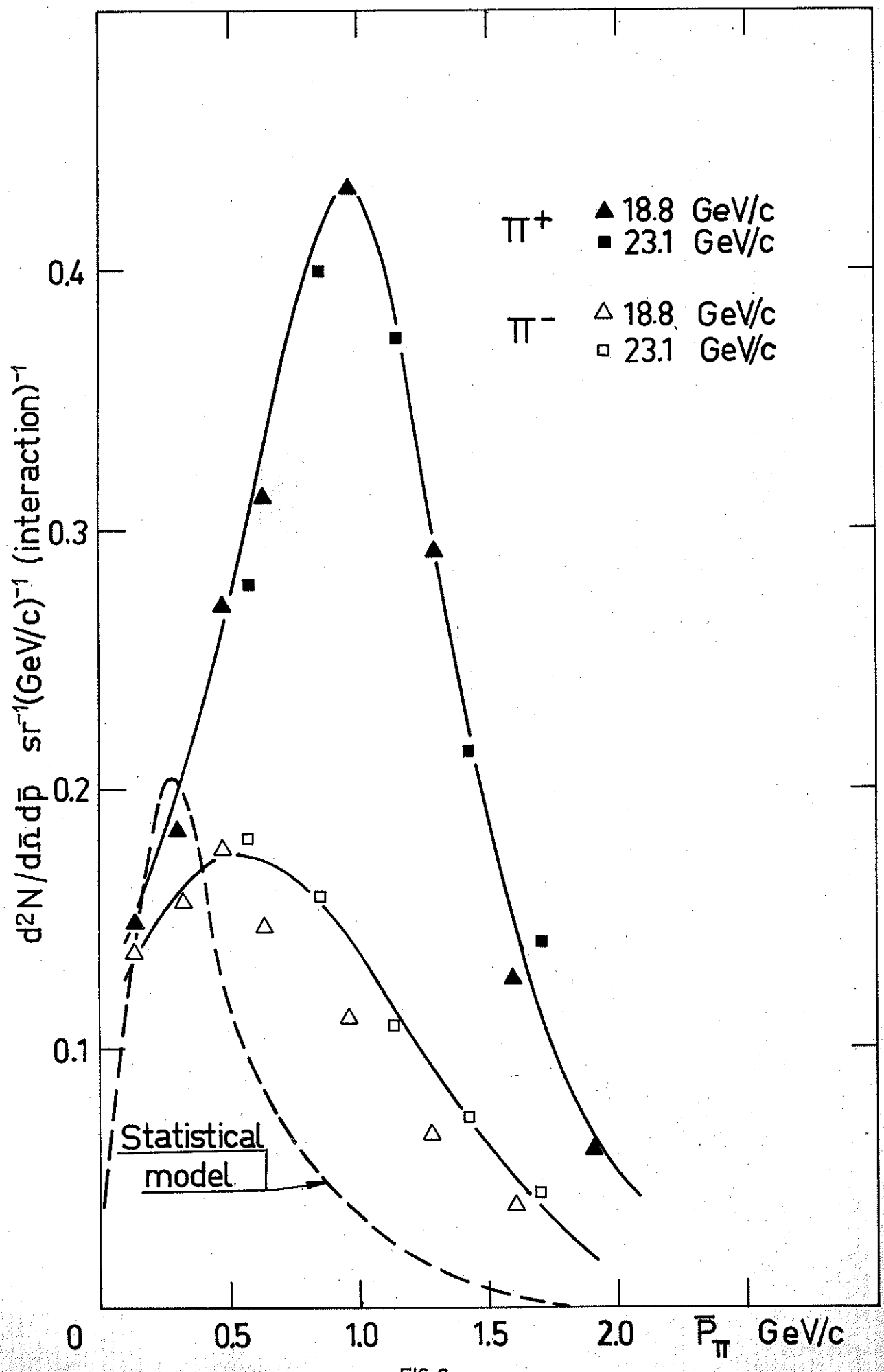
π+
18.8 GeV/c
23.1 GeV/c
π−
18.8 GeV/c
23.1 GeV/c
Statistical model
d²N/dΩ̄ dp̄ sr⁻¹(GeV/c)⁻¹ (interaction)⁻¹
0.4
0.3
0.2
0.1
0
0.5
1.0
1.5
2.0
P̄π GeV/c

FIG. 7

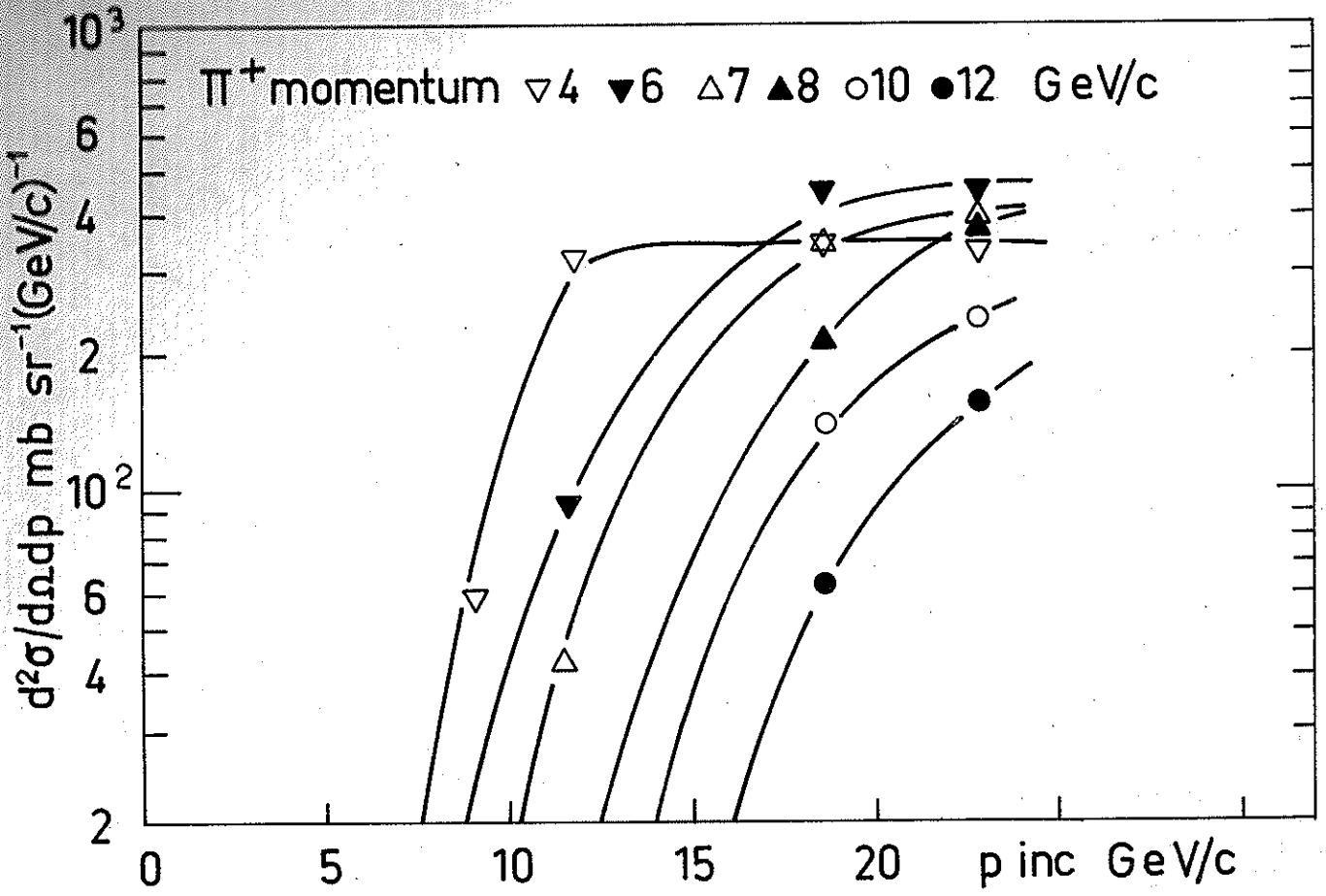
π^+ momentum ▽4 ▼6 △7 ▲8 ○10 ●12 GeV/c
$d^2\sigma/d\Omega dp$ mb $sr^{-1}(GeV/c)^{-1}$
10^3
6
4
2
10^2
6
4
2
0
5
10
15
20
p inc GeV/c

FIG. 8a

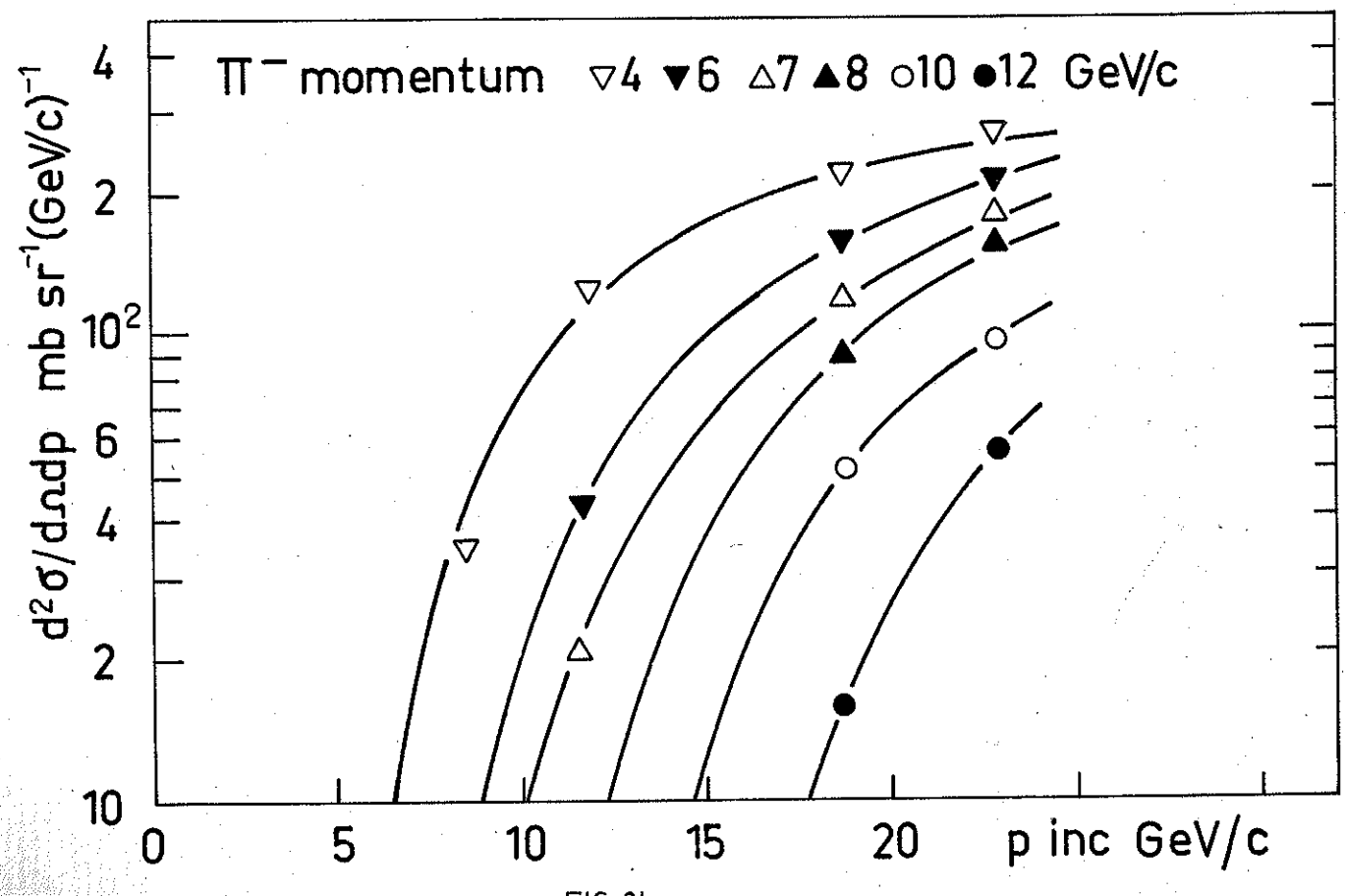
π^- momentum ▽4 ▼6 △7 ▲8 ○10 ●12 GeV/c
$d^2\sigma/d\Omega dp$ mb $sr^{-1}(GeV/c)^{-1}$
4
2
10^2
6
4
2
10
0
5
10
15
20
p inc GeV/c

FIG. 8b

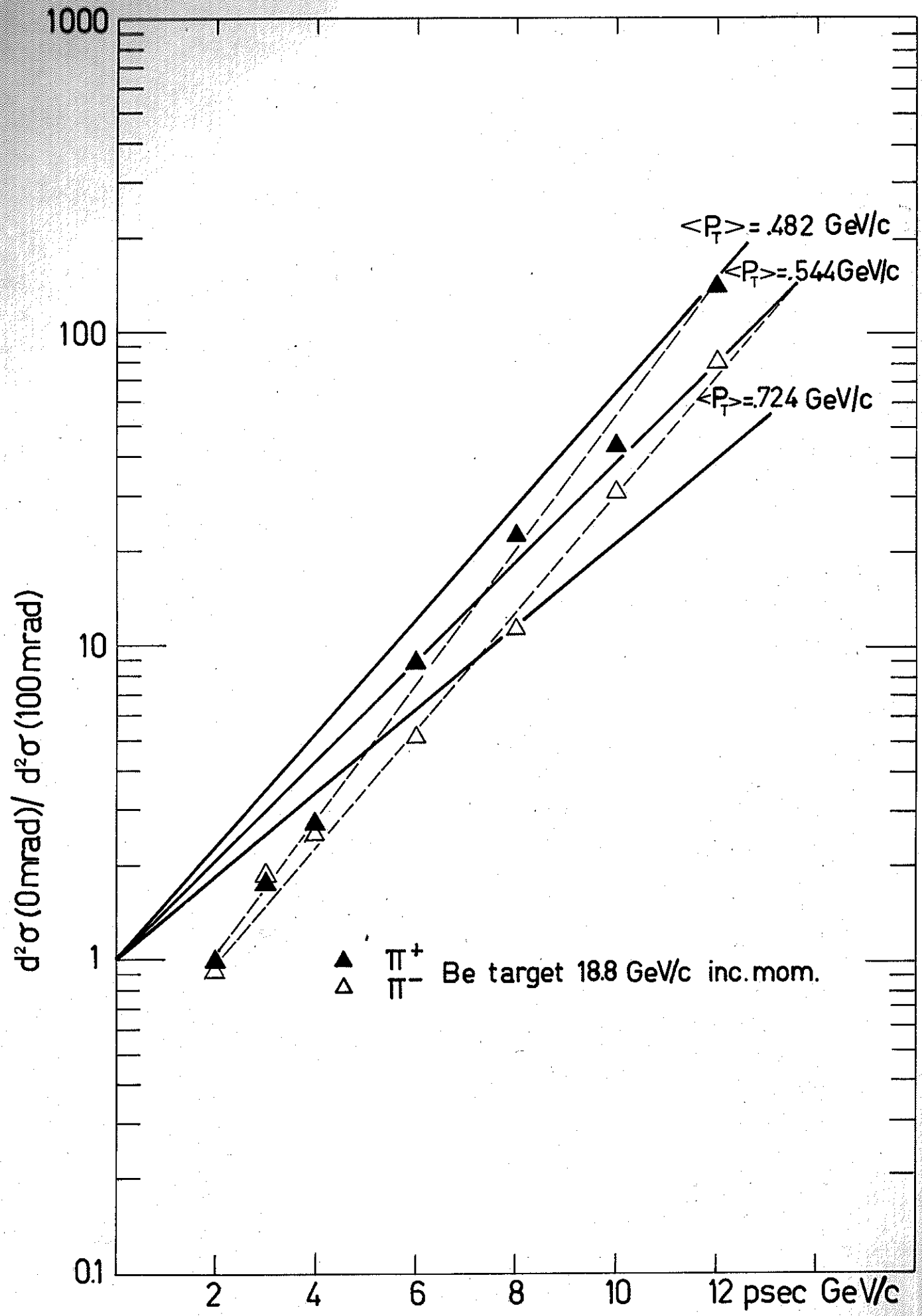
1000
100
10
1
0.1
$d^2\sigma$ (0mrad)/ $d^2\sigma$ (100mrad)
<P_T>= .482 GeV/c
<P_T>=.544GeV/c
<P_T>=.724 GeV/c
π^+
π^- Be target 18.8 GeV/c inc.mom.
2
4
6
8
10
12 psec GeV/c

FIG. 9

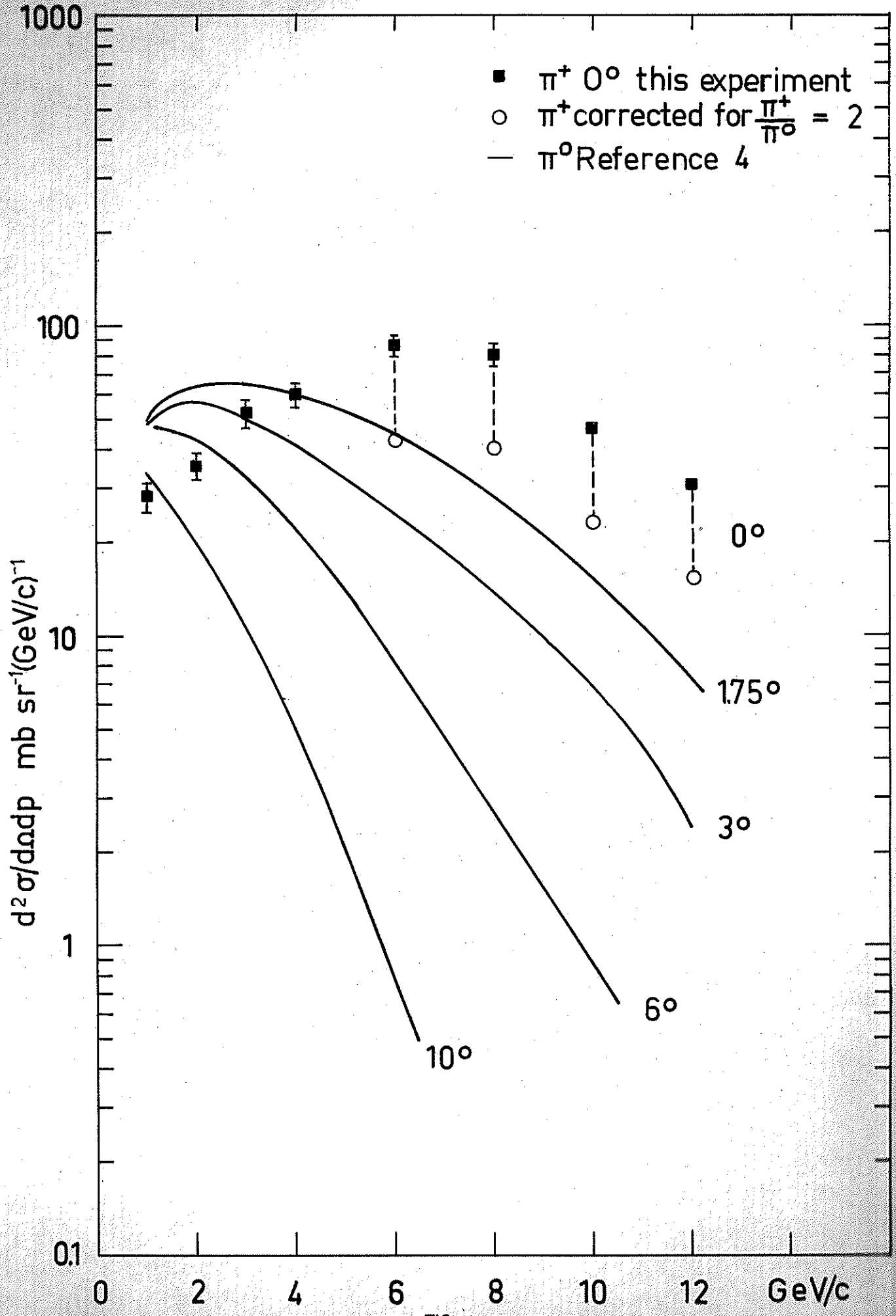
1000
100
10
1
0.1
$d^2\sigma/d\Omega dp$ mb $sr^{-1}(GeV/c)^{-1}$
π^+ 0° this experiment
π^+ corrected for $\frac{\pi^+}{\pi^0}$ = 2
π^0 Reference 4
0°
1.75°
3°
6°
10°
0
2
4
6
8
10
12
GeV/c

FIG. 10

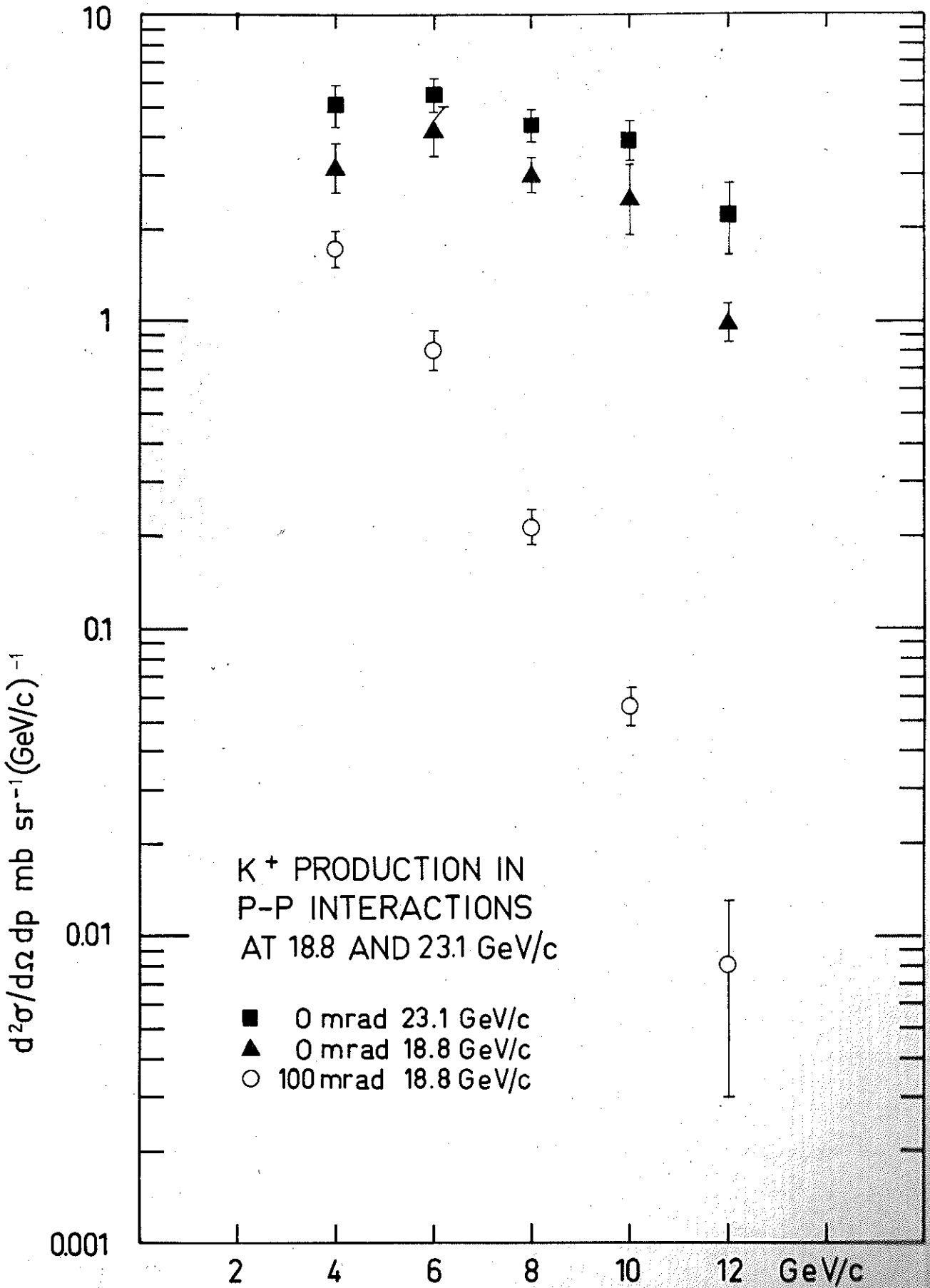

FIG. 11a

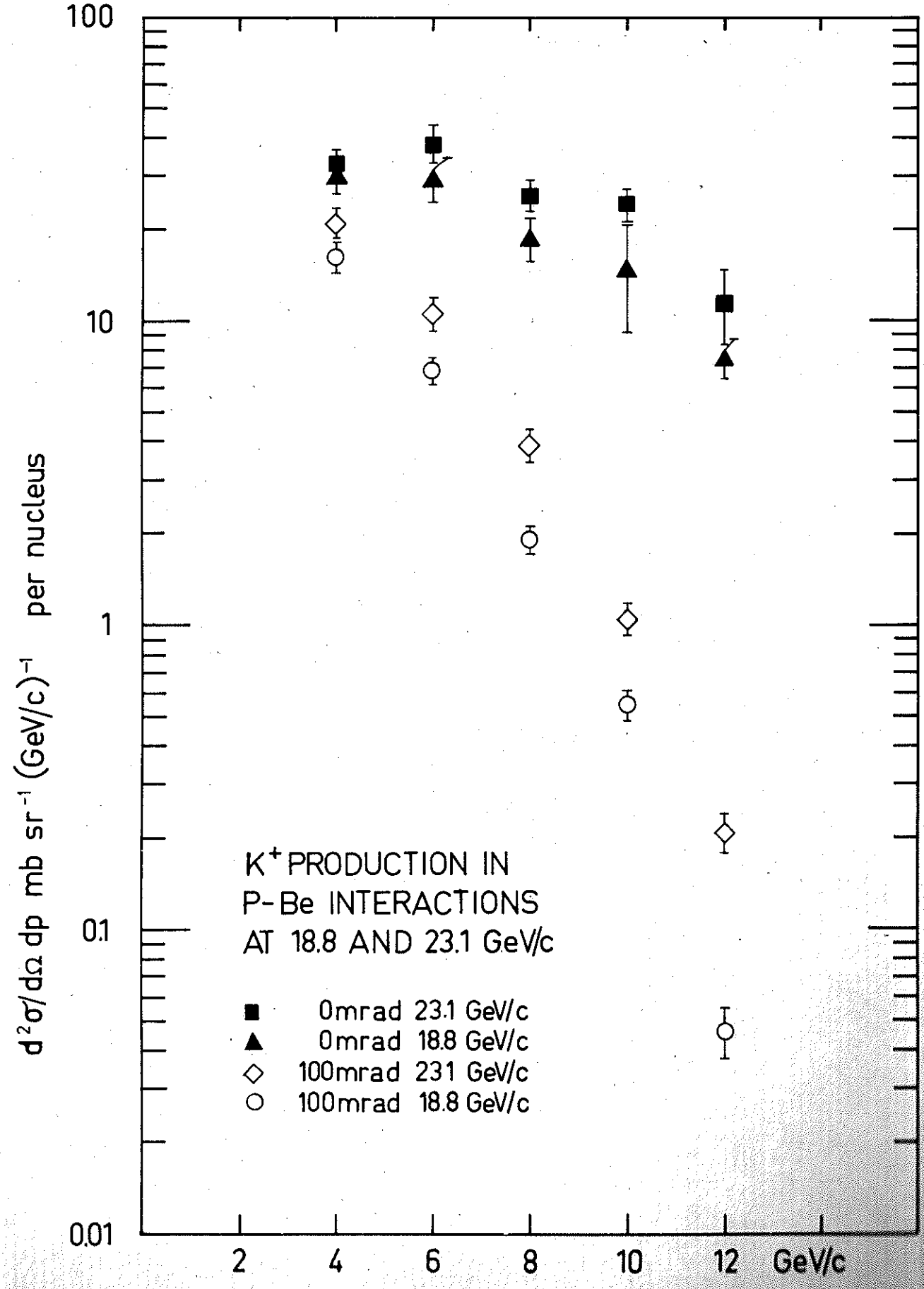

FIG.11b

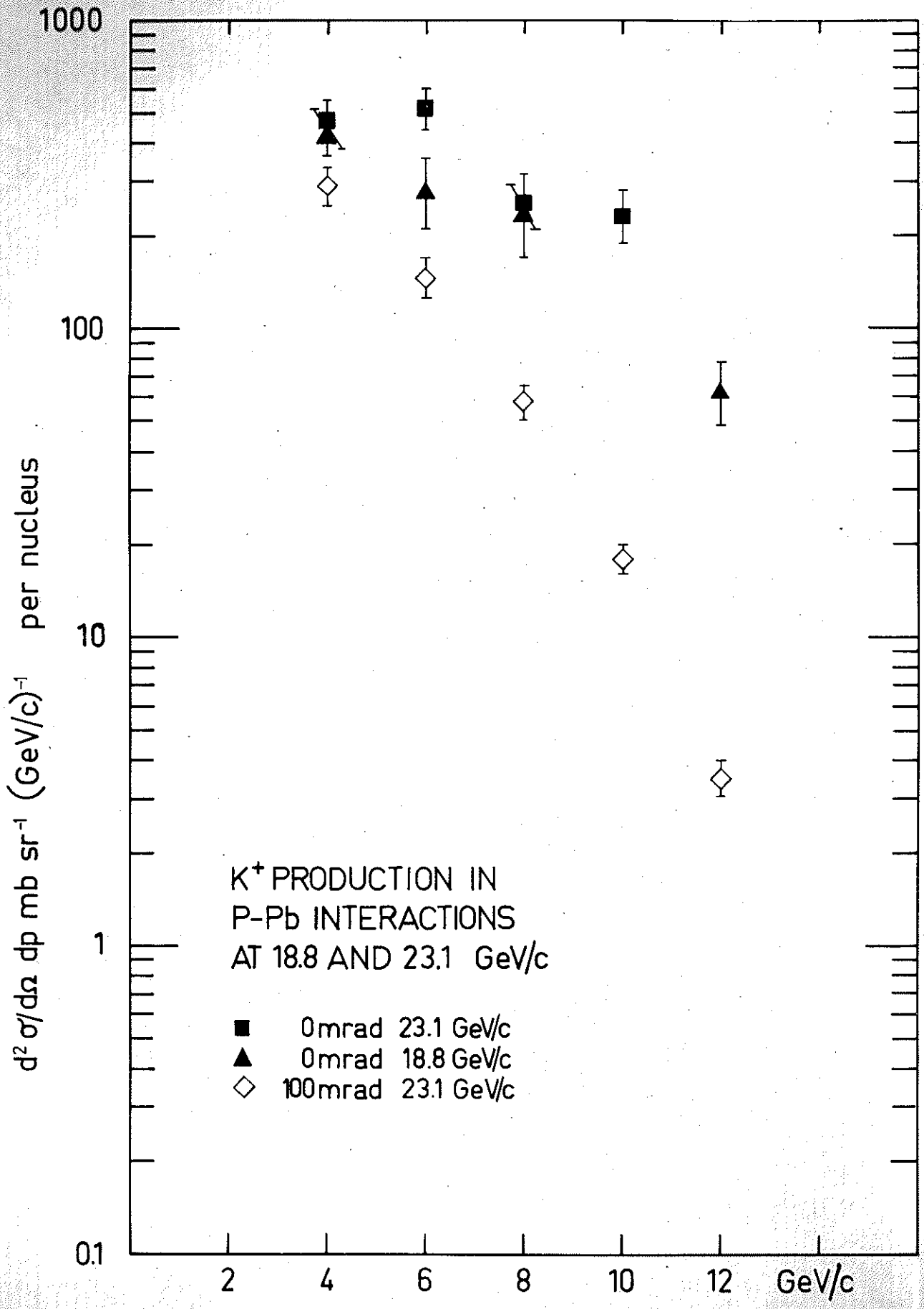
1000
100
10
1
0.1
2
4
6
8
10
12
GeV/c
$d^2\sigma/d\Omega\, dp$ mb sr^{-1} (GeV/c)$^{-1}$ per nucleus
K^+ PRODUCTION IN
P-Pb INTERACTIONS
AT 18.8 AND 23.1 GeV/c
0 mrad 23.1 GeV/c
0 mrad 18.8 GeV/c
100 mrad 23.1 GeV/c

FIG.11c

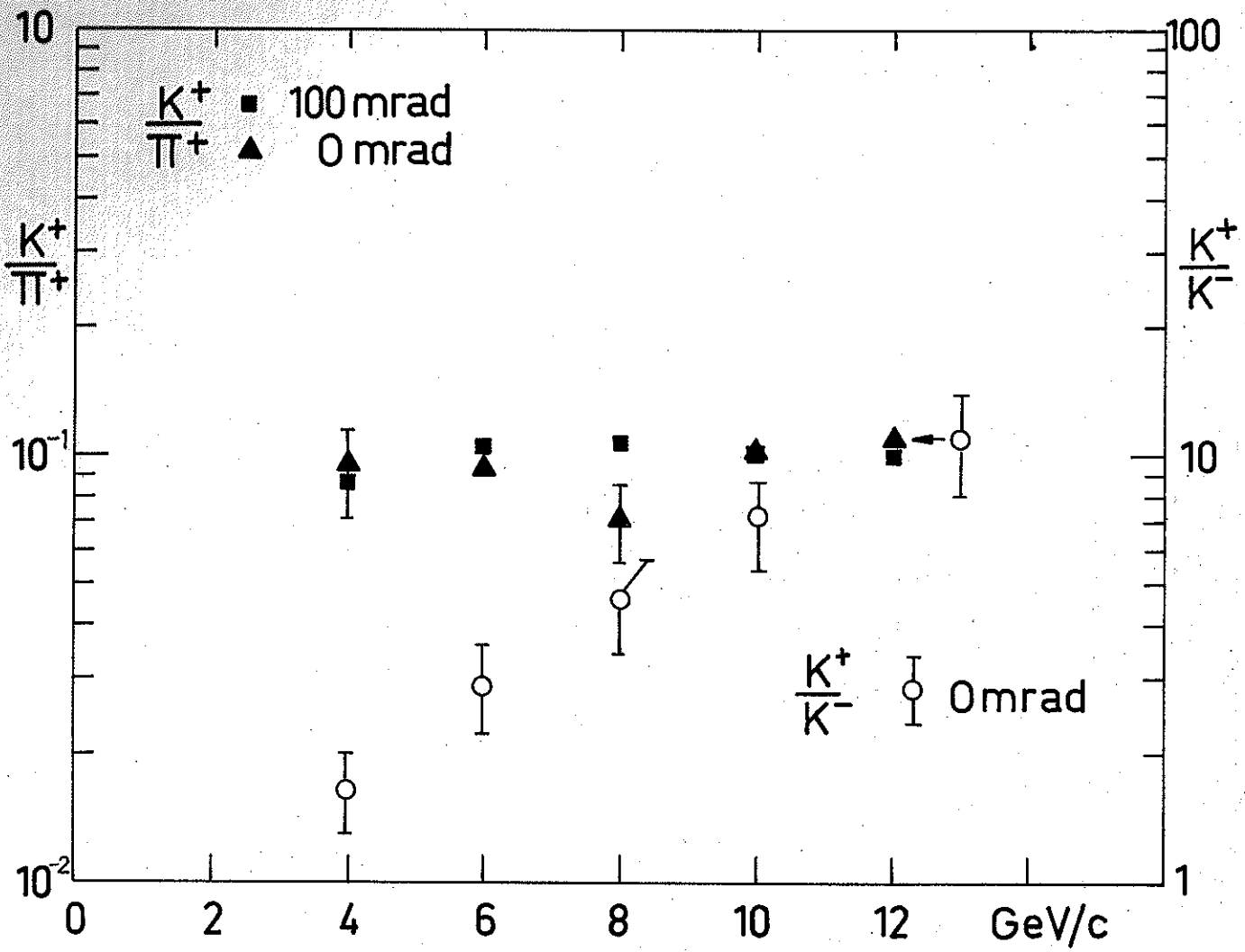
10
10^{-1}
10^{-2}
$\frac{K^+}{\pi^+}$
$\frac{K^+}{\pi^+}$ ■ 100 mrad
▲ 0 mrad
100
10
1
$\frac{K^+}{K^-}$
$\frac{K^+}{K^-}$ 0 mrad
0
2
4
6
8
10
12
GeV/c

FIG. 12

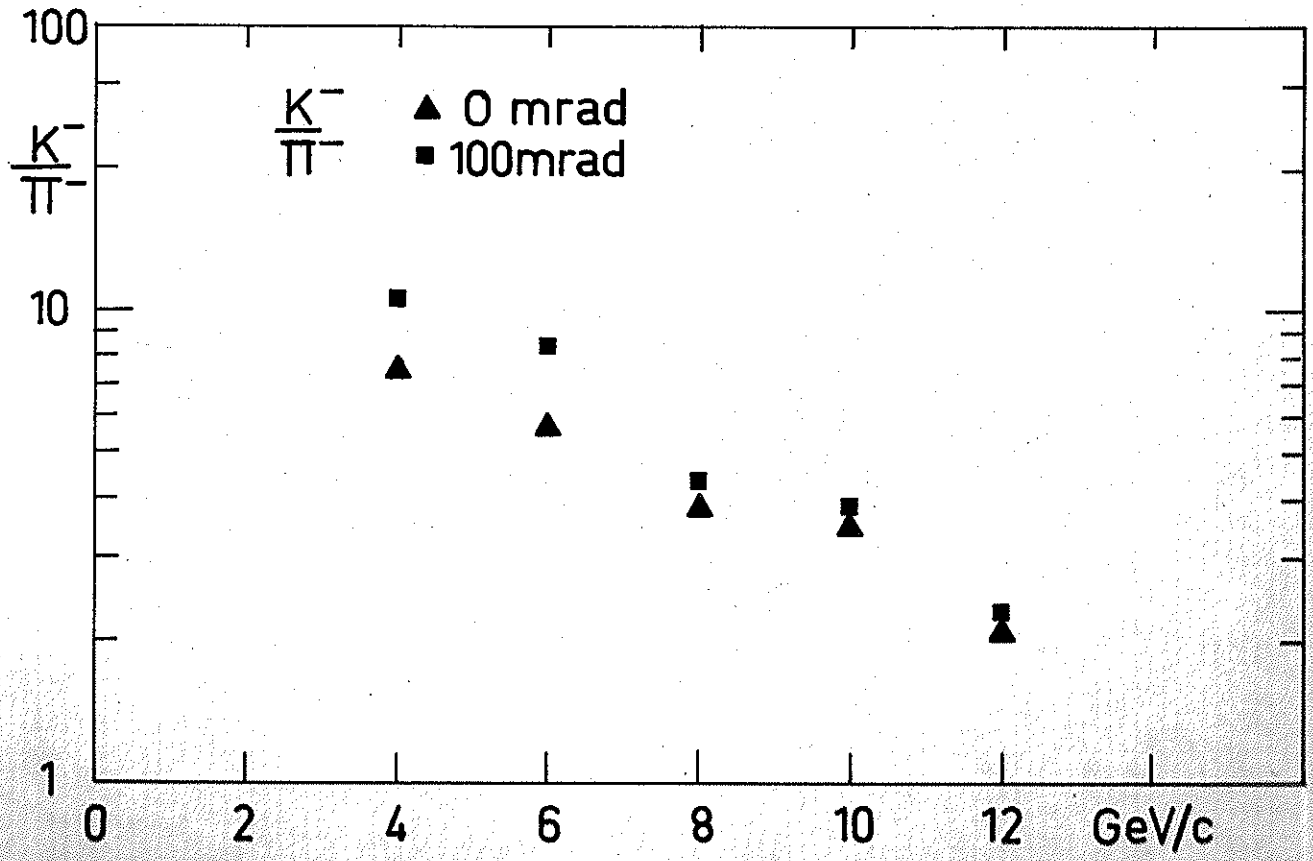
100
10
1
$\frac{K^-}{\pi^-}$
$\frac{K^-}{\pi^-}$ ▲ 0 mrad
■ 100 mrad
0
2
4
6
8
10
12
GeV/c

FIG. 13

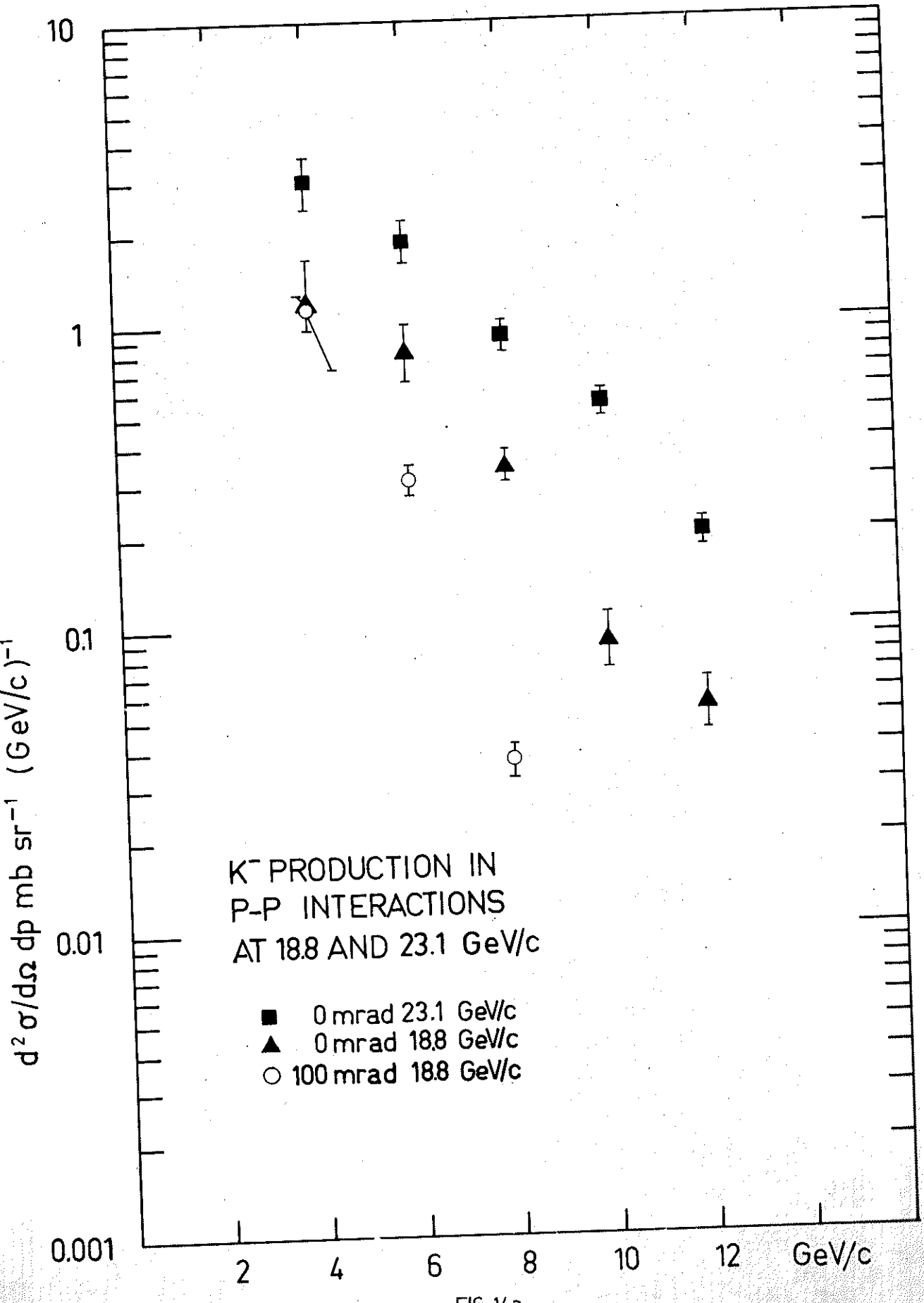

FIG. 14a

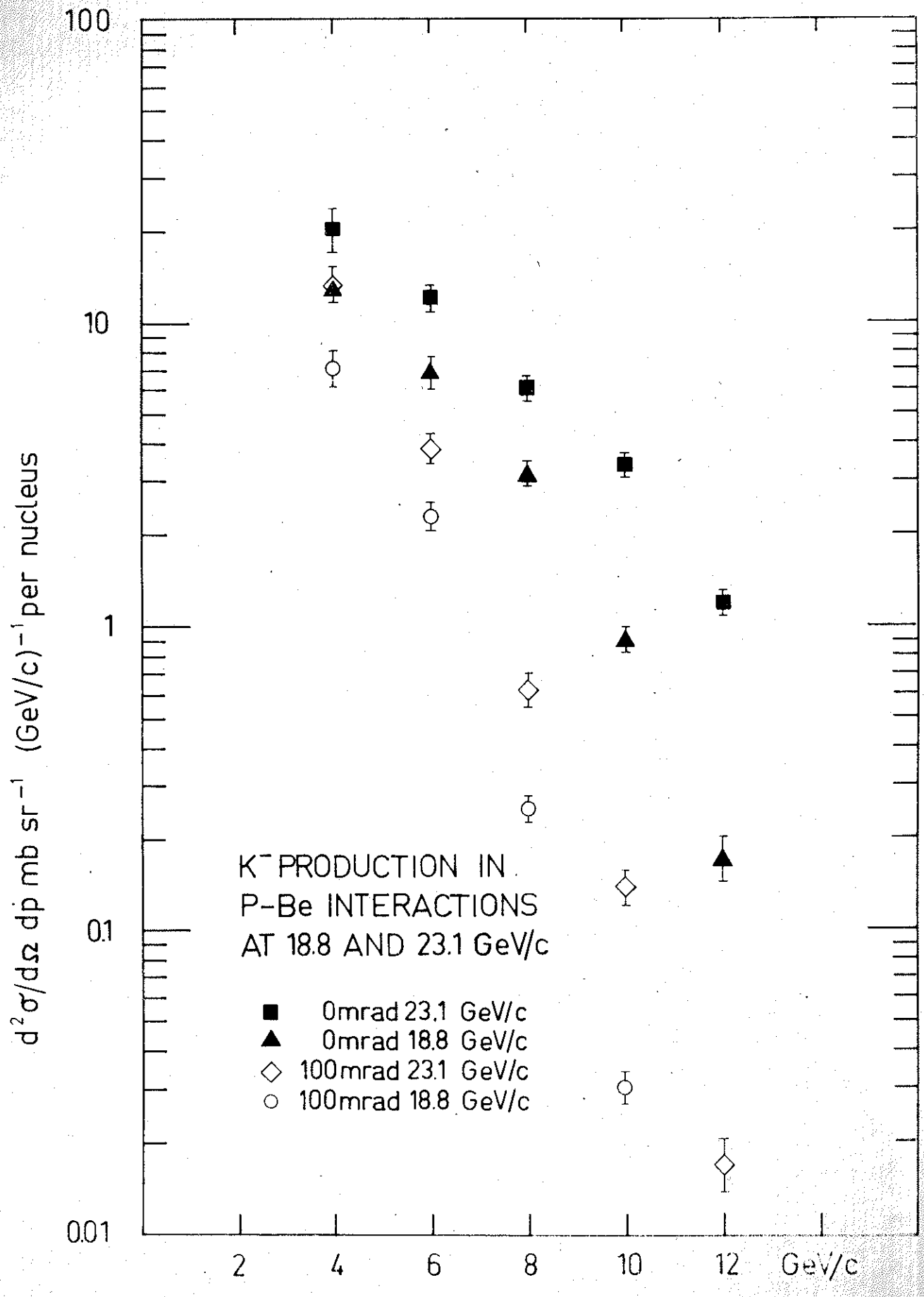

FIG. 14b

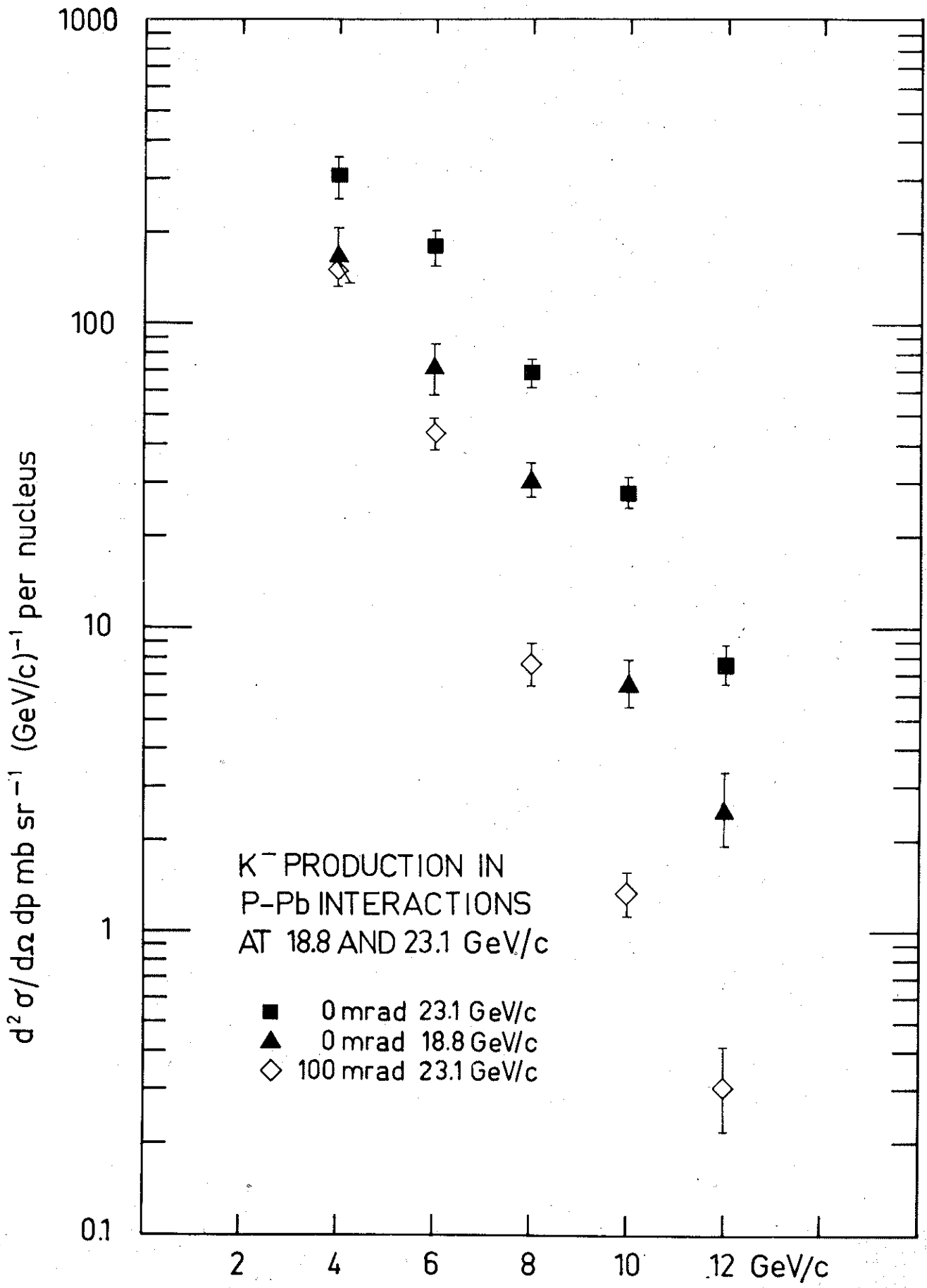

FIG. 14c

DIA - 1986

SIS/R/8558

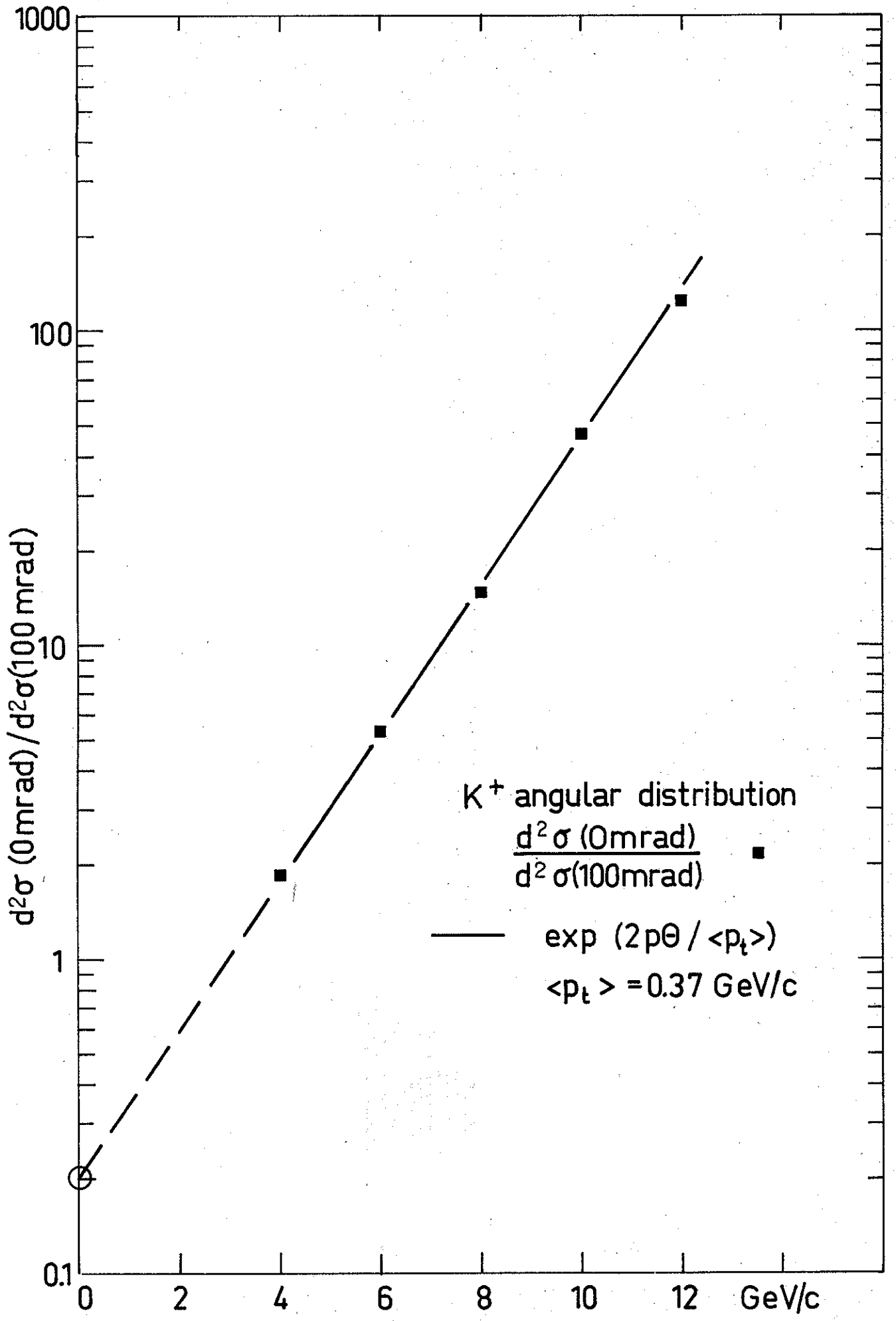

FIG. 15

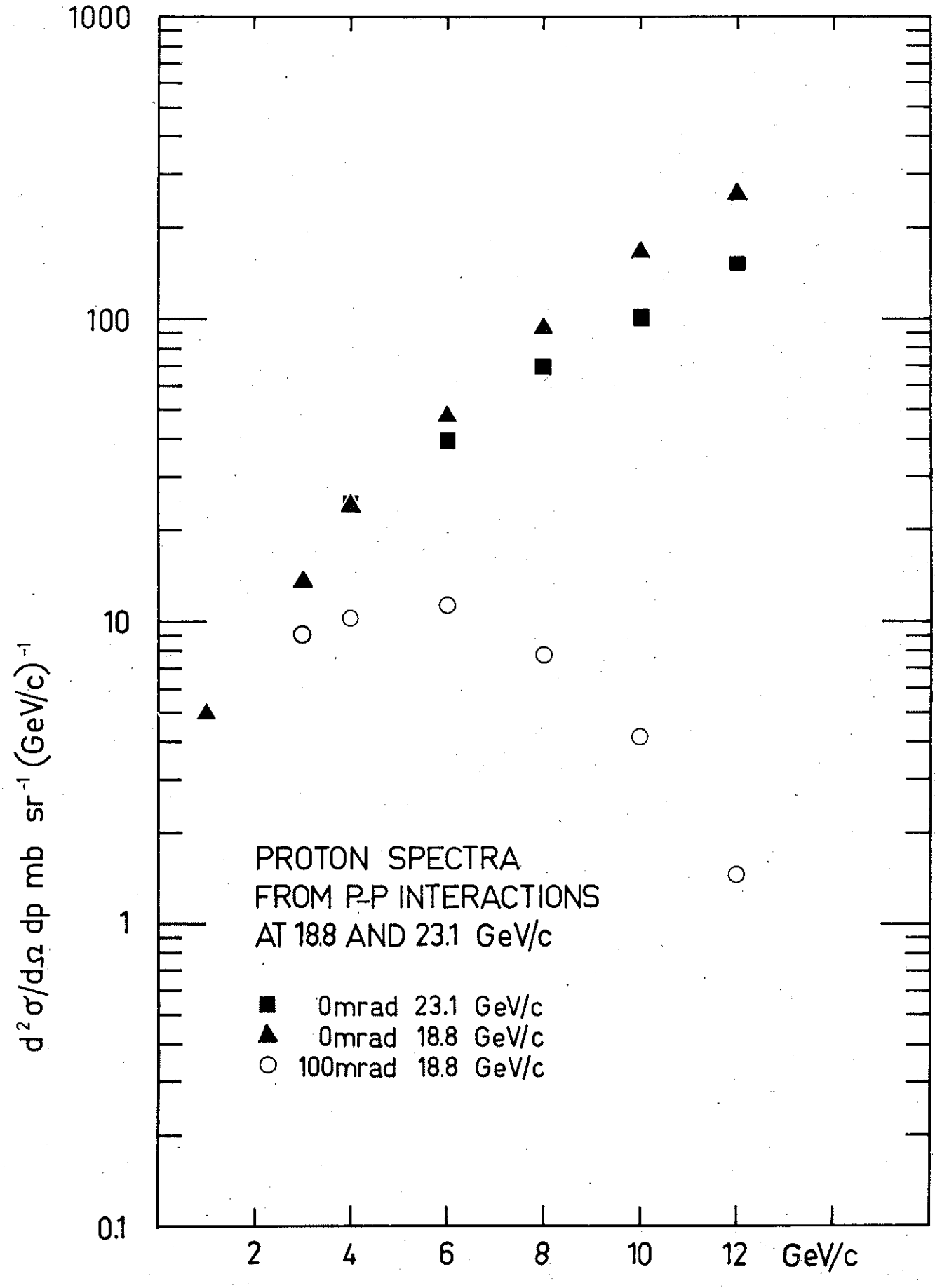

FIG. 16a

DIA - 19861

SIS/R/8557

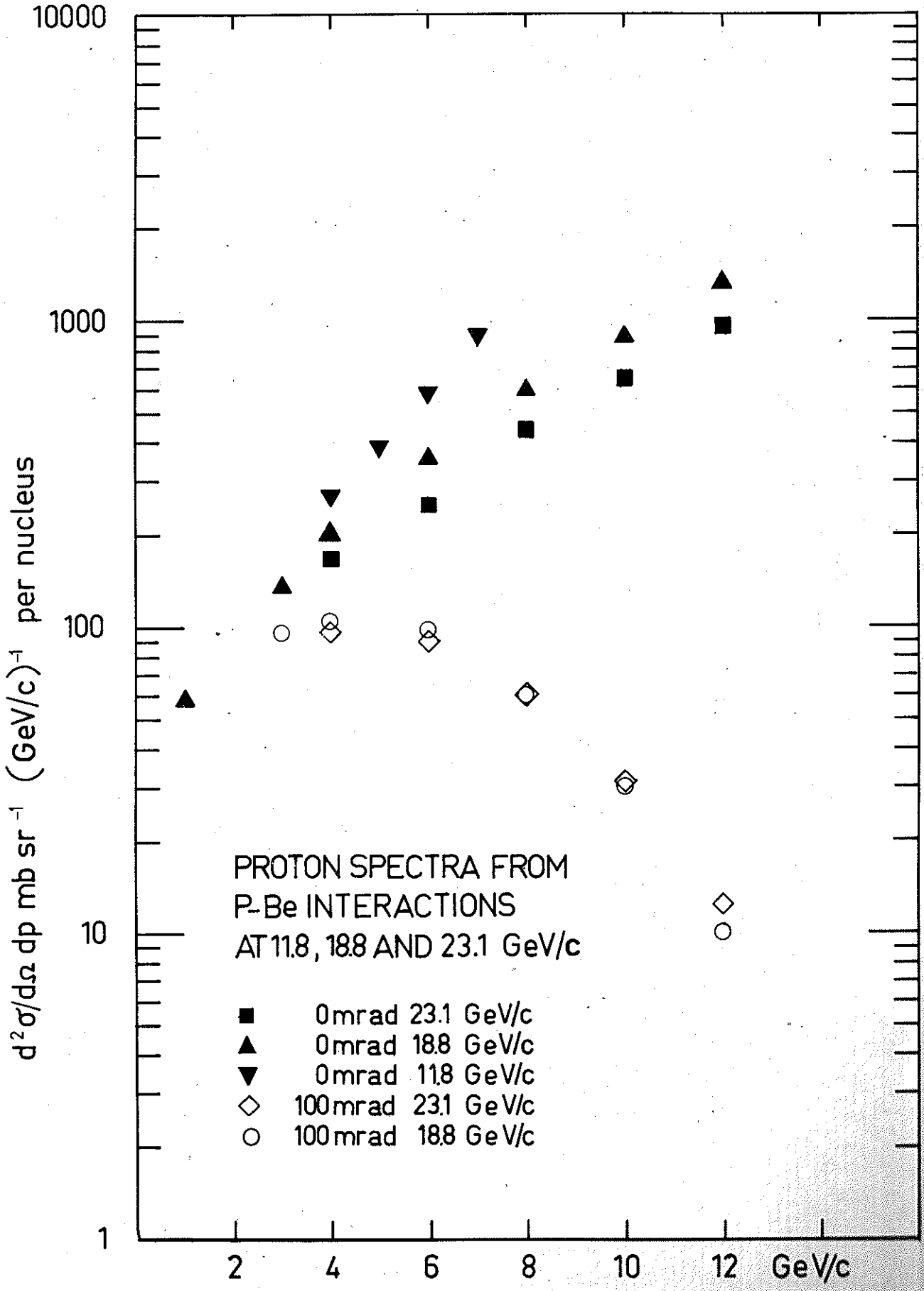

FIG. 16b

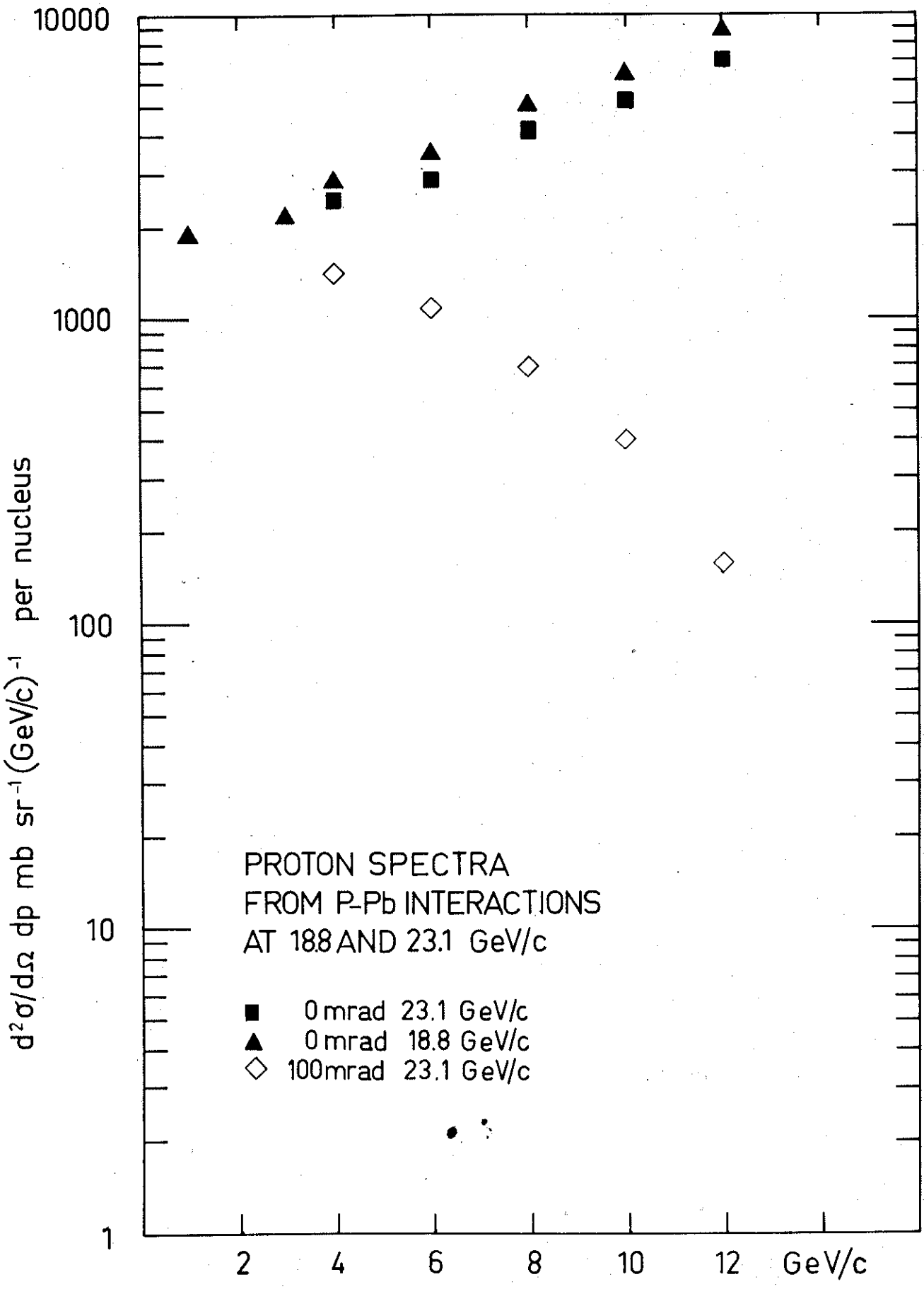

FIG. 16c

DIA - 19859

SIS/R/8554

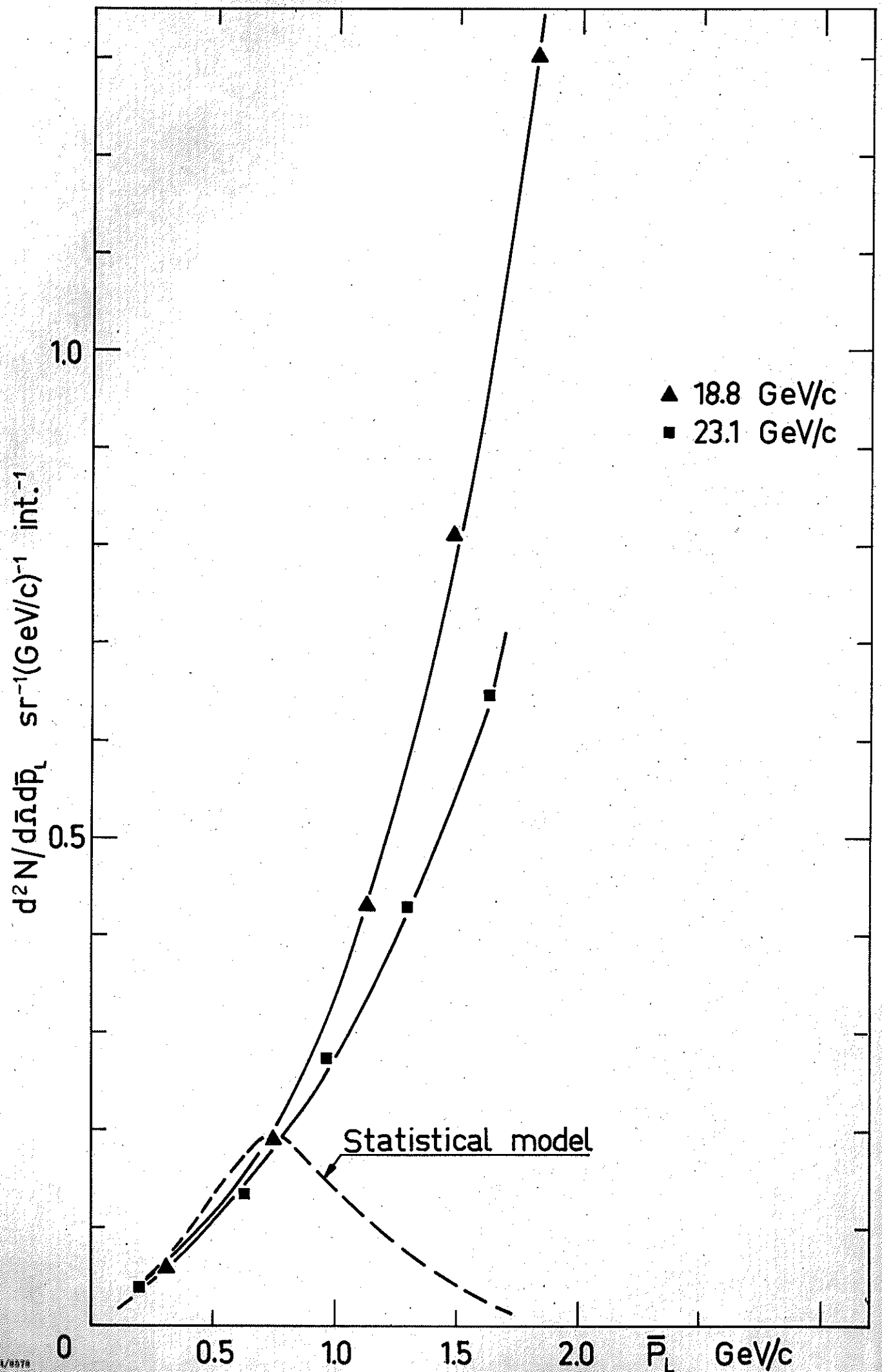
1.0
0.5
0
0.5
1.0
1.5
2.0
$\bar{P}_L$ GeV/c
$d^2N/d\bar{\Omega}d\bar{P}_L$ $sr^{-1}(GeV/c)^{-1}$ int.$^{-1}$
▲ 18.8 GeV/c
■ 23.1 GeV/c
Statistical model

FIG. 17

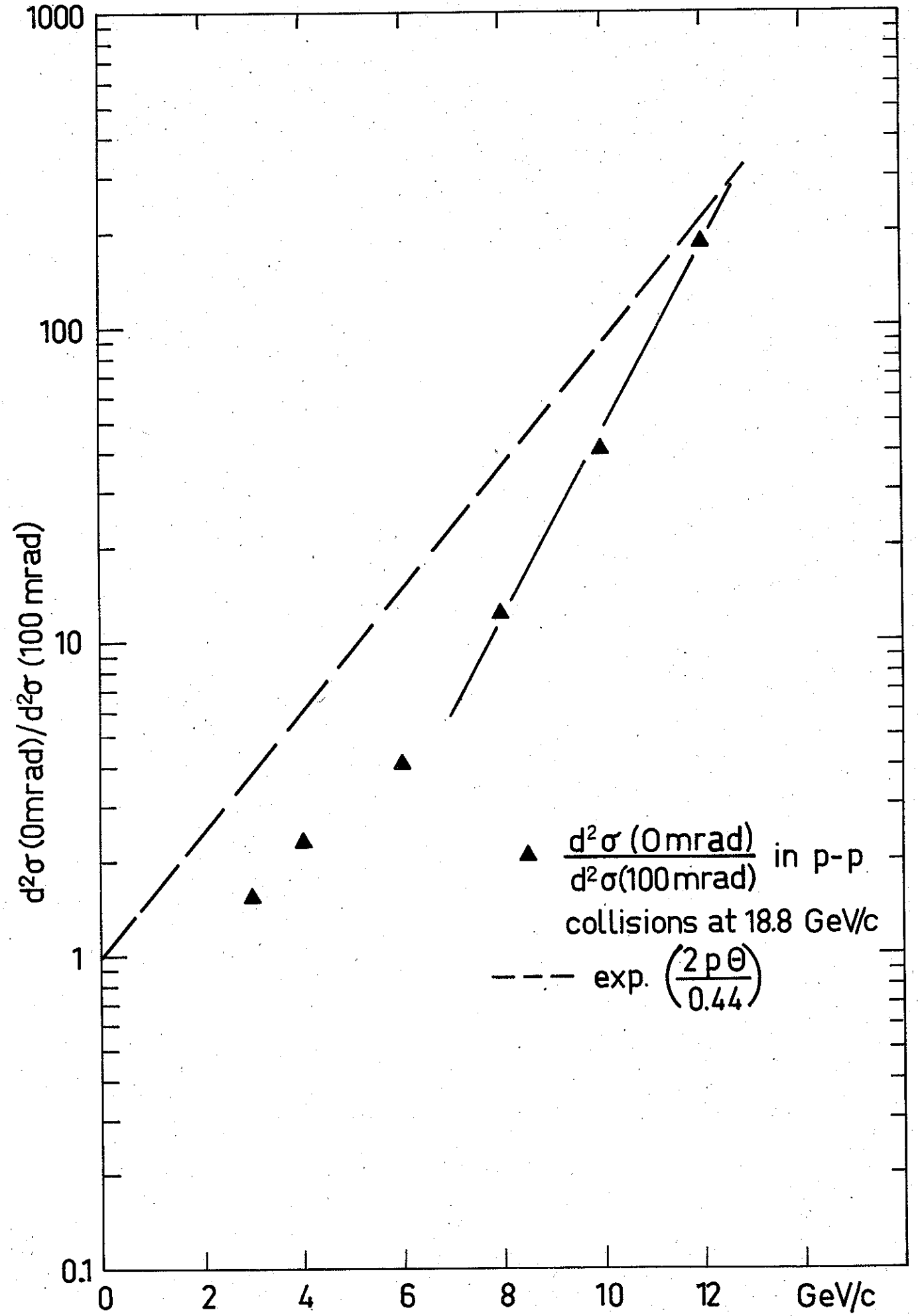
1000
100
10
1
0.1
0
2
4
6
8
10
12
GeV/c
$d^2\sigma$ (0mrad)/$d^2\sigma$ (100 mrad)
$\frac{d^2\sigma\,(0\,mrad)}{d^2\sigma(100\,mrad)}$ in p-p
collisions at 18.8 GeV/c
exp. $\left(\frac{2\,p\,\Theta}{0.44}\right)$

FIG. 18

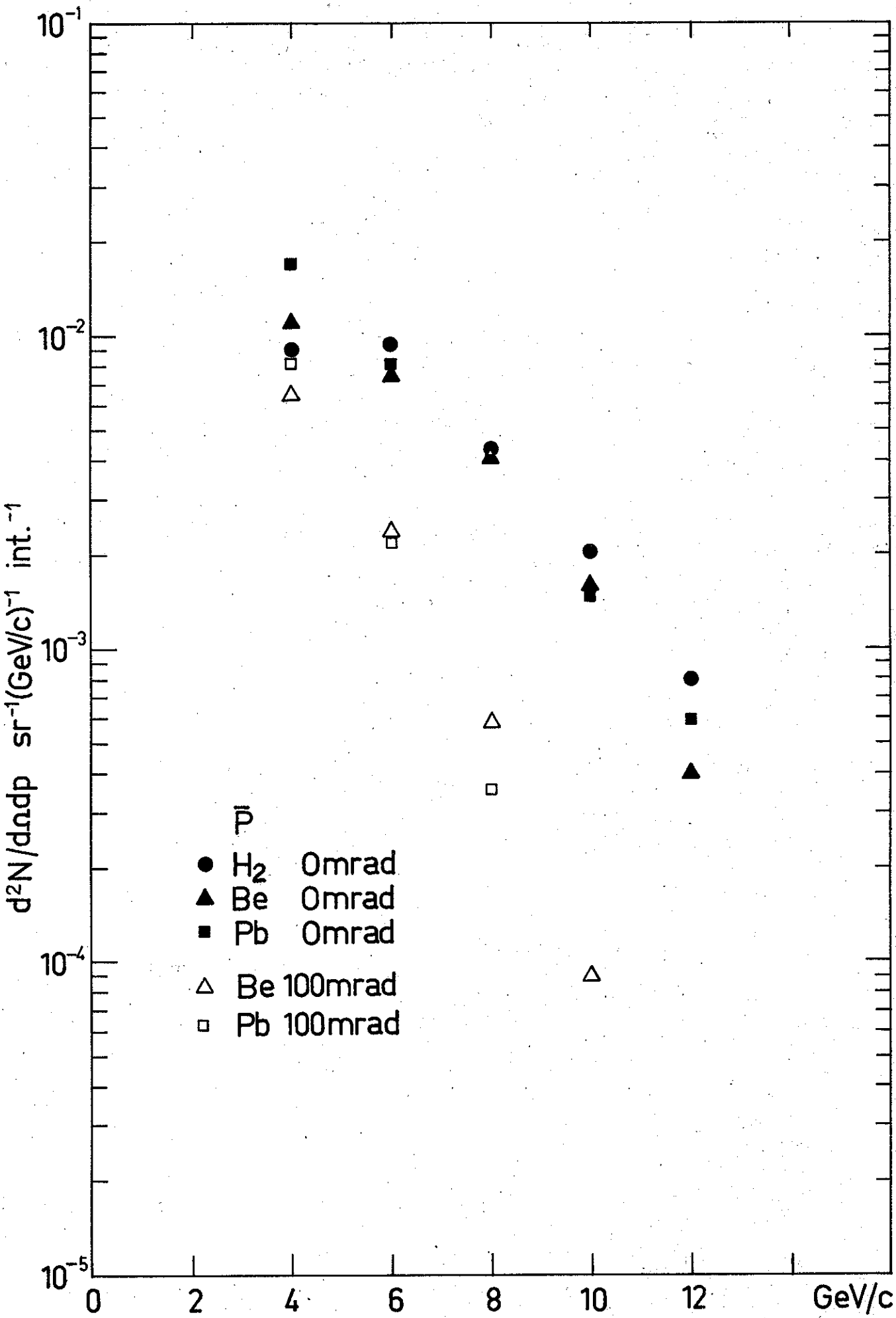
10^{-1}
10^{-2}
10^{-3}
10^{-4}
10^{-5}
$d^2N/d\Omega dp$ sr^{-1}(GeV/c)$^{-1}$ int.$^{-1}$
0
2
4
6
8
10
12
GeV/c
$\vec{P}$
H_2 0mrad
Be 0mrad
Pb 0mrad
Be 100mrad
Pb 100mrad

FIG. 19

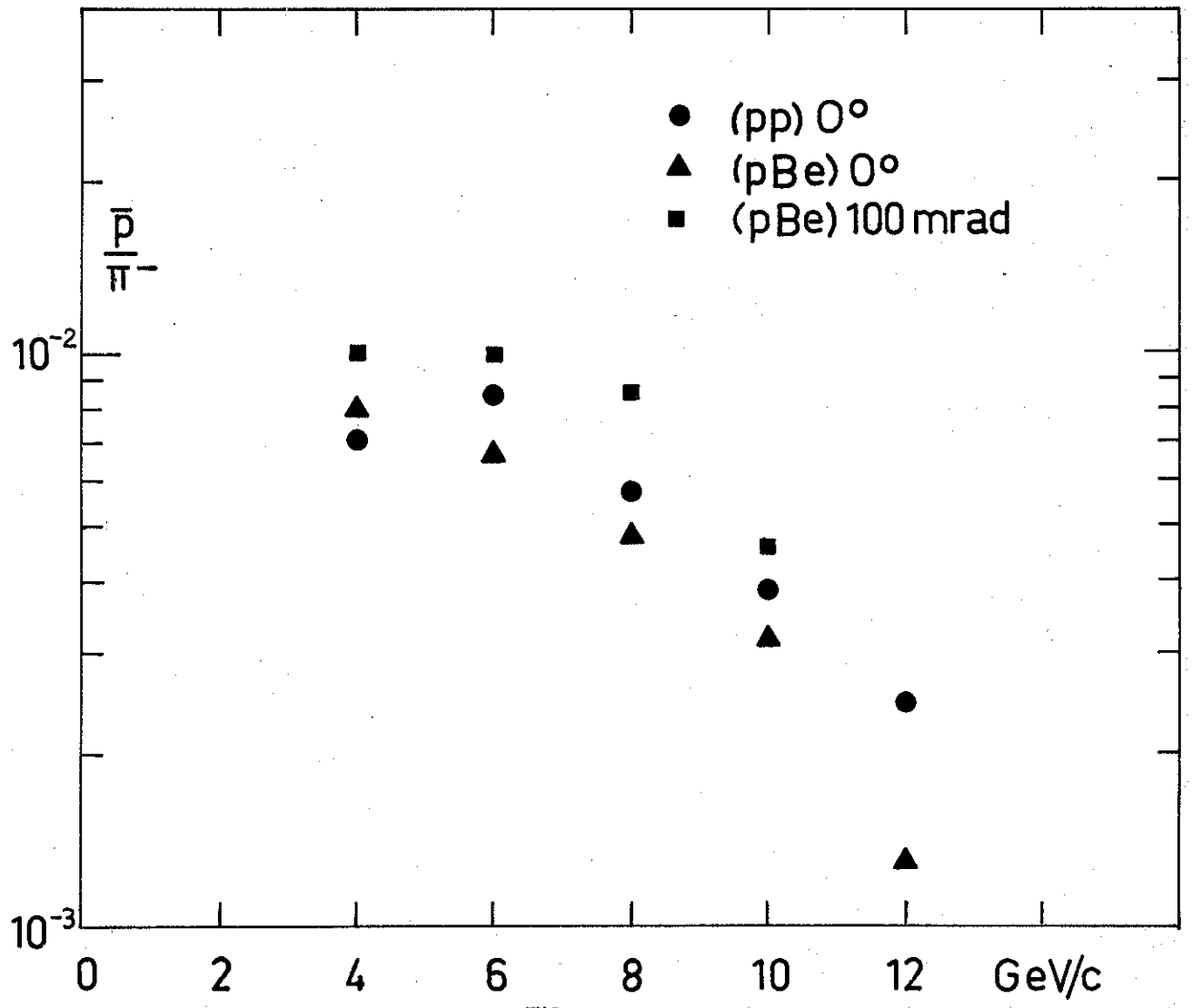

FIG. 20

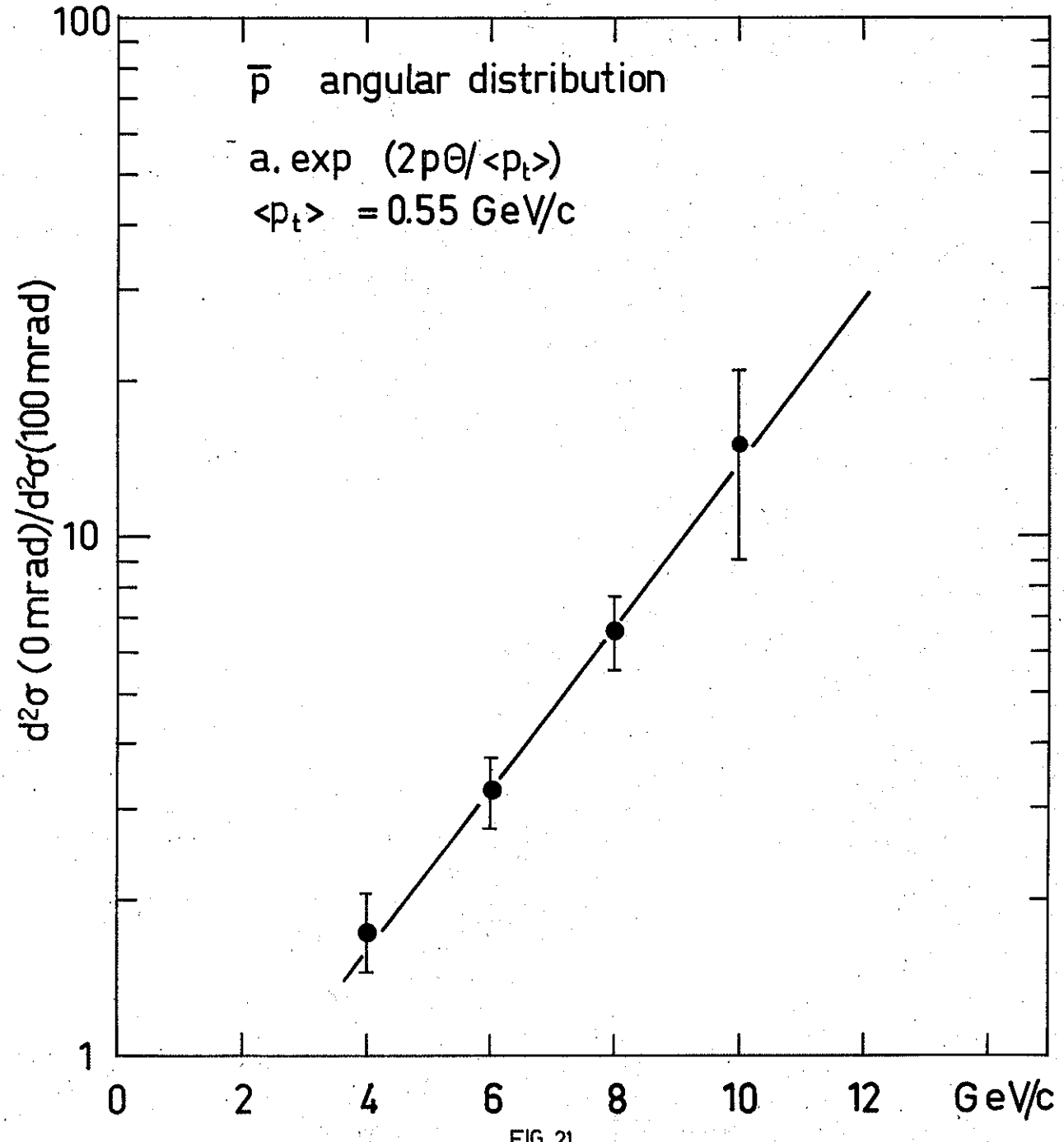
$\bar{p}$ angular distribution
a. exp $(2p\Theta/\langle p_t \rangle)$
$\langle p_t \rangle$ = 0.55 GeV/c
$d^2\sigma$ (0 mrad)/$d^2\sigma$(100 mrad)
100
10
1
0
2
4
6
8
10
12
GeV/c

FIG. 21

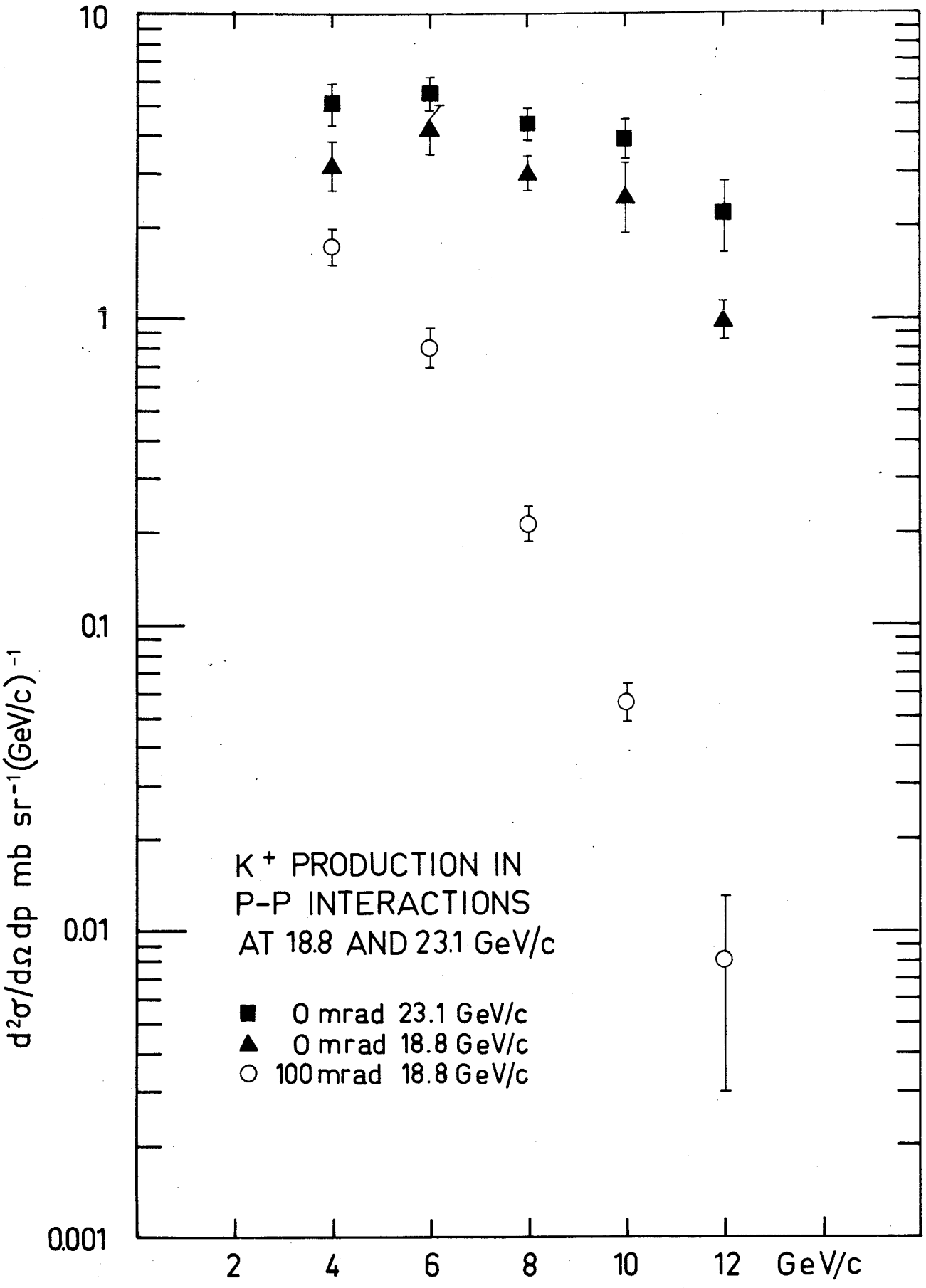

FIG. 11a

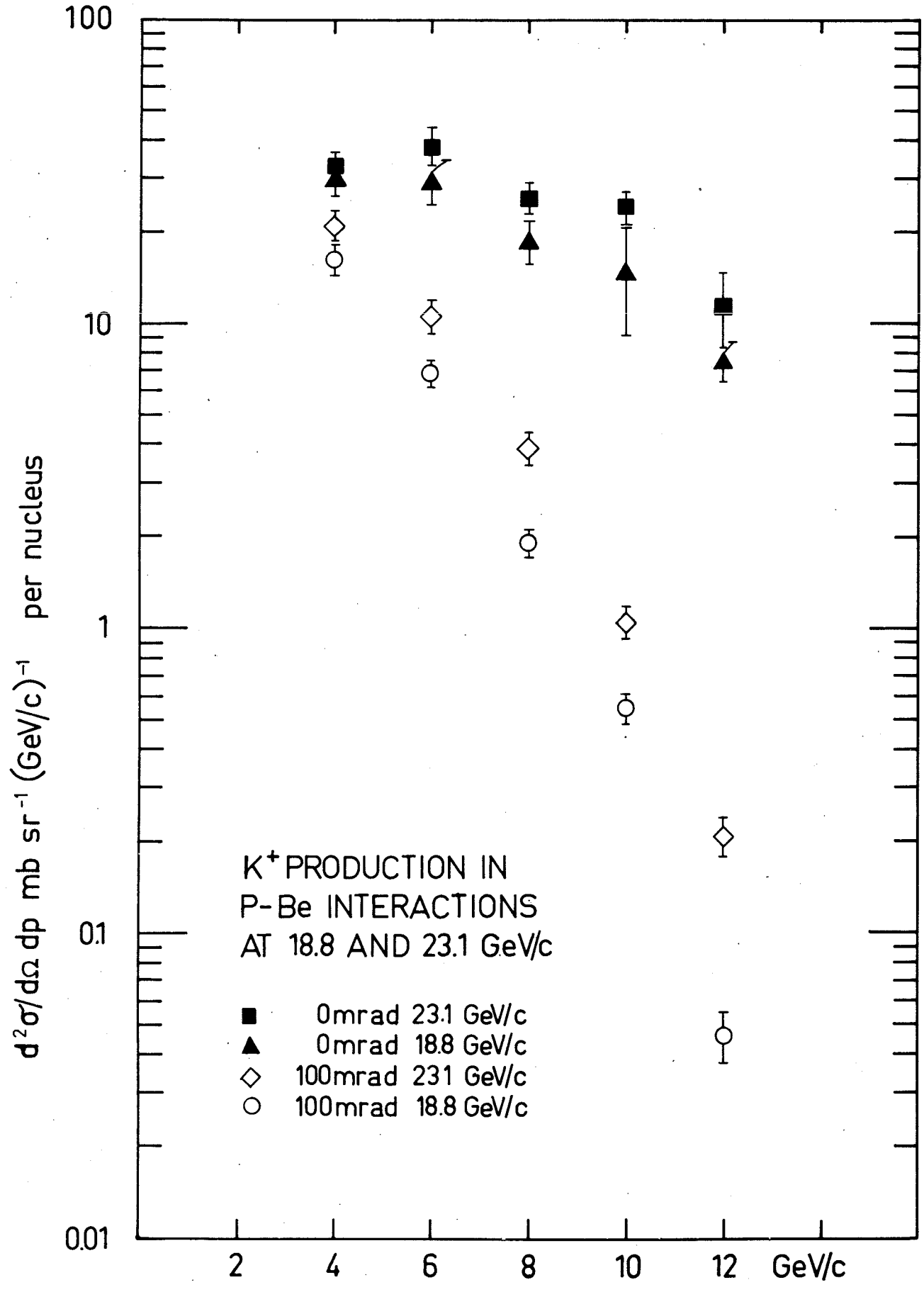

FIG.11b

DIA - 19855

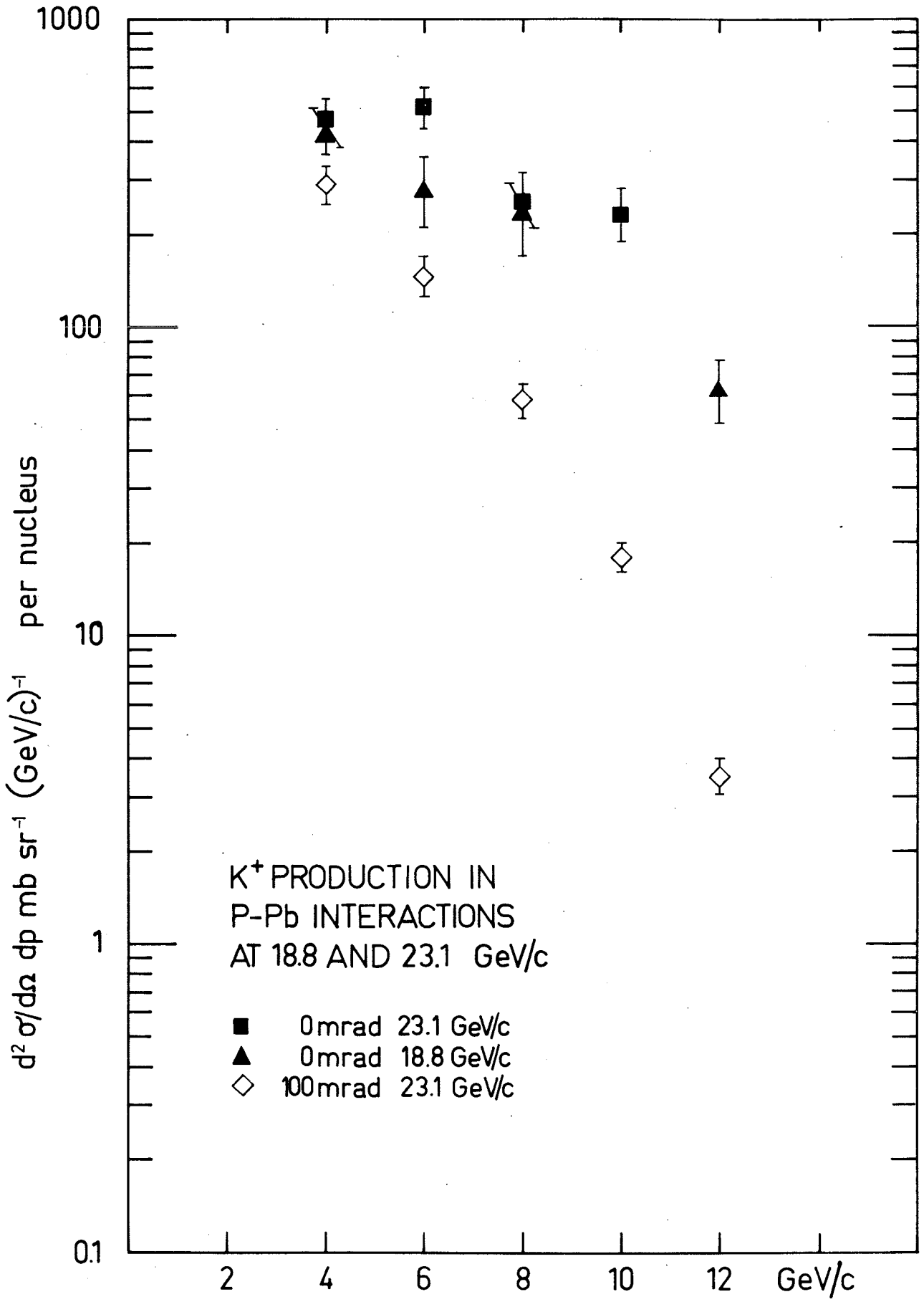

FIG.11c

DIA - 11560

SIS/R/8560

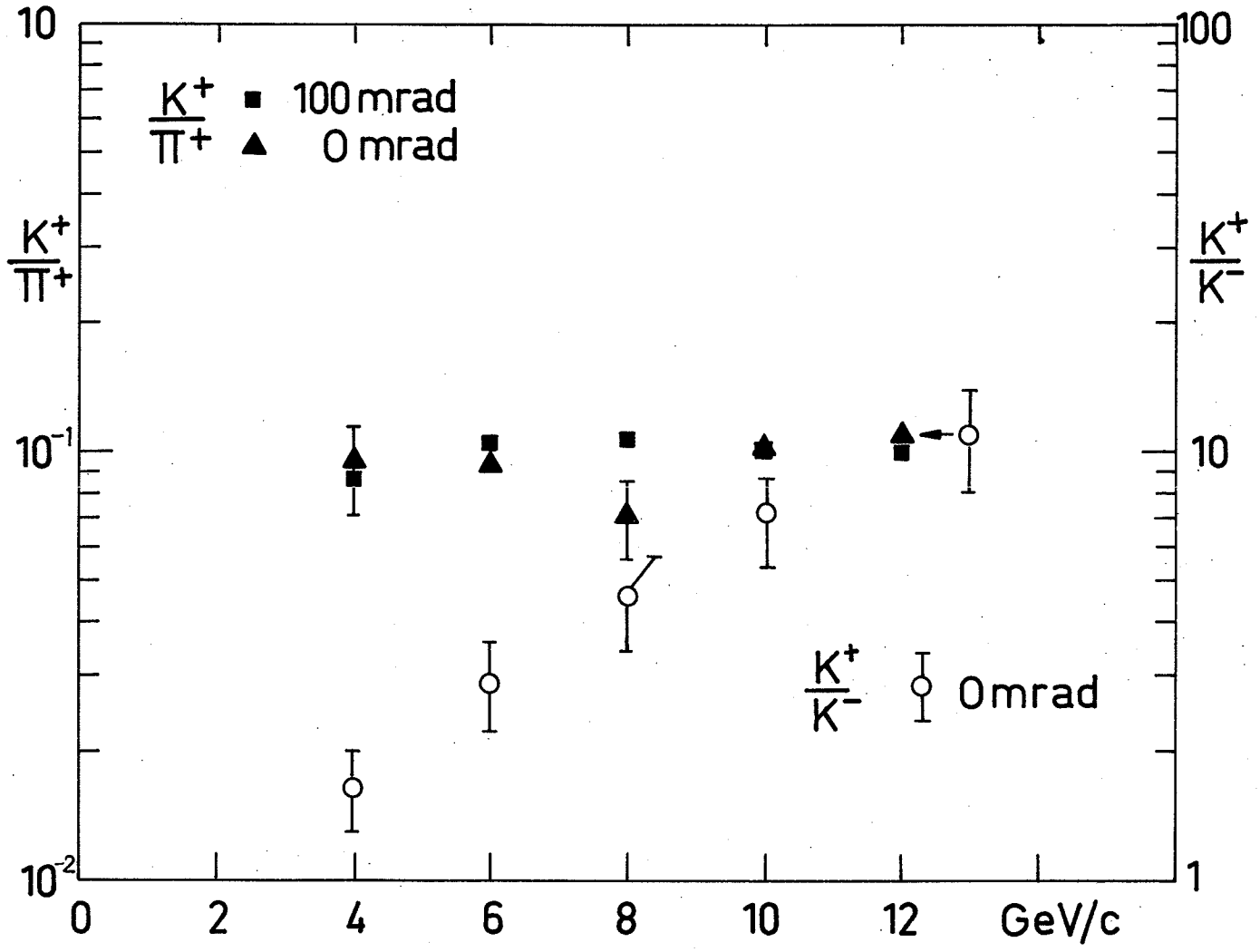
10
100
$\frac{K^+}{\pi^+}$ ■ 100 mrad
▲ 0 mrad
$\frac{K^+}{\pi^+}$
$\frac{K^+}{K^-}$
10^{-1}
10
$\frac{K^+}{K^-}$ 0 mrad
10^{-2}
1
0 2 4 6 8 10 12 GeV/c

FIG. 12

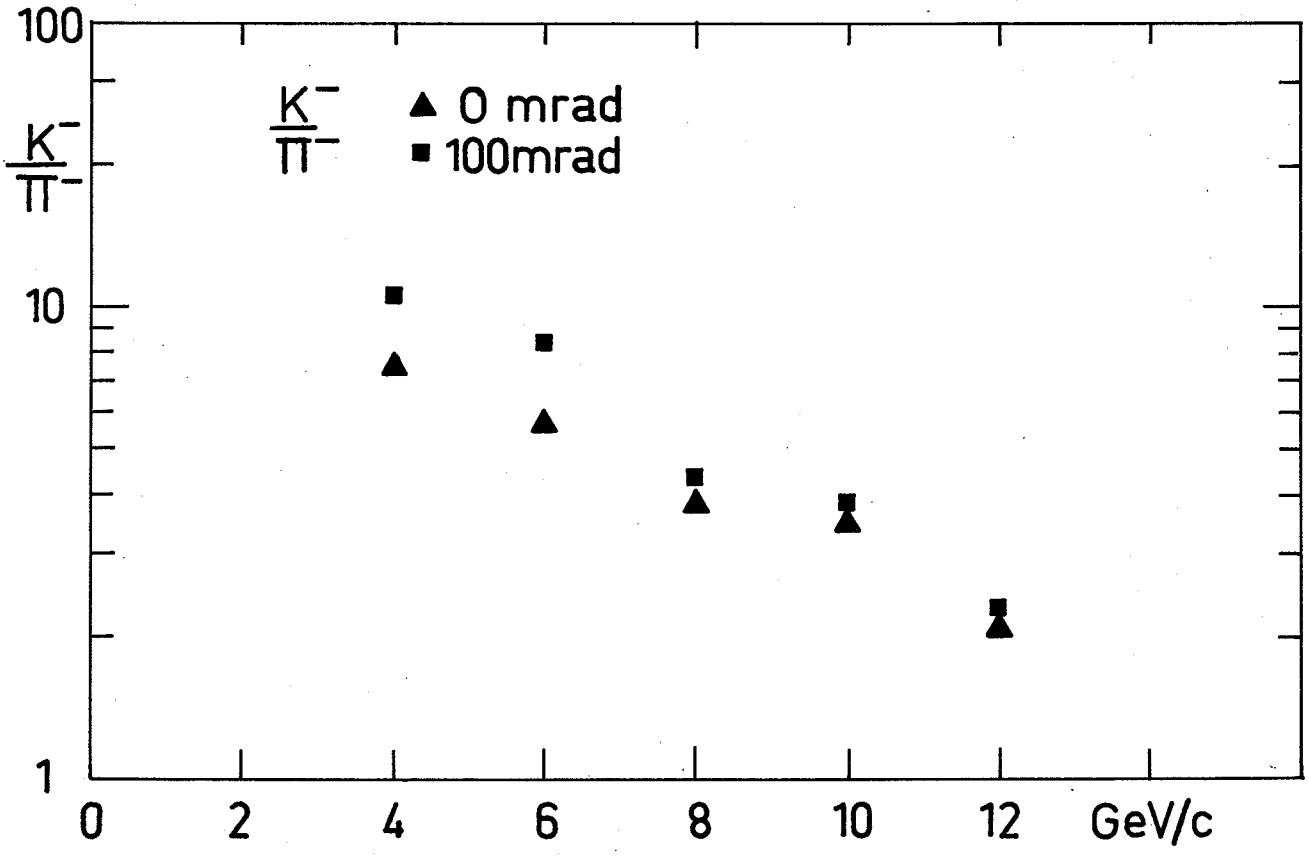
100
$\frac{K^-}{\pi^-}$
▲ 0 mrad
■ 100 mrad
10
1
0 2 4 6 8 10 12 GeV/c

FIG. 13

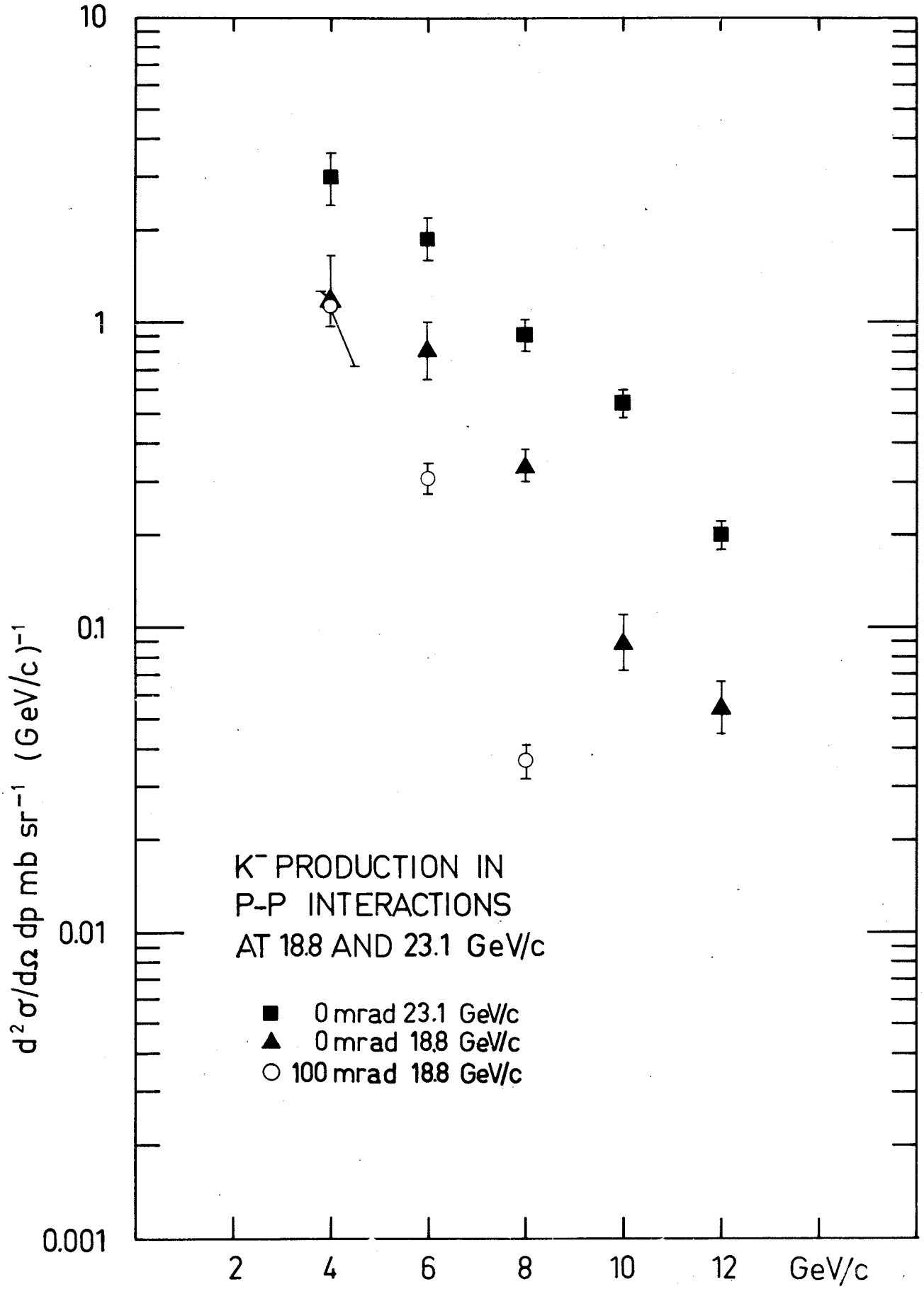

FIG. 14a

DIA - 19860

SIS/R/8561

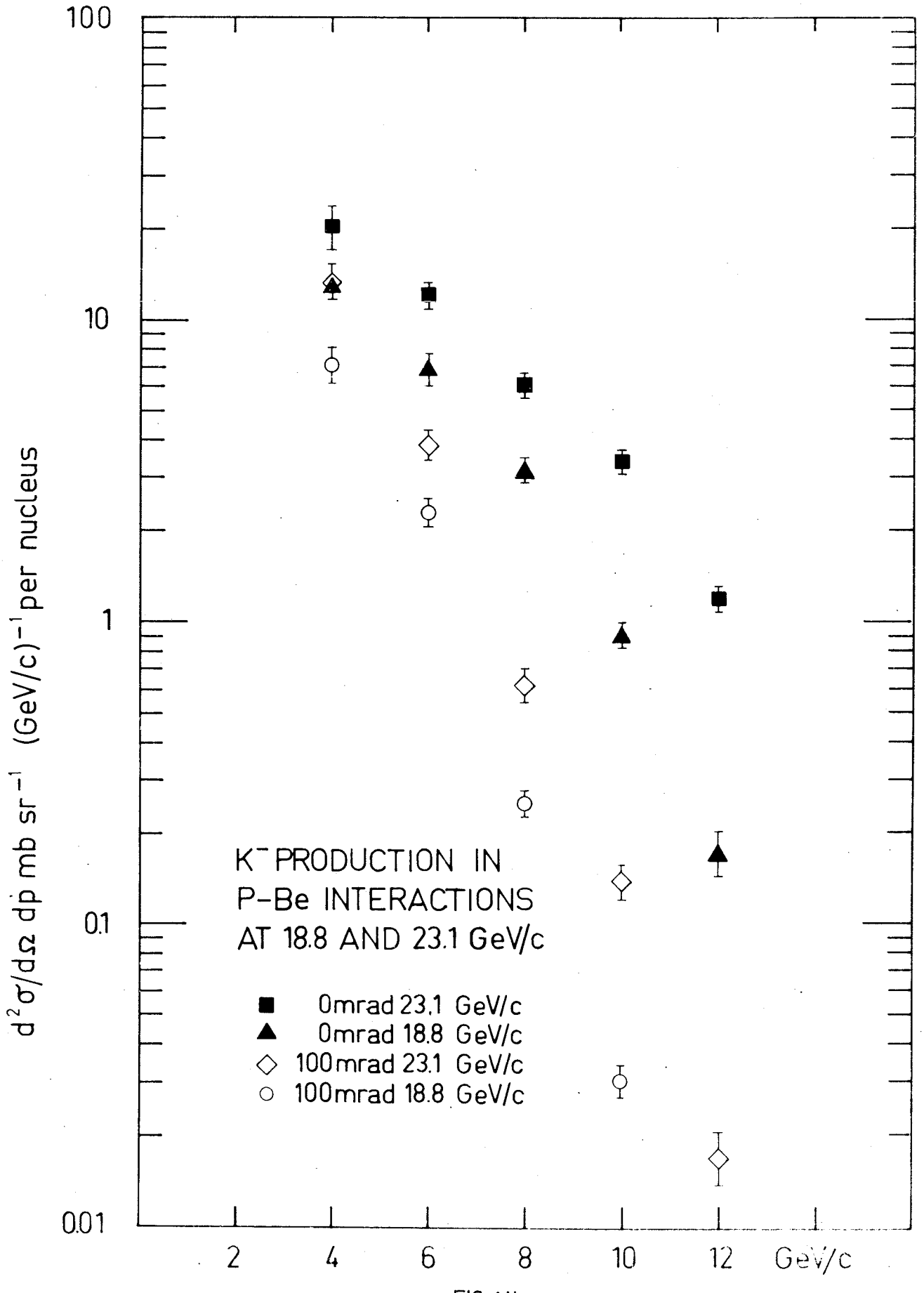

FIG. 14b

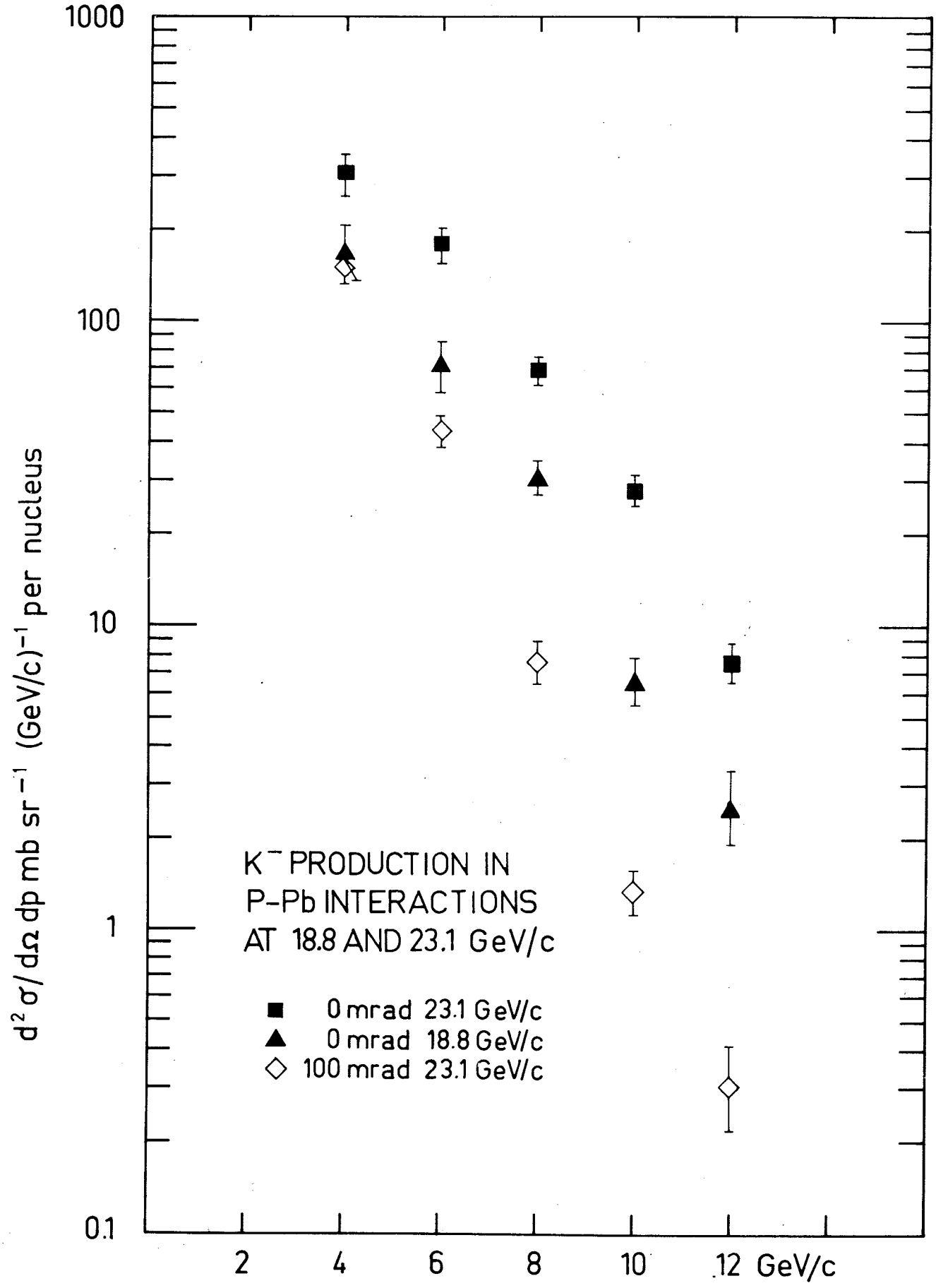

FIG. 14c

D/A - 1986

SIS/R/8558

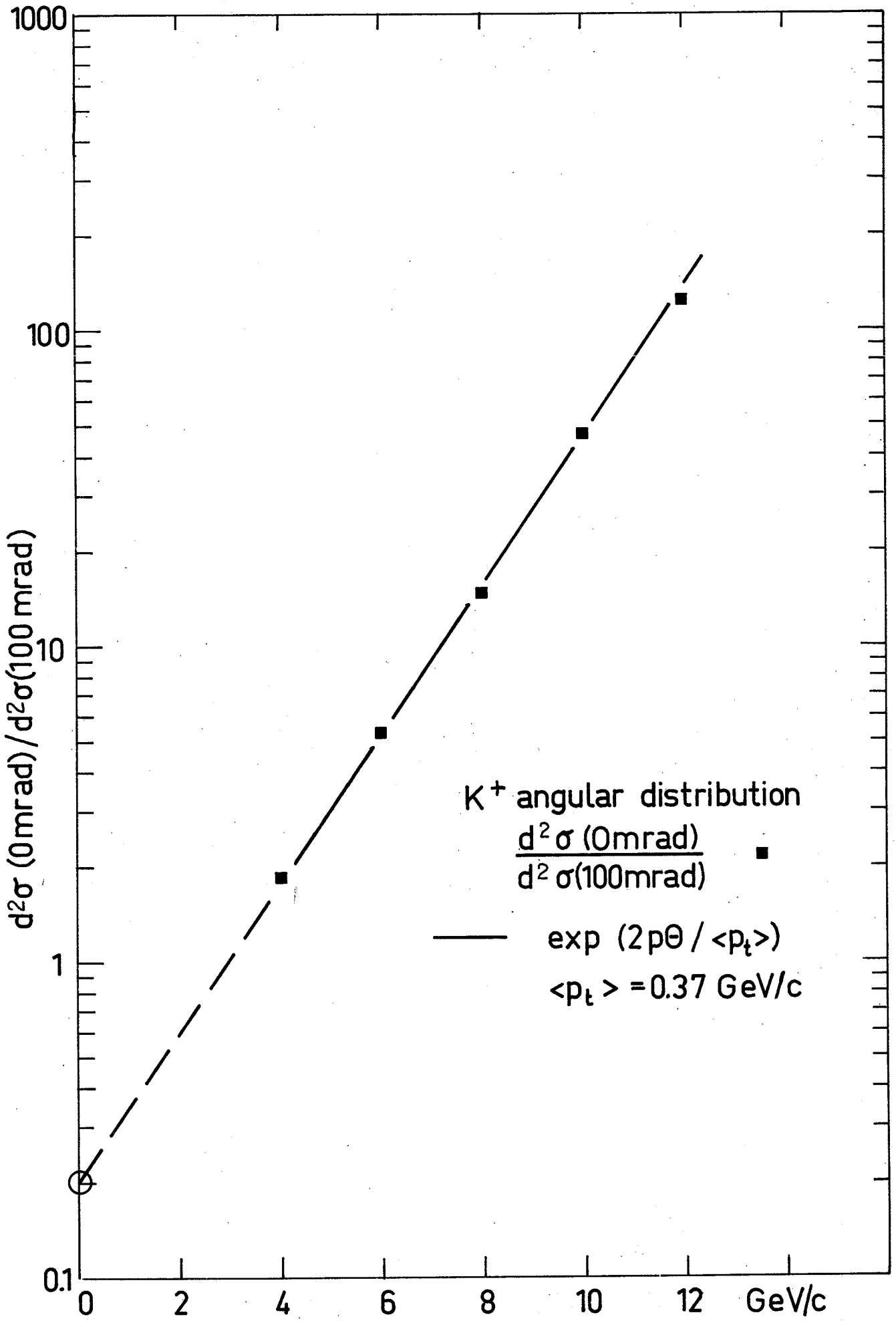

FIG. 15

SIS/R/8575

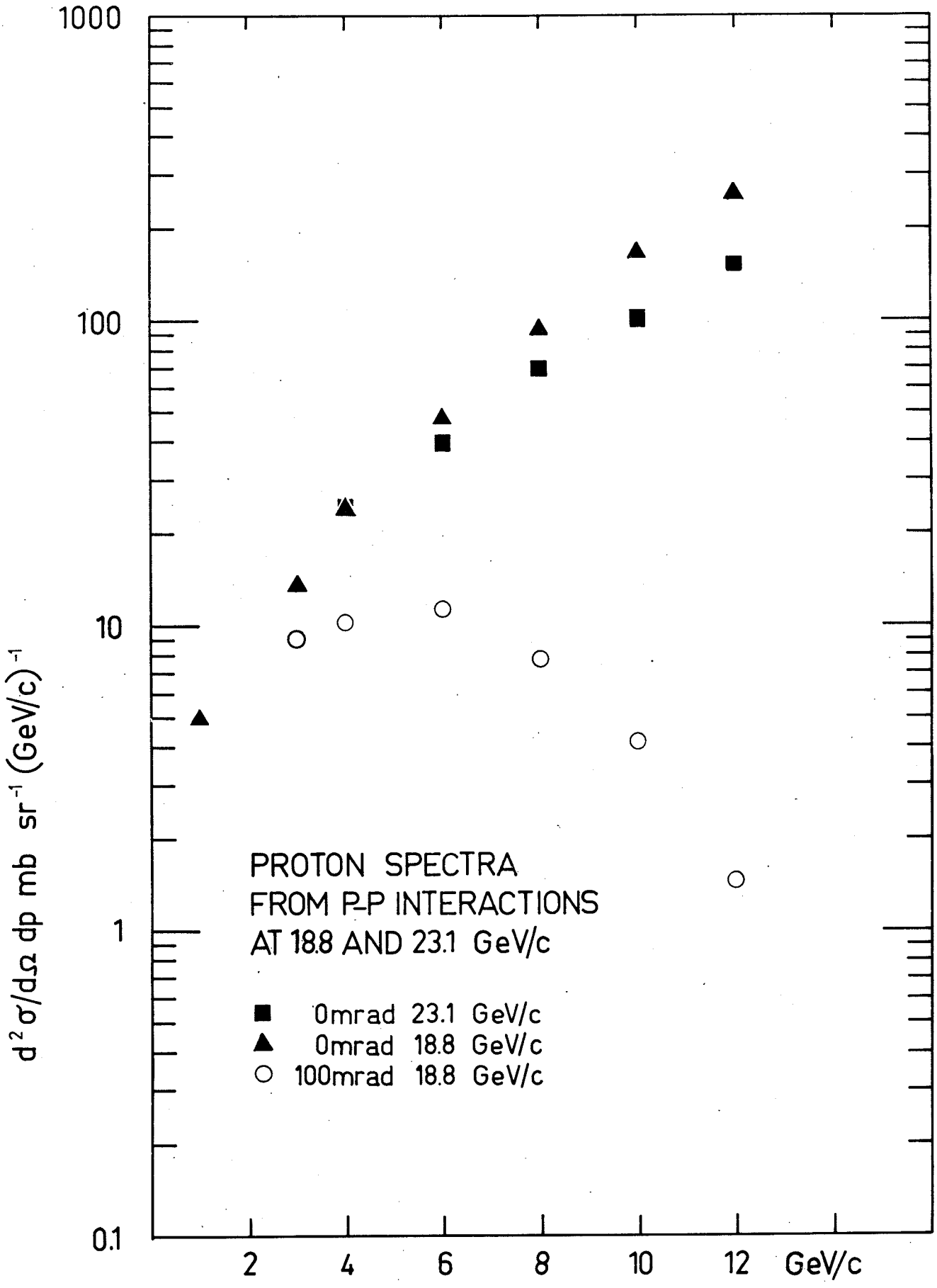

FIG. 16a

DIA - 19861

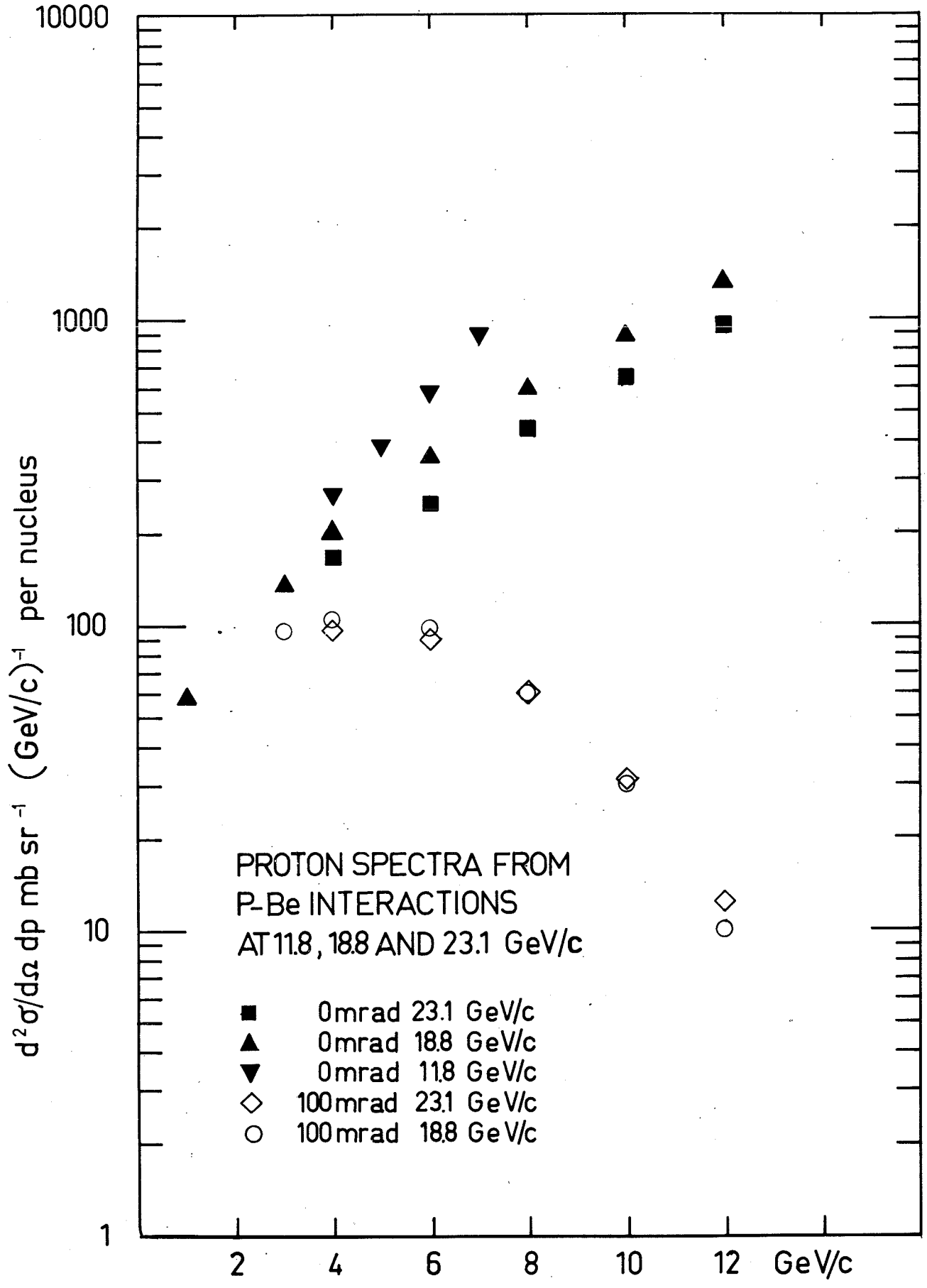

FIG. 16b

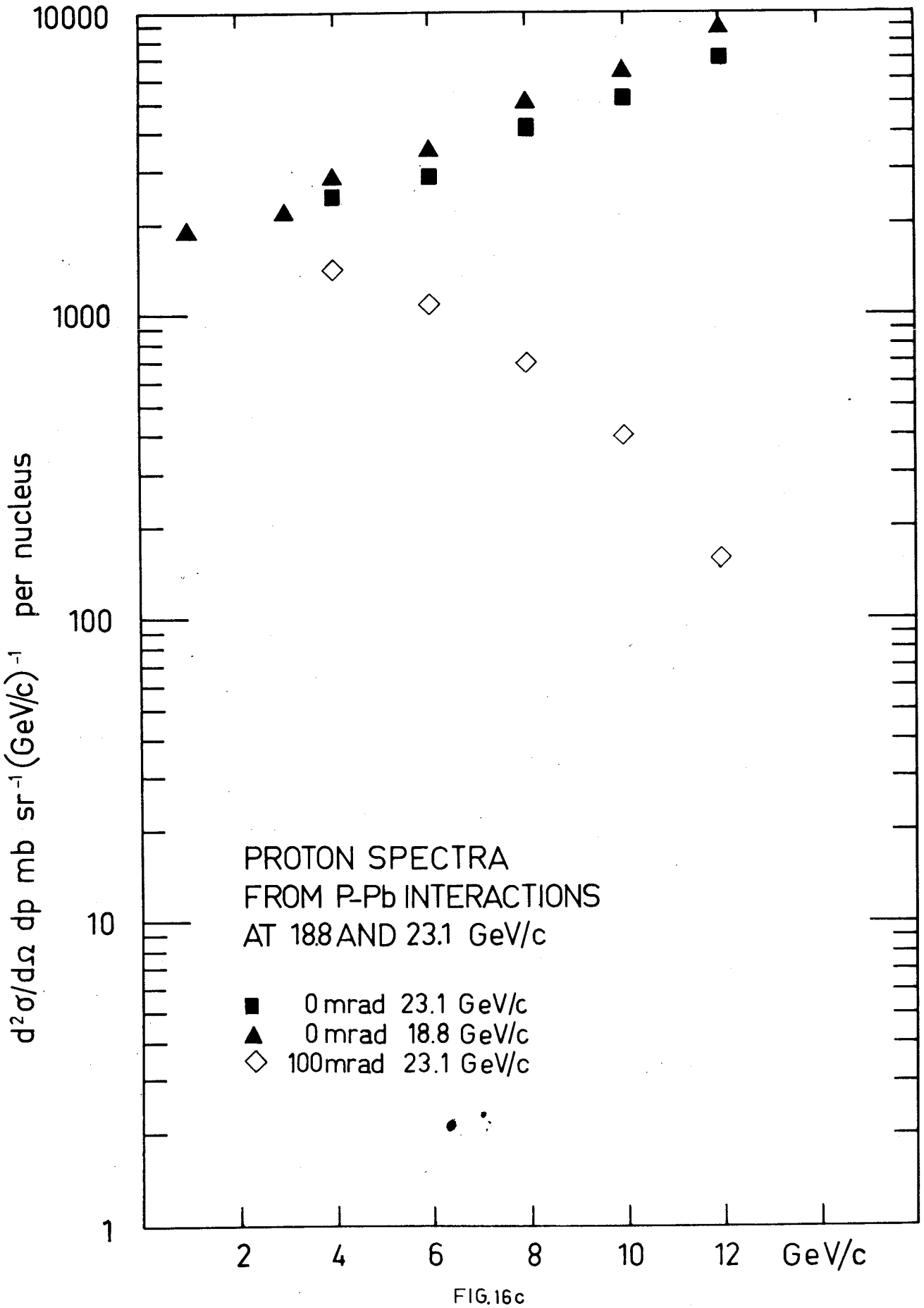

FIG. 16c

DIA - 19859

SIS/R/8554

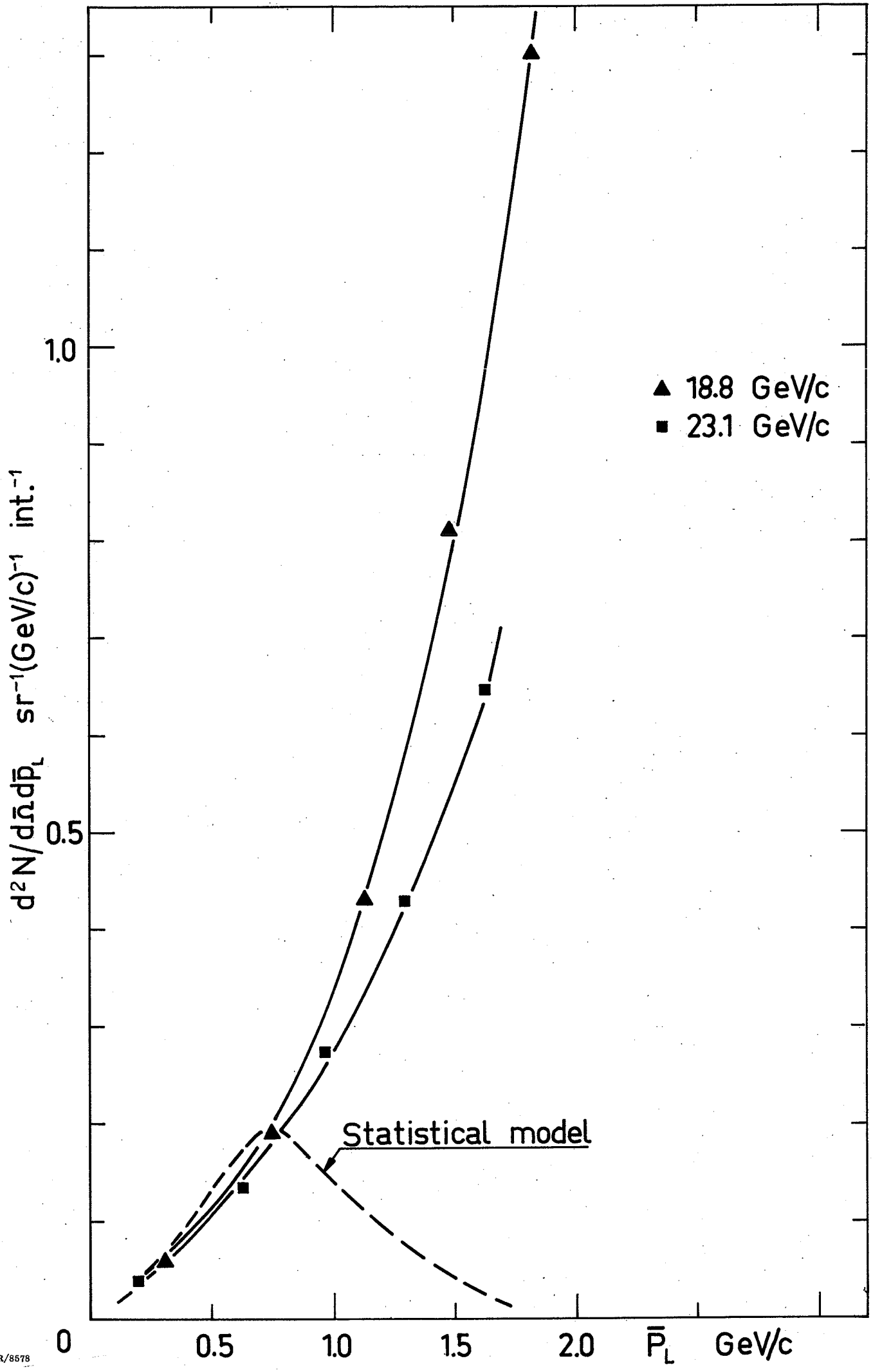

SIS/R/8578

FIG. 17

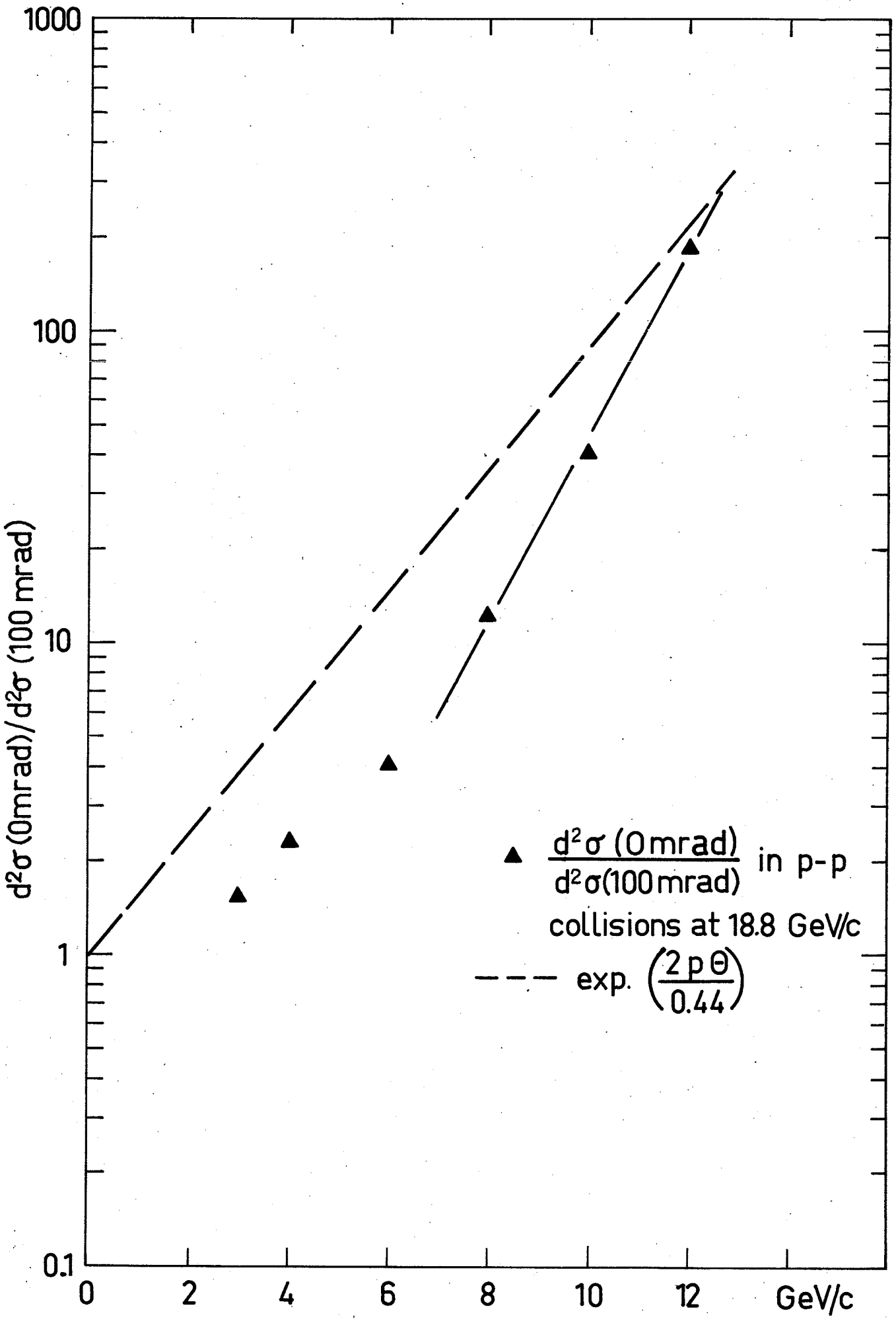
1000
100
10
1
0.1
0
2
4
6
8
10
12
GeV/c
d²σ (0mrad)/d²σ (100 mrad)
d²σ (0mrad) / d²σ(100mrad) in p-p
collisions at 18.8 GeV/c
exp. (2pΘ / 0.44)

FIG. 18

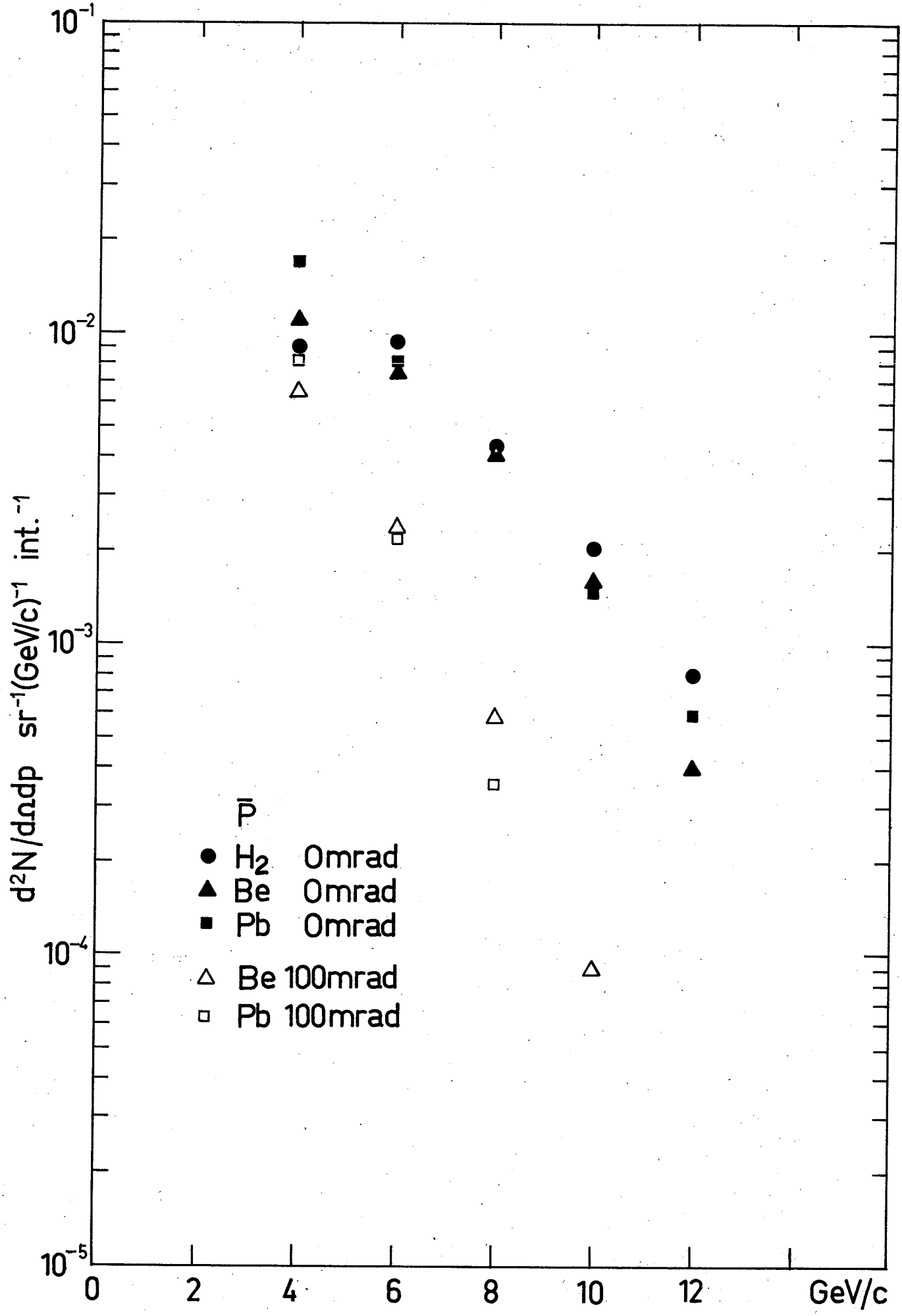
10^{-1}
10^{-2}
10^{-3}
10^{-4}
10^{-5}
$d^2N/d\Omega dp$ $sr^{-1}(GeV/c)^{-1}$ int.$^{-1}$
$\bar{P}$
H_2 0mrad
Be 0mrad
Pb 0mrad
Be 100mrad
Pb 100mrad
0
2
4
6
8
10
12
GeV/c

FIG. 19

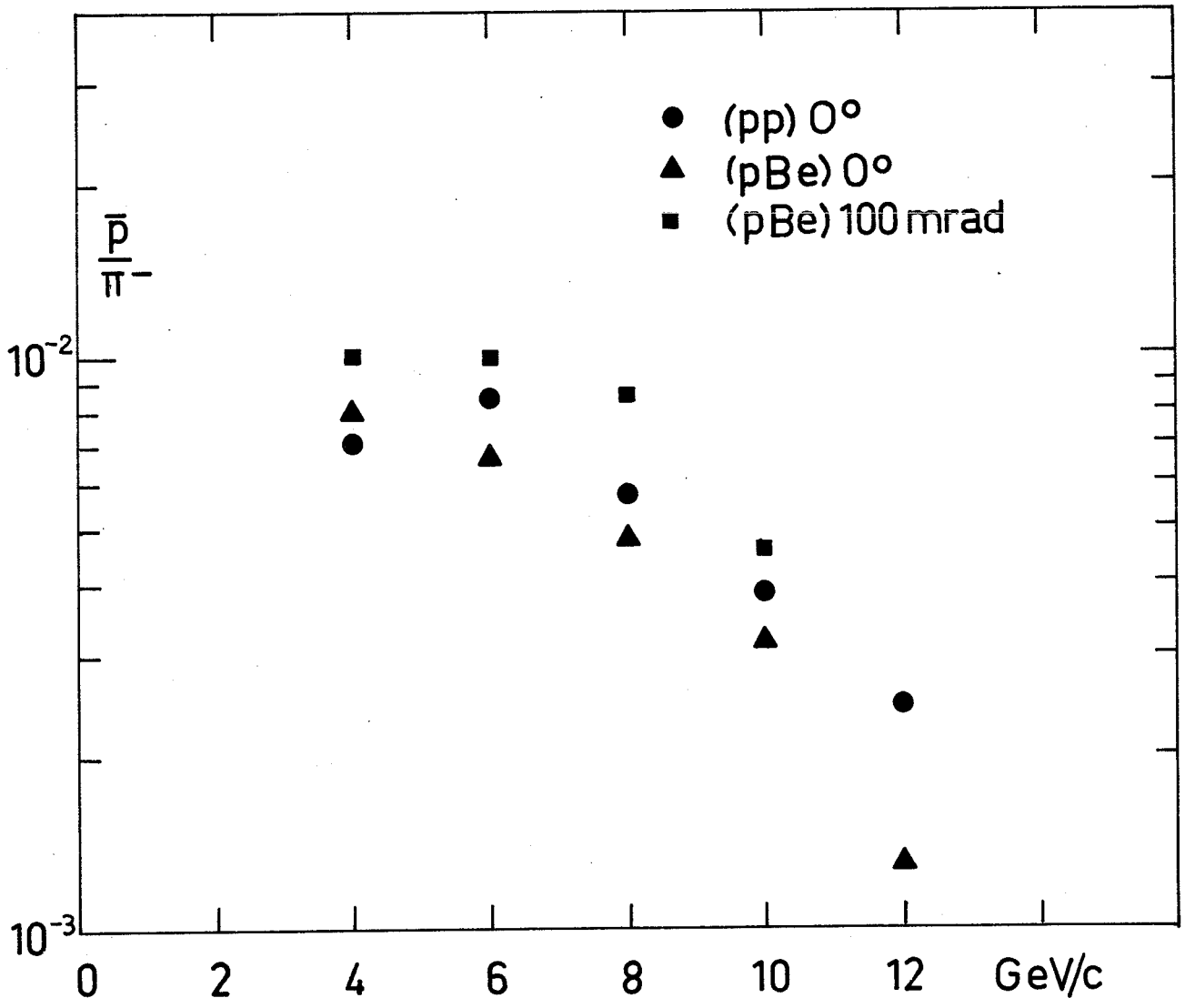

FIG. 20

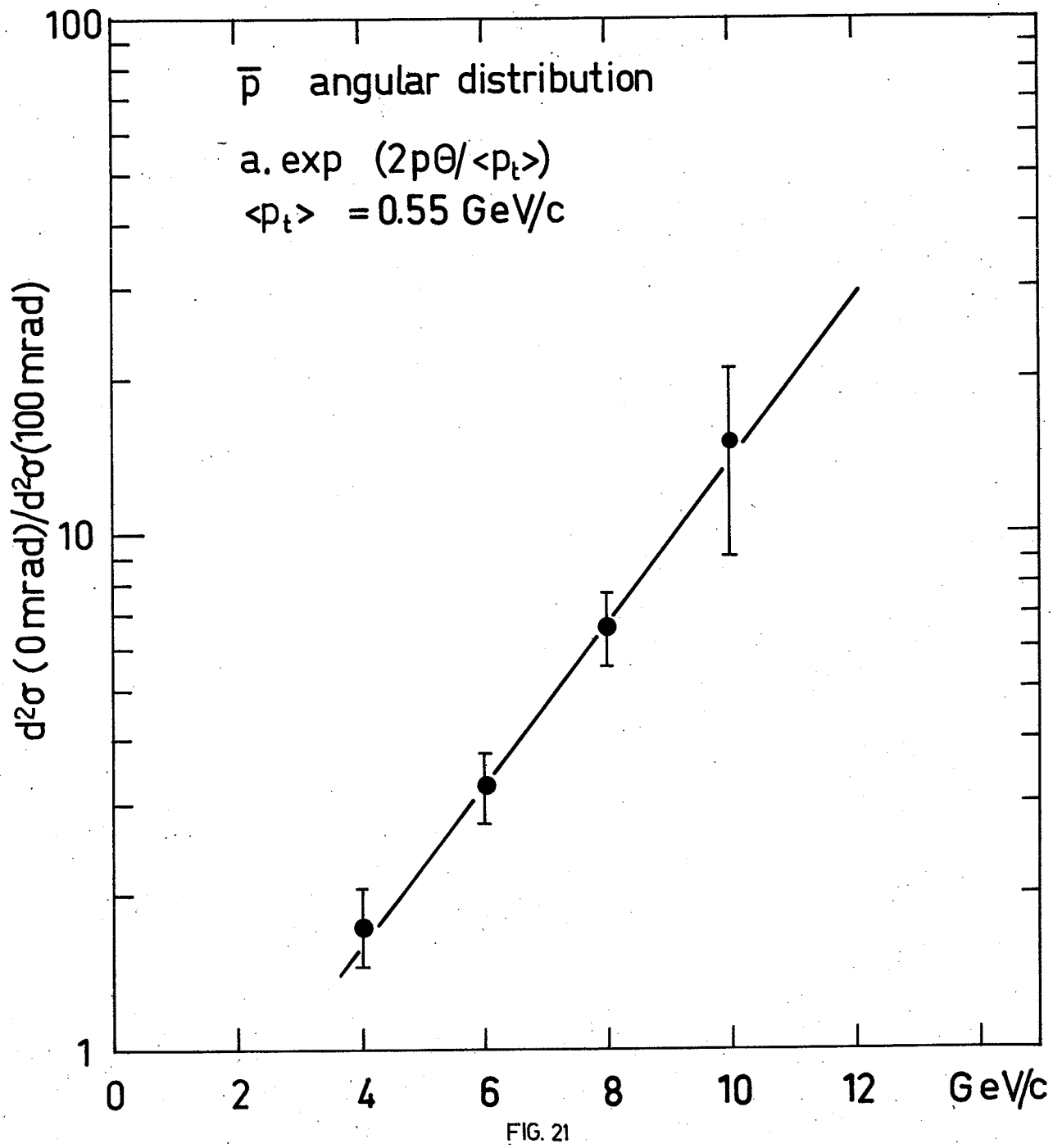
100
10
1
$\bar{p}$ angular distribution
a. exp $(2p\Theta/\langle p_t \rangle)$
$\langle p_t \rangle$ = 0.55 GeV/c
$d^2\sigma(0\,mrad)/d^2\sigma(100\,mrad)$
0
2
4
6
8
10
12
GeV/c

FIG. 21